RADC-TR-78-81
Final Technical Report
May 1978

LEVEL III

COST-EFFECTIVE GaAs READ IMPATT TRANSMITTERS

Raytheon Research Division

DDC
RECEIVED
AUG 7 1978
A

ROME AIR DEVELOPMENT CENTER
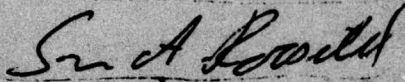AIR FORCE SYSTEMS COMMAND
GRIFFISS AIR FORCE BASE, NEW YORK 13441

AD No.
DDC FILE COPY

ADA056996

78 08 01 056

This report has been reviewed by the RADC Information Office (OI) and is releasable to the National Technical Information Service (NTIS). At NTIS it will be releasable to the general public, including foreign nations.

RADC-TR-78-81 has been reviewed and is approved for publication.
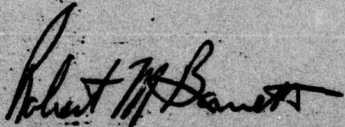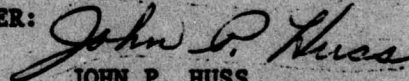
APPROVED: *[signature]*

SVEN A. ROOSILD
Project Engineer

APPROVED: *[signature]*

ROBERT M. BARRETT, Director
Solid State Sciences Division

FOR THE COMMANDER: *[signature]*

JOHN P. HUSS
Acting Chief, Plans Office

REPORT DOCUMENTATION PAGE		READ INSTRUCTIONS BEFORE COMPLETING FORM
1. REPORT NUMBER RADC-TR-78-81	2. GOVT ACCESSION NO.	3. RECIPIENT'S CATALOG NUMBER
4. TITLE *(and Subtitle)* COST-EFFECTIVE GaAs READ IMPATT TRANSMITTERS.		5. TYPE OF REPORT & PERIOD COVERED Final Report 29 May 76 - 31 Oct 77 3/29/76 - 10/31/77
		6. PERFORMING ORG. REPORT NUMBER S-2294
7. AUTHOR(s) R. N. Wallace		8. CONTRACT OR GRANT NUMBER(s) F30602-76-0143
9. PERFORMING ORGANIZATION NAME AND ADDRESS Raytheon Research Division 28 Seyon Street Waltham, MA 02154		10. PROGRAM ELEMENT, PROJECT, TASK AREA & WORK UNIT NUMBERS 62702F 46001820
11. CONTROLLING OFFICE NAME AND ADDRESS Deputy for Electronic Technology (RADC) Hanscom AFB, MA 01731 Contact Monitor: Sven Roosild/ESE		12. REPORT DATE May 1978
		13. NUMBER OF PAGES 186 P.
14. MONITORING AGENCY NAME & ADDRESS(if different from Controlling Office)		15. SECURITY CLASS. (of this report) Unclassified
		15a. DECLASSIFICATION/DOWNGRADING SCHEDULE N/A

16. DISTRIBUTION STATEMENT *(of this Report)*

Approved for public release; distribution unlimited.

17. DISTRIBUTION STATEMENT *(of the abstract entered in Block 20, if different from Report)*

18. SUPPLEMENTARY NOTES

19. KEY WORDS *(Continue on reverse side if necessary and identify by block number)*

Gallium Arsenide	Microwave Power Combiners
IMPATT Diodes	Microstrip Circuits
Microwave Devices	Epitaxial Material
	Semiconductors

20. ABSTRACT *(Continue on reverse side if necessary and identify by block number)*

The objective of this program was to develop a low-cost 5-GHz 40-W FM CW transmitter, using GaAs Read IMPATT diodes as RF power-generating elements, suitable for data-link applications. The transmitter actually produced during the course of the program met most of the RF performance goals established initially, but the goals for size, weight, cost, and primary power consumption were not achieved.

298320

78 08 01 056

The transmitter system was divided into four major subassemblies: a VCO-driver, a multidiode output stage, a multichannel current regulator, and a DC-to-DC inverter. The VCO-driver produced a 3.3W CW output in the 4.97 - 5.03 GHz operating band, and was capable of more than 20 MHz peak-to-peak frequency deviation with modulating frequencies between 50 kHz and 12 MHz. The output stage combined four high-power single-diode modules, operating in the injection-locked oscillator mode, through a nonresonant multi-port hybrid. Compact coaxial cavity oscillator circuits were used for the diode modules. The four-port hybrid was formed by cascading two-port power splitters of the type described by Gysel. The power combining circuitry was constructed in trapped inverted microstrip (TIM) line. The transistorized multichannel current regulator permitted control of the operating bias of the output stage without excessive power dissipation. The commercially-available DC-to-DC inverter permitted operation of the complete transmitter from a single 28 V supply.

Development of the output stage was aided by the availability of GaAs Read IMPATT diodes capable of 15 W CW output in the 5 GHz frequency range. Six diodes representative of those used in the transmitter output stage were delivered to RADC at the end of each month's effort until a total of 72 diodes was reached. Ten of twelve epitaxial wafers selected for processing produced diodes which reached or exceeded 15 W (nominal) power output. The best diode result obtained during the program was 21.9 W CW output at 4.85 GHz with 29.7 percent efficiency. Six high-power diodes were combined in a cavity-type oscillator to produce 120 W CW output at 5 GHz with 25 percent efficiency in a demonstration of the ultimate power capability of the diodes.

In actual tests of the transmitter, up to 42 W CW output was obtained near 5 GHz. DC-to-RF conversion efficiency of the output stage was 18 percent, and combining efficiency was 75 percent. The overall efficiency of the complete transmitter from 28 V prime power to RF output was about 9 percent. Improvements in the inverter and minor refinements in the RF portion of the circuit should increase this overall efficiency to 14-15 percent, making it possible to reduce the current drain from the 28 V supply below 10 A, the original program goal.

Engineering to reduce size, weight, and cost of the transmitter was not completed during the program. The transmitter as presently designed would cost about $ 15,000 to produce in quantities of 500, well in excess of the $ 2,000 goal. Size and weight of the transmitter exceed the $6.4 \times 1.7 \times 3.6$ in.^{3} and 3.5 lb goals, but present projections indicate that the complete unit except for the DC-to-DC inverter could be reduced to these limits.

A-044-034

EVALUATION

The prime objective of this contract was to build a small, efficient, prototype 40 watt solid state power transmitter to be operated at 5 Gigahertz with a 60 MHz tuning range. In addition, size, weight, and prime power objectives were imposed on the overall transmitter.

In general, the solid state power transmitter effort was very successful. The state of the art for output from individual IMPATT diodes was advanced. Furthermore, an innovative technological approach for combining the output of individual diodes was shown to function very satisfactorily. The objectives for size, weight, cost and primary power consumption were not met. The difficulties encountered were not fundamental in nature and can be overcome with additional effort.

SVEN A. ROOSILD
Project Engineer

TECHNICAL REPORT SUMMARY

The objective of this program was to develop a deliverable breadboard model of a low-cost 5 GHz FM transmitter having 40 W CW output suitable for data link applications. Gallium arsenide Read IMPATT diodes were to be used as RF power-generating elements in the transmitter. This final report describes the complete program effort during the period 29 March 1976 through 31 October 1977.

The transmitter actually delivered at the end of the technical effort achieved most of the major RF performance goals which had been established at the outset of the program. It produced somewhat more than 40 W CW output at 5 GHz, and demonstrated FM capability with more than 20 MHz peak-to-peak frequency deviation for modulating frequencies from 50 kHz to 12 MHz. The transmitter operated from a single 28 V DC source. Reliability sufficient to meet the program goals (5000 hours operating life, 7 years storage life) appeared to be possible. However, the goals for size, weight, cost, and primary power consumption were not achieved.

The complete transmitter consisted of four main subassemblies. These were the VCO-driver, the multiple-diode power output stage, the multichannel current regulator feeding the output stage, and the DC-to-DC inverter supplying high voltage ($\sim$ 120 V) to all IMPATT diodes in the transmitter.

Design, fabrication, and preliminary testing of the VCO-driver sub-assembly were carried out by the Raytheon Special Microwave Devices Opera-tion. This unit was essentially a low-power FM transmitter, which accepted a baseband input signal (typically between 70 kHz and 10 MHz) and produced $\sim$ 3.3 W CW output at 5 GHz. The full 4.97 to 5.03 GHz operating range pro-jected for the transmitter was covered by electronic tuning during preliminary tests of this unit.

Development of the multiple-diode power output stage was the major program task. This subassembly consisted of four single-diode oscillator modules combined through a nonresonant power splitter. The diode modules

used a compact coaxial cavity circuit, and each was operated under DC bias conditions which would produce 12.5 W CW output at 5 GHz with 24 percent efficiency. The power combining circuit used a cascade of two-port hybrids of the type described by Gysel. These hybrids were constructed using trapped inverted microstrip (TIM) line for low loss and improved isolation between diodes. Power outputs up to 42 W with a DC-to-RF conversion efficiency of 18 percent were obtained in this output stage, indicating that the combining efficiency of the circuit was 75 percent.

The development of the output stage was simplified by the availability of GaAs Read IMPATT diodes having 15 W or more CW power output capability in the 5 GHz region. The design and fabrication techniques for such diodes are now fairly well in hand. This was demonstrated by the fact that 10 of 12 epitaxial GaAs wafers selected for diode processing during the program produced diodes which reached or exceeded the 15 W (nominal) power output level. Operation of such diodes in the transmitter at the 12.5 W level produced a junction temperature of only 175°C, which is consistent with a long operating lifetime. The best diode performance achieved during the program was 21.9 W CW output at 4.85 GHz with 29.7 percent efficiency. Six diodes from the same lot producing this result were combined in a resonant cavity oscillator circuit to produce 120 W CW output at 5.0 GHz with 25 percent overall DC-to-RF conversion efficiency. This provided a demonstration of the high-power capability of the diodes.

The multichannel current regulator used both active and passive circuit techniques to provide the high bias circuit source impedance necessary to stabilize the operating points of the output stage diodes while suppressing bias circuit oscillations. In the deliverable transmitter, a dissipation of ~ 50 W occurred in this unit. However, a reduction of this loss to ~ 10 W should be possible. The regulator included protective circuitry to shut down the output stage whenever a failure of any of the output stage diodes occurred.

To avoid expending a major portion of the program effort in further development of the relatively mature power supply technology, a standard commercially-available DC-to-DC inverter was selected. The unit chosen

could supply the power requirements of the transmitter, but was a major contributor to the size and weight overruns in the deliverable unit. Also, its efficiency under full load, 67 percent, was less than the 80 percent value assumed in planning the transmitter, and this caused the total power consumption to be larger than originally projected.

The transmitter delivered at the conclusion of the program effort *could be refined further, without major technological innovations, to reduce* the size, weight, and power consumption. Present projections indicate that the RF portion of the transmitter could fit within the original size and weight constraints, but that the DC-to-DC inverter would have to be packaged separately. Total drain from the 28 V supply could be reduced to less than the original 10 A goal.

Further value engineering will be required to reduce the manufacturing cost of the transmitter toward the $2,000 unit cost goal in quantities of 500. The present design, which is not really suitable for quantity production, would cost ~ $15,000 to produce in lots of 500.

PREFACE

The objective of this program was to produce a prototype of a low-cost FM CW transmitter capable of producing 40 W output at 5 GHz for data link applications. The transmitter was to use GaAs Read IMPATT diodes as active elements.

Most of the RF performance goals established in the program were achieved by the transmitter actually constructed. The output stage combined four high-power GaAs diodes to produce slightly more than 40 W at 5 GHz. However, the size, weight, cost, and primary power consumption objectives for the transmitter were not achieved. Prospects for achieving or closely approaching these original objectives with further development work are good.

The program work was carried out by the Research Division of Raytheon Company, Waltham, Massachusetts. The work was sponsored by the Air Force Systems Command, Rome Air Development Center, Hanscom AFB, Massachusetts under Contract No. F30602-76-0143.

At Raytheon, the work was carried out under the supervision of R. W. Bierig, Manager of the Microwave Semiconductor Laboratory at the Research Division. The growth and characterization of the gallium arsenide epitaxial wafers were directed by S. R. Steele. Design and fabrication of GaAs Read IMPATT diodes were under the direction of Dr. M.G. Adlerstein. Diode evaluation and circuit development were the responsibility of Dr. R. N. Wallace. Development of the VCO-driver subassembly in the transmitter was subcontracted to the Raytheon Special Microwave Devices Operation.

The Air Force Project Engineer was Mr. S. A. Roosild, RADC/ETSD. This report covered the period 29 March 1976 through 31 October 1977. The Raytheon internal report number is S-2294.

TABLE OF CONTENTS

TABLE OF CONTENTS (Cont'd.)

LIST OF ILLUSTRATIONS

LIST OF ILLUSTRATIONS (Cont'd.)

LIST OF ILLUSTRATIONS (Cont'd.)

LIST OF ILLUSTRATIONS (Cont'd.)

LIST OF ILLUSTRATIONS (Cont'd.)

LIST OF TABLES

1.0 INTRODUCTION

This final report describes the technical effort toward the development of a deliverable breadboard model of a cost-effective GaAs Read IMPATT transmitter. The transmitter was to produce 40-W CW output at 5 GHz with FM capability suitable for data link applications. This basic objective was in fact achieved. High-power, high-efficiency GaAs Read IMPATT diodes were used as active elements in the power-generating stages of the transmitter. The work reported herein was carried out at the Raytheon Company Research Division during the period 29 March 1976 through 31 October 1977.

A number of specific performance goals were initially set for the breadboard transmitter. These goals are listed below, along with the performance actually obtained from the unit delivered. Performance of this unit was witnessed by the RADC project engineer.

	Goal	Test Result
Center Frequency	5 GHz	5 GHz (Initial Test)
Tunable Bandwidth	60 MHz	60 MHz (Driver, Initial Test) > 200 MHz (Output Stage)
Instantaneous Bandwidth	10 MHz (-1 dB)	> 20 MHz (-1 dB)
Power Output	40 W CW	42.1 W CW (Maximum) 40 W CW (Typical)
Input Power	28 V DC 10 A	28 V DC 16.7 A
Operating Life	5000 hours	> 5000 hours (Projection)
Shelf Life	7 years	> 7 years (Projection)

1

	<u>Goal</u>	<u>Test Result</u>
Modulation	FM 70 kHz < f_m < 10 MHz; 10 MHz p-p deviation; Modulation sensitivity flat + 0, -1 dB from 70 kHz to 10 MHz	FM 50 kHz < f_m < 12 MHz; < 20 MHz p-p deviation; Modulation sensitivity 35.5 MHz/V, ± 0.2 dB from 200 kHz to 10 MHz, rising + 1 dB at 140 kHz, and + 2.1 dB at 70 kHz.
Form Factor	6.4 x 1.7 x 3.6 in.^{3} (39.2 in.^{3})	1109.4 in.^{3}
Weight	3.5 lb	25.6 lb
Noise (Total AM and FM)	30 dB or more below carrier level in a 1 kHz bandwidth 100 MHz from the carrier frequency.	90 dB or more below carrier level under specified conditions.
Cost	$2000 each, in quantities of 500	~ $15,000 each in quantities of 500

From these tabulated results, one can see that most of the RF performance objectives for the transmitter were achieved. Prospects for achieving those objectives not reached by the prototype are considered in detail in the body of this report, but a few preliminary comments on possible improvements will be made here.

The power consumption for the transmitter was substantially in excess of the goal. This was caused primarily by the relatively low efficiency of the DC-to-DC inverter used to supply the operating voltage required by the IMPATT diodes and by a larger-than-necessary voltage drop across the current regulator feeding these diodes. Both of these problems can be attacked directly, and when improvements here are combined with minor refinements in the RF circuitry, a total current drain less than 10 A should be possible.

2

The only flaw in the modulation characteristics of the transmitter was a rise in modulation sensitivity at low frequencies. This can be cured by changing the values of the L-C network used to couple the modulating signal to the Gunn-diode VCO in the driver section of the transmitter.

Size and weight of the transmitter were much larger than the program goals, since the components were constructed as first laboratory prototypes. Our recent projections indicate that the RF portion of the transmitter, excluding only the DC-to-DC inverter used to convert 28 V prime power to the higher voltage required by the IMPATT diodes, can eventually be reduced to fit within the size and weight goals.

Value engineering of the transmitter was not completed. The present transmitter configuration, which differs from a unit which would be useable in the field, would cost about $15,000 in quantities of 500. This is substantially more than the $2000 program goal. Some reduction should be possible as the transmitter is redesigned mechanically and electrically. Some of the constraints and tradeoffs in the design, fabrication and operation, and cost of the transmitter are discussed within the body of this report.

The fabrication of a successful prototype transmitter was dependent on a supply of high-power, high-efficiency GaAs Read IMPATT diodes. Six diodes representative of those to be used in the transmitter output stage were delivered to RADC at the end of each month of the program until a total of 72 diodes was reached. Diodes capable of more than 15 W CW output at 5 GHz were available for use in the transmitter. There, they were operated at low (175°C) junction temperature for long life. The design and fabrication of such devices was under fairly good control as demonstrated by the fact that ten of twelve GaAs epitaxial wafers meeting doping profile specifications produced IMPATT diodes which reached or exceeded the 15 W (nominal) power level. The best diode result obtained during the program was 21.9 W CW output at 4.85 GHz with 29.7 percent efficiency. The possible application of such diodes in high-power sources was demonstrated when six diodes in a cavity-type oscillator circuit produced 120 W CW output at 5 GHz with 25 percent DC-to-RF conversion efficiency.

3

In the remaining sections of this report, we first give an overall description of the prototype transmitter which was delivered (Sec. 2). The development of the subassemblies which made up this transmitter is described in Sec. 3. Test results are given in Sec. 4, along with projections of the performance which can reasonably be expected with further development. Section 5 describes the cost projections for the transmitter in its present early stage of development. Section 6 summarizes the hardware deliveries that were made during the program. In Sec. 7 we give some major conclusions derived from the work, along with suggestions for future work. References are listed in Section 8.

2.0 TRANSMITTER SYSTEM DESCRIPTION

Figure 1 shows a functional block diagram for the deliverable transmitter in its final form. Four major subassemblies — the VCO-driver, the power output stage, the multichannel current regulator, and the DC-to-DC inverter – make up the complete unit. The details of the development of each subassembly are described in Sec. 3 of this report. The system design for the transmitter is essentially the same as that originally proposed, but there have been some changes within the individual subassemblies. Also, an interstage isolator (terminated circulator) has been added to avoid undesirable interaction between the driver and the output stage.

The VCO-driver subassembly accepts a baseband input signal in the range 70 KHz to 10 MHz and provides 3.3-W CW (typical) of frequency-modulated RF output at 5 GHz. The full 4.97-to-5.03-GHz tuning range specified for the transmitter is covered by electronic tuning. The power output of this driver is more than sufficient to provide 10 MHz of electronic tuning (locking bandwidth) in the subsequent power output stage. The subassembly includes in a single package a low-power (100-150 mW) voltage-controlled Gunn oscillator, two injection-locked oscillator stages using GaAs IMPATT diodes to increase the output power to ~3.3 W, and the voltage and current regulators required for the Gunn and IMPATT stages. The total power consumption of the subassembly is ~61 W, substantially above the 33 W projected in the original Technical Proposal. The design, fabrication and initial testing of the VCO-driver subassembly were carried out by the Raytheon Special Microwave Devices Operation.

The output stage, designed and fabricated at the Research Division, required the largest development effort during the program. It consists of four high-power GaAs Read IMPATT diode oscillators whose power outputs are summed in a nonresonant parallel-type combining circuit. The oscillators use a compact coaxial cavity circuit, and each one is operated at a bias current level which produces a nominal 12.5 W CW output at 5 GHz with 24 percent efficiency. The four-diode power combining circuit is made by cascading 3-dB hybrids of the type described by Gysel.[5] To help reduce

5

Power Output Stage
(Injection-Locked Oscillator)

VCO-Driver

Modulation
Input

− + − +
28V 120V

3 W
5 GHz

40 W
5 GHz

Divider

GaAs Read
IMPATT
Diode
Oscillators

Multi-channel
Current Regulator

− +

120 V
− +

DC-DC Inverter

− 28V +
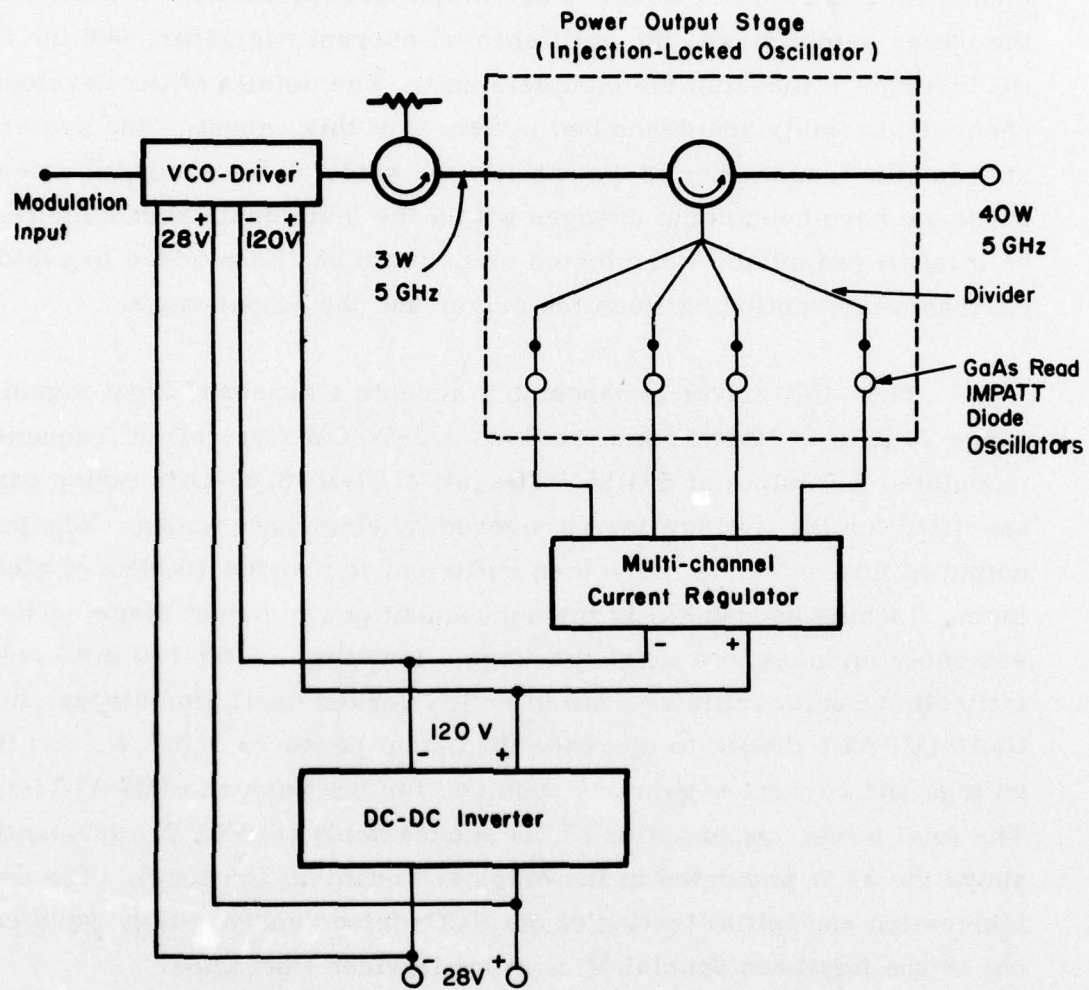
Figure 1   Functional Block Diagram of the Transmitter.

losses and improve isolation in the hybrids, trapped inverted microstrip (TIM) line[6] was used as the circuit medium.

The output stage has produced up to 42 W CW power within the nominal 4.97 to 5.03 GHz operating band of the transmitter. Junction temperatures of the high-power IMPATT diodes are typically $\sim 175°C$, which represents a conservative operating condition. With the existing VCO-driver, a locking bandwidth of 48 MHz has been demonstrated, well in excess of the 10 MHz requirement for electronic tuning, but less than the full 60 MHz operating band of the transmitter. Covering the full operating band of the transmitter requires mechanical tuning of the oscillators in the output stage. The tuning procedure is simple, and a mechanical tuning range in excess of 200 MHz is possible. Power consumption of the output stage is ~ 210 W, somewhat less than the 230 W projected in the Technical Proposal, which helps to offset the overrun in the power required for the VCO-driver. The efficiency with which the power outputs of the diodes are combined, including the effects of the input and output circulator losses, is 75 percent, somewhat better than the 70 percent projected.

The multichannel current regulator provides four individually adjustable current-regulated bias outputs to operate the diodes in the power output stage. This regulator is an extension of the single-channel regulator developed during the previous program.[2] While the regulator consumes essentially no current, there is a voltage drop of ~ 20 V across the circuit during operation. This drop represents about 50 W of dissipated power. A reduction of the voltage drop to as little as 5 V with no change in the RF performance of the transmitter appears possible. This would improve the overall system efficiency and, assuming use of the present inverter, would reduce current drain from the 28 V prime power source by ~ 1.5 A.

The DC-to-DC inverter produces 120 V DC nominal output from the 28-V DC primary power for operation of the IMPATT diodes in the VCO-driver subassembly and in the output stage. (The Gunn oscillator in the VCO-driver is operated directly from the 28-V primary power source through a voltage

7

regulator.) To achieve lower overall cost and to avoid spending a large part of the program effort in power supply development, a standard, commercially available inverter was used. The unit selected is the CEA2-C-130Z-252 inverter produced by the CEA Division of Berkleonics, Inc., San Luis Obispo, California. The efficiency of this inverter is typically ~70 percent under the normal operating conditions present in the transmitter, somewhat less than the 80 percent originally projected. The inverter alone exceeds the size and weight limits originally given for the entire transmitter package. Possibilities for reducing the size and weight of the inverter and for obtaining still higher efficiency have been discussed with the manufacturer.

Using the present inverter, the total load current imposed on the 28-V primary power source by the complete transmitter package is ~16.7 A This is higher than the 13.5 A originally projected principally because the voltage drop across the current regulator is larger than necessary and because the inverter efficiency was smaller than expected.

3.0   DEVELOPMENT OF TRANSMITTER COMPONENTS

3.1   VCO-Driver Subassembly

The VCO-driver subassembly is a 3-W CW FM transmitter which operates at 5 GHz. Power consumption of this subassembly is relatively small compared with that of the complete 40-W transmitter. Consequently, little improvement in overall transmitter efficiency can be obtained by refining the VCO-driver subassembly.

The performance required from the VCO-driver is similar to that of sources and amplifiers produced routinely by the Raytheon Special Microwave Devices Operation (SMDO) using established IMPATT and Gunn diode technology. For this reason, and because little was to be gained in transmitter efficiency by exploiting new technology in this subassembly, the unit was ordered from SMDO. The VCO-driver subassembly was received in final form from SMDO in September 1976.

Figure 2 shows a functional block diagram and a schematic mechanical layout of the VCO-driver subassembly as it was finally received. It consists of a Gunn diode VCO followed by two IMPATT diode amplifier stages, which operate in the injection-locked oscillator mode. Interstage and output circulators are used to prevent undesired interactions between stages or with the subsequent transmitter output stage. The Gunn diode is operated from the 28-V primary power supply through a voltage regulator. The current regulator for the IMPATT diodes accepts 120-V input, which is derived from the DC-to-DC inverter. A photograph of the finished subassembly is shown in Fig. 3.

The Gunn oscillator stage, fabricated in air-dielectric coaxial line, produces 150 mW output at 5 GHz. Tuning over the 4.97 to 5.03 GHz range is accomplished by adjusting the operating bias voltage. A potentiometer that controls the voltage regulator integral to the subassembly is provided for this adjustment. Frequency modulation is accomplished by an independent

9
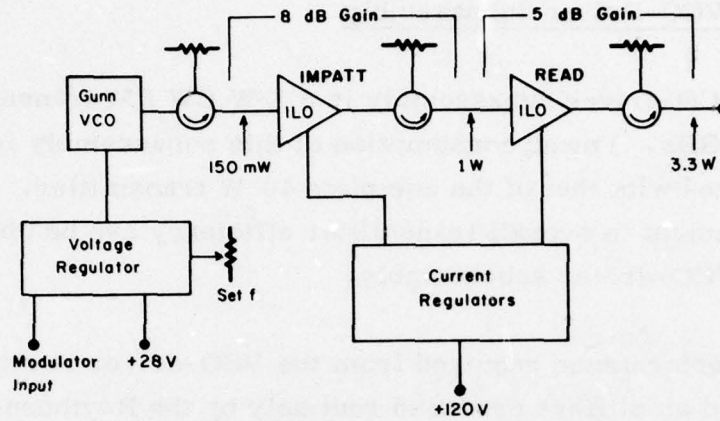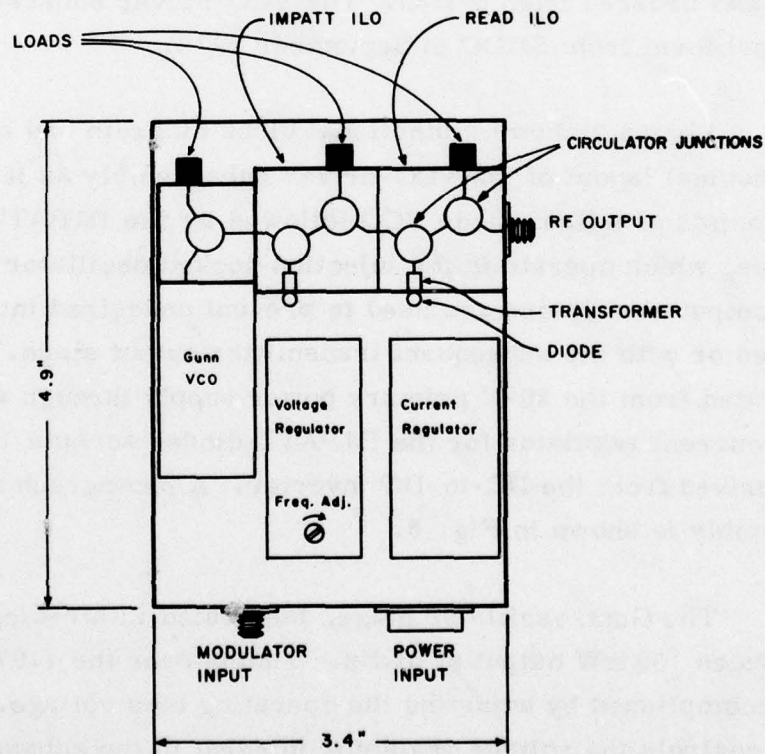
Figure 2   Functional Block Diagram and Schematic Mechanical
                  Layout of the VCO-Driver Subassembly.

10
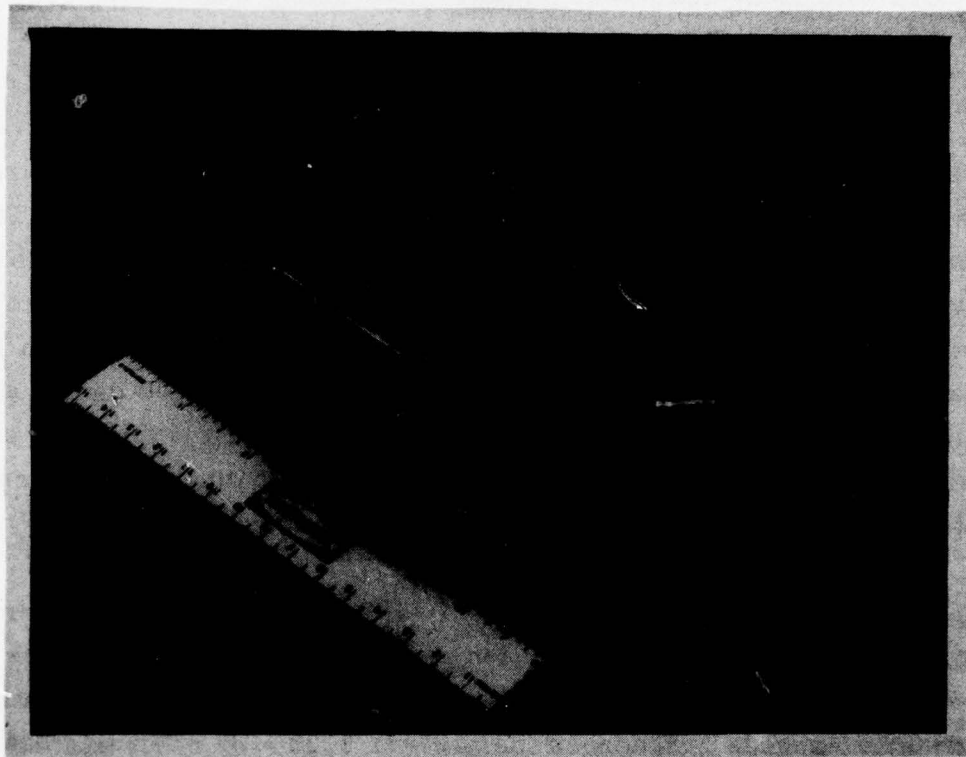
Figure 3   Photograph of the Completed VCO-Driver Subassembly.

11

variation of the bias voltage. The use of bias tuning and bias modulation results in some change in the output amplitude of the oscillator across the operating band. This change is less than 1 dB and is relatively unimportant because succeeding stages operate as high-gain injection-locked oscillators with saturated power output. Bias tuning was chosen because it provides a simpler RF circuit than could be realized with varactor tuning.

The two IMPATT diode stages are fabricated in ferrite-substrate microstrip configuration so that the required interstage and output circulators can be included simply, without resorting to composite substrates. The first of these stages uses a flat-profile GaAs diode operating as an injection-locked oscillator. Locking is maintained across the full 4.97 to 5.03 GHz operating band without mechanical tuning. The stage produces 1-W output with 100 mW input at 5 GHz. The second IMPATT stage uses a GaAs Read diode, also operating as an injection-locked oscillator. As in the first IMPATT stage, locking is maintained across the full operating band without mechanical tuning. The stage produces 3.3W (nominal) output with 1 W input at 5 GHz.

Performance of the complete VCO-driver subassembly is summarized in Table 1. While the gain distribution and power levels of the stages differ somewhat from those originally proposed, the RF performance is satisfactory. Power output exceeds 3 W across the 4.97 to 5.03 GHz operating band.

The specifications used in producing the VCO-driver subassembly were derived from the performance objectives of the transmitter and from experience gained during the previous program[2]. The proposed and actual characteristics of the complete subassembly are compared in Table 2. In general, the RF performance goals were met or exceeded, but size, weight, and power consumption were somewhat larger than planned.

Considering Table 2 in detail, note that the operating band of the driver, measured during initial acceptance tests, coincided with that of the complete transmitter. A slight shift of this operating band occurred when additional shielding was applied to the driver to improve frequency stability, as will be described in Section 4.

12

TABLE 1

VCO-DRIVER PERFORMANCE

Nominal Operating Conditions:

IMPATT diodes	-	120 VDC
		350 mA
Gunn diode	-	28 VDC
		670 mA

Power Output:

f(GHz)	P_o(W)
4.97	3.16
4.98	3.31
4.99	3.46
5.00	3.54
5.01	3.54
5.02	3.54
5.03	3.54

13

TABLE 2

COMPARISON OF PROPOSED AND ACTUAL
VCO-DRIVER SUBASSEMBLY CHARACTERISTICS

PROPOSED	ACTUAL
1. Operating Frequency 4.97 - 5.03 GHz	1. Operating Frequency 4.97 - 5.03 GHz, by adjustment of potentiometer controlling Gunn diode bias voltage
2. Power Output 3 W (+0, -0.5 dB)	2. Power Output 3.54 W (+0, -0.5 dB)
3. Instantaneous Bandwidth 10 MHz (+0, -1 dB)	3. Instantaneous Bandwidth Demonstrated >40 MHz (+0, -0.5 dB) In any 10-MHz band, +0, -0.2 dB or better
4. Modulation FM, modulation frequency from 70 kHz to 10 MHz Modulation sensitivity constant (± 0.5 dB) within this range	4. Modulation FM, modulation frequencies from 50 kHz to 12 MHz demonstrated Modulation sensitivity 35.5 MHz/V, ± 0.2 dB from 200 kHz to 10 MHz Sensitivity rises at low frequencies: + 1 dB at 140 kHz and +2.1 dB at 70 kHz

14

TABLE 2 (Cont'd.)

COMPARISON OF PROPOSED AND ACTUAL
VCO-DRIVER SUBASSEMBLY CHARACTERISTICS

PROPOSED	ACTUAL
5. Noise (Total AM and FM) -40 dB relative to the carrier in a 1-kHz bandwidth 100 MHz from the carrier	5. Noise (Total AM and FM) -85 dB relative to the carrier in a 1-kHz bandwidth 100 MHz from the carrier demonstrated
6. Input Power 120 V, 200 mA DC 28 V, 300 - 350 mA DC (33 W total)	6. Input Power 120 V, 350 mA DC 28 V, 670 mA DC (61 W total)
7. Operating Life 5000 hours	7. Operating Life Standard sources and amplifiers of similar construction have demonstrated more than 10,000 hours MTF in field service
8. Shelf Life 7 years	8. Shelf Life 7 years or more possible
9. Size $3.5 \times 4 \times 1$ in.^{3}	9. Size $3.4 \times 4.9 \times 1.25$ in^3 (top compartment only) $4 \times 5.75 \times 1.45$ in.^{3} (overall, including base plate)

TABLE 2 (Cont'd.)

COMPARISON OF PROPOSED AND ACTUAL
VCO-DRIVER SUBASSEMBLY CHARACTERISTICS

PROPOSED	ACTUAL
10. Weight	10. Weight
~ 1 lb.	1.11 lb. (top compartment)
	1.67 lb. (total, including base plate)

Power output was specified at 3 W, a level large enough to insure a 10-MHz locking bandwidth in the following output stage. In fact, more than 3.5 W could be obtained at some frequencies. In previous work,[2] 330 mW of input signal had provided 6 MHz of locking bandwidth with a 60-W high-Q multiple-diode output stage. The locking bandwidth varies as $(2/Q_e) \sqrt{P_i/P_o}$, where P_i is the RF input power, P_o is the RF output power, and Q_e is the external Q of the locked stage. Thus, 3 W input would be expected to give at least 20 MHz of locking bandwidth in a 40-50 W output stage, even if the external Q remained large. The Q of the present output stage, using a nonresonant power combining structure, was expected to be lower than that of the previous cavity-type circuit. In fact, external Q's of 30-40 were measured for the oscillators in the output stage. This provided more than 40 MHz of locking bandwidth in the complete transmitter, even with the output of the VCO-driver attenuated by passage through two circulator junctions. Thus, the instantaneous bandwidth goals for the VCO-driver and for the complete transmitter were surpassed. It was not possible, however, to cover the full 4.97 to 5.03 GHz band of the transmitter by electronic tuning alone.

The subassembly demonstrated frequency modulation capability from 50 kHz to 12 MHz. There is a low-frequency cutoff of modulation sensitivity imposed by the AC-coupling of the modulation to the Gunn diode VCO through an L-C network. This general behavior is considered acceptable because FDM-FM communications links often do not use baseband frequencies below about 70 kHz. A resonance in the coupling network caused a peak in the low-frequency modulation sensitivity near 50 kHz before the final low-frequency cutoff. This condition could be corrected by changing the inductance and capacitance of the coupling network to move the resonance below the desired range of modulating frequencies. With the present coupling network, modulation sensitivity is essentially constant from 200 kHz to 10 MHz.

Total noise and spurious output from the transmitter were far below the specification set for the VCO-driver. This specification included a margin of 10 dB over that required for the complete transmitter to allow for excess noise which might be contributed by the output stage.

Input power requirements exceeded those originally proposed by almost a factor of two. This did not cause any substantial overrun in the total load imposed by the transmitter since the output stage was somewhat more efficient than planned. The low efficiency of the Gunn VCO contributes significantly to the large power consumption of the subassembly. It now appears that substantial reductions in the power consumption of the unit could be achieved by using FET's as active elements, as will be discussed further in Section 7.0.

No direct study of the operating life or shelf life of the VCO-driver subassembly was made in the present work. However, microwave transmitters having the same general circuit configuration and operating power level as the unit tested here are available from SMDO as standard catalog items. These units have demonstrated more than 10,000 hours MTBF in actual field use. Thus, a 5000-hour operating lifetime is achievable in the present unit. So long as the unit is hermetically sealed, only degradation of the electrolytic capacitors in the control and regulating circuitry would be a limiting factor for shelf life. Such capacitors can be obtained with 10-year lifetime, so the shelf life goal for the VCO-driver should also be achievable.

Size and weight limits for the VCO-driver were exceeded. However, if the base plate is considered a part of the main heat sink for the transmitter, the size and weight overruns are small. The use of FET's in the driver could result in a substantial size reduction, since most of the circulators required in the injection-locked oscillator circuitry would be eliminated.

18

3.2 Output Stage

3.2.1 High efficiency GaAs Read IMPATT diodes

3.2.1.1 Background

As a part of the previous RADC program,[2] high-power, high-efficiency
GaAs IMPATT diodes capable of operation at 5 GHz were developed. These
diodes used the low-high-low modified Read doping profile and had platinum
Schottky-barrier junctions. The required GaAs material was produced by
vapor phase epitaxial growth. For improved power output, reduced electrical
series resistance, and reduced thermal impedance, each high-power diode was
made up of four mesas in a 2 × 2 square array on an integral gold plated heat
sink. Typical mesa diameters were 7 - 8 mils. Each four-mesa chip was
bonded into a standard microwave diode package.

With diodes operating as oscillators, the best performance achieved
in the previous work was 13.3-W CW output with 24 percent efficiency in the
4.8 - 4.9 GHz range. Diodes from two different wafers reached this perform-
ance level.   More typical of the better diodes fabricated was 10 - 11 W CW
output with 22 - 23 percent efficiency in the 5-GHz range. These diodes had
thermal resistances in the range 4.5 - 5.0°C/W, which allowed them to
produce their rated power output with junction temperatures of ~200°C.
Initial plans called for the use of five such diodes in the output stage of the
transmitter. The design for these diodes was well in hand. This was
demonstrated by the fact that eleven of thirteen epitaxial wafers selected
for device processing toward the end of the previous program produced
diodes with 10 W or more CW output.[3]

The reliability of such high-power GaAs Read IMPATT diodes, both
under storage and operating conditions, is still under investigation. The
present program included no independent study of device reliability, and
was to make use of separately-gathered reliability data to project the
transmitter lifetime. Most reliability data have been obtained using single-
mesa diodes. A detailed study of four-mesa diodes is to be undertaken

19

at out laboratory in the near future. Until that work is complete, data from
single-mesa diodes having similar construction and operating with similar
junction temperatures can be used to make preliminary projections of the
reliability of four-mesa diodes. First, there appears to be no inherent or
fundamental limitation on shelf life. As long as the diode surface is kept
clean during manufacture and the integrity of the hermetic seal of the package
is maintained, the IMPATT diodes should not be a limiting factor in achieving
the 7-year shelf-life goal. Second, regarding lifetime under operating con-
ditions, the work of Coleman et al. [7] indicates that Pt Schottky-barrier de-
vices should have operating lifetimes approaching 10^5 and 10^4 hours with
junction temperatures of 180°C and 230°C, respectively. Our own independent
work on multilayer (Pt-Ti-Au) Schottky barrier metallization for low-high-low
Read diodes indicates that lifetimes in excess of 10^6 hours are achieved at
junction temperatures of 200°C. In all cases, the limitation on lifetime occurs
because of the ongoing chemical reaction between the GaAs material and the
Schottky-barrier metallization. These results indicate that the high-power
four-mesa IMPATT diodes should not be a limiting factor in achieving a
5000 hour operating lifetime for the transmitter.

The present program included no diode development effort. The high-
power GaAs Read diodes required both for the transmitter and for the in-
cidental monthly diode deliveries were to be produced using existing tech-
nology, namely, that technology used during the previous program. This
technology, including material growth, diode fabrication, and diode eval-
uation, was described in the final report of the previous program. [3]

Material growth and diode fabrication procedures are continually
being refined in our laboratory as the result of a number of ongoing IMPATT
diode programs sponsored by Raytheon and by outside agencies. For this
reason, there are several differences between the diodes produced for this
program and those developed for the previous program. First, silicon
(as SiH_4) rather than sulfur (as H_2S) is used as the n-type dopant during
vapor phase growth of the GaAs epitaxial material. Silicon does not diffuse
as rapidly as sulfur in GaAs, and silicon doping allows more precise con-
trol of the doping profile. Also, silicon-doped buffer layers of lower

resistivity than those produced with sulfur doping can be obtained. This reduces the series resistance of any IMPATT diode and increases efficiency. Second, the doping profile specifications for the new diodes were refined based on experimental results obtained toward the end of the previous program. The changes involved an increase in electric field step and a decrease in drift region doping to raise the diode efficiency. Clearly, diode efficiencies of 25 to 30 percent, instead of 20 to 25 percent as typically obtained in previous work, would improve the overall transmitter efficiency. Third, a gold-germanium ohmic back contact has now been adopted as standard for all of our IMPATT diodes. This results in somewhat lower series resistance and higher efficiency, and somewhat more repeatable diode characteristics than could be achieved with the previous chrome-gold back contact. Finally, by comparison of the older C-band diodes with X-band diodes produced for another program, it became evident that the junction areas of the early C-band diodes were quite small compared with the maximum which could be tolerated in typical circuits. Accordingly, the diameters of the mesas on the four-mesa chips were increased to 10 mils from the 7 - 8 mils used previously. This change permitted power outputs of 15 W (nominal) from each diode package. A four-diode output stage, having simpler bias and RF circuitry than would be used in the five-diode output stage originally proposed, then became possible.

3.2.1.2 Diode fabrication and test for the present program

The general form of the low-high-low doping profile used in the high-power diodes produced for this program is shown in Fig. 4, along with the electric field profile present in the reverse-biased diode. Notation for Fig. 4 is explained in Table 3. The doping profile specifications to which the material was grown are shown in Table 4. The initial specifications were refined during the course of the work in order to bring the optimum operating frequencies closer to 5 GHz.

An epitaxial reactor was calibrated for the growth of C-band wafers, and the first wafer meeting the specifications of Table 4 was delivered
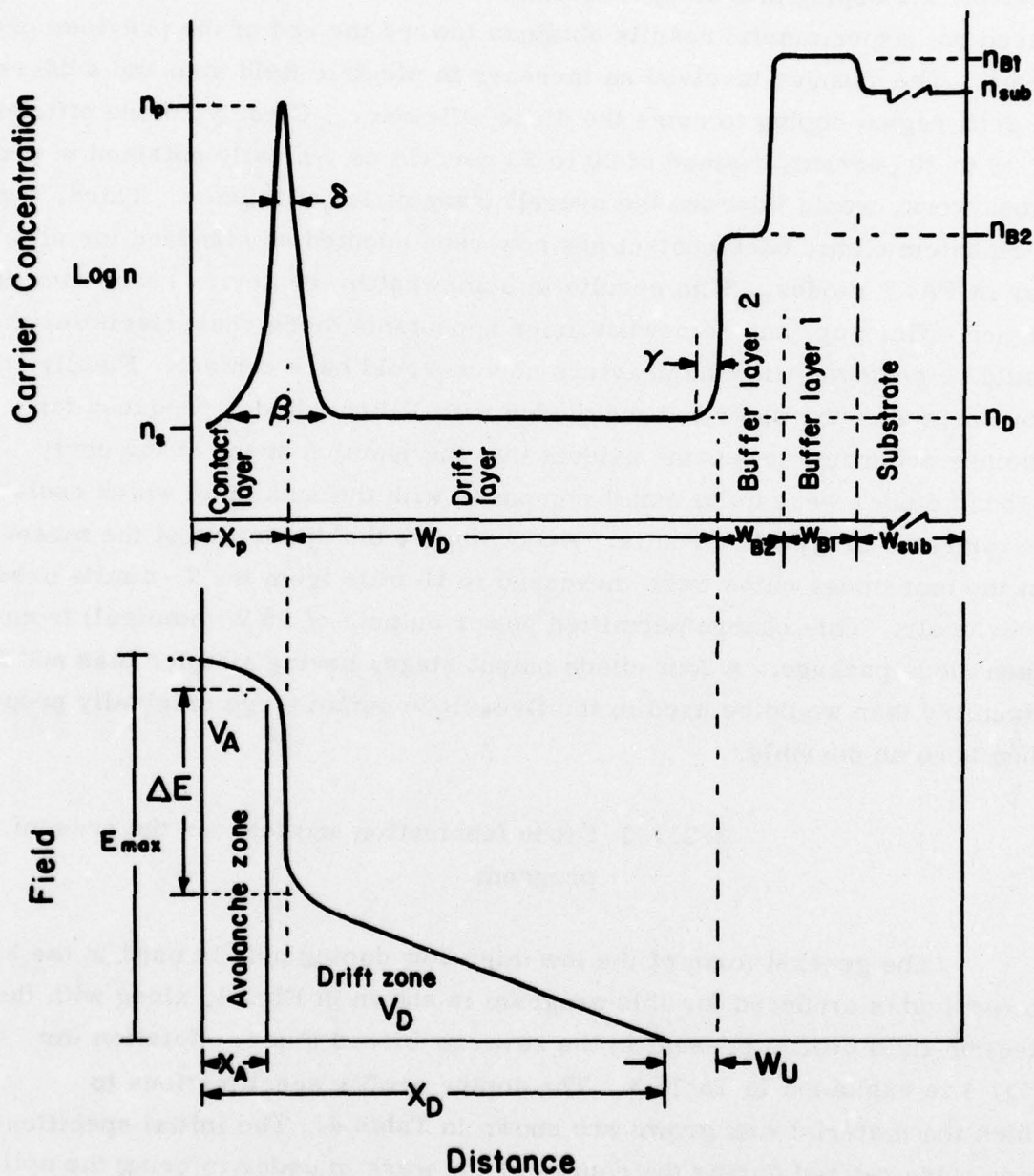
Figure 4   Schematic Representation of the Donor-Density
Profile and the Electric-Field Profile of a Stepped-
Field (LHL) Read Diode. The notation used in this
figure is identified in Table 3.

TABLE 3

IDENTIFICATION OF NOTATION

W_{B1} Thickness of epitaxial buffer layer 1 as grown

W_{B2} Thickness of epitaxial buffer layer 2 as grown

W_C Thickness of epitaxial contact layer from spike to surface as grown

W_D Thickness of epitaxial drift layer from spike to buffer layer 2 as grown

W_{sub} Thickness of substrate material

W_u Width of undepleted epi zone in diode

X_A Depth of avalanche zone-distance in diode at breakdown measured from junction, or Schottky barrier

X_D Total depletion depth-distance in diode at breakdown measured from junction, or Schottky barrier

X_p Spike depth-distance in diode measured from junction, or Schottky barrier

E_D Electric field at beginning of the linear field portion of the drift zone in diode at breakdown

E_{max} Electric field at junction or Schottky barrier in diode at breakdown

ΔE Field step occurring across doping spike in diode at breakdown

n_{B1} Electron concentration of buffer layer 1

n_{B2} Electron concentration of buffer layer 2

n_D or n_2 Electron concentration of drift layer

n_p Measured electron concentration at peak of doping spike

n_{sub} Electron concentration of substrate

n_S or n_1 Electron concentration measured with zero bias applied to junction or Schottky barrier

β Base width of doping spike measured at 1.5 n_D

δ Full width of doping spike measured at half height (0.5 n_p)

γ Width of doping transition from drift layer to buffer layer 2

TABLE 4

INITIAL SPECIFICATIONS FOR 5 GHz READ WAFERS

W_{sub} ~400 micrometers $n_{sub} > 1 \times 10^{18}$ cm^{-3}
             (thinned in processing)

W_{B1} 5-10 micrometers $n_{B1} \sim 2 \times 10^{18}$ cm^{-3}

W_{B2} ~1.5 micrometers $n_{B2} \sim 2 \times 10^{16}$ cm^{-3}

W_D 8-10 micrometers $n_D \sim 2.5 \times 10^{15}$ cm^{-3}
             (preferably ~9)

X_p ~0.25 micrometers $n_s < 2 \times 10^{16}$ cm^{-3}

δ ~0.04 micrometers $n_p \sim 4.8 \times 10^{17}$ cm^{-3}

ΔE ~3.3 $\times 10^5$ V/cm

CHANGES IMPLEMENTED IN THE SECOND GROWTH SERIES

W_D = 9-11 micrometers (preferably ~10)

X_p = 0.26 micrometers

ΔE = 3.0-3.3 $\times 10^5$ V/cm

n_D = 2.0-2.4 $\times 10^{15}$ cm^{-3}

(Other parameters remain unchanged)

24

during April 1976. A total of six wafers was delivered during the April-through-June time period. Diode processing was started on these wafers as they were received. Toward the latter portion of the growth series, recurring problems with poor wafer surfaces were encountered. These difficulties were eventually traced to a small leak in the reactor tube, which was repaired. This first reactor was then dedicated to other programs. A second epitaxial reactor was calibrated for C-band growth during September 1976. This reactor, working to the modified specifications shown in Table 4, was used to grow the remaining wafers required for the program during October 1976. Six epitaxial wafers meeting the modified specifications were delivered for diode processing during October 1976. In addition, two wafers from this second growth series having characteristics deviating slightly from the specification were processed in March 1977 to provide a back-up supply of diodes for development of the transmitter output stage.

A four-mesa plated-heat-sink chip typical of those used in the diodes is shown in Fig. 5.   The pictured chip has ten-mil-diameter mesas mounted on 20-mil centers. The completed chip is approximately 40 mils square. The chips were soldered into microwave packages, and gold mesh was used to contact the mesa tops as is shown in the cut-away view of Fig. 6. Lids were welded on the packages to complete a hermetic seal of each diode. An outline drawing of the package is included in Fig. 6 to indicate the size of the finished device.

Table 5 shows the best results obtained in CW oscillator tests of all diode lots fabricated for this program. With one exception, lot 951, the diodes used four-mesa PHS chips with 10-mil-diameter mesas. Thermal resistances were typically 4°C/W, and maximum powers were generally achieved with junction temperatures in the 200 to 220°C range. Where "best power" and "best efficiency" occurred under substantially different conditions, both results are listed. "Top hat" oscillators of the type shown in Fig. 7, constructed in WR-137 and WR-187 waveguide sections, were used in this test series.

Figure 5   Scanning Electron Micrograph of a Four-Mesa PHS Diode Chip.

TABLE 5

BEST RESULTS IN CW OSCILLATOR TESTS

Diode Lot	Wafer	P_o(W)	f (GHz)	η (%)
(First Series)				
904	81905	12.8	6.510	23.3
905	81907	14.9	5.835	26.2
906	81908	15.4	5.735	26.9
907	81910	19.2	5.201	28.1
909	81915	21.9	4.847	29.7
910	81934	17.6	4.929	29.8
(Second Series)				
946	41334A	17.5	5.024	25.1
947	41336B	16.9	4.964	26.0
948	41337A	11.9	5.747	22.9
949	41337B	15.5	5.215	27.9
951[†]	41338A	17.0	6.190	26.1
952	41338B	14.8	5.212	26.1
		13.3	5.197	27.3
970	41337C[*]	14.1	5.207	24.5
971	41338C[*]	15.3	5.164	26.5
		11.7	5.251	27.5

[*] Wafers not conforming to specifications (low Δ E).

[†] 12-mil mesas, etched in package.

27

PBN-77-699
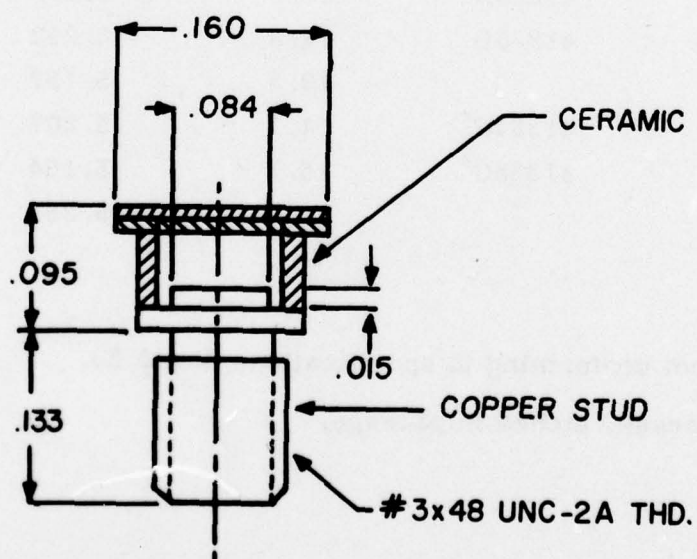
Figure 6   Photograph and Outline Drawing of Packaged Diode.

28
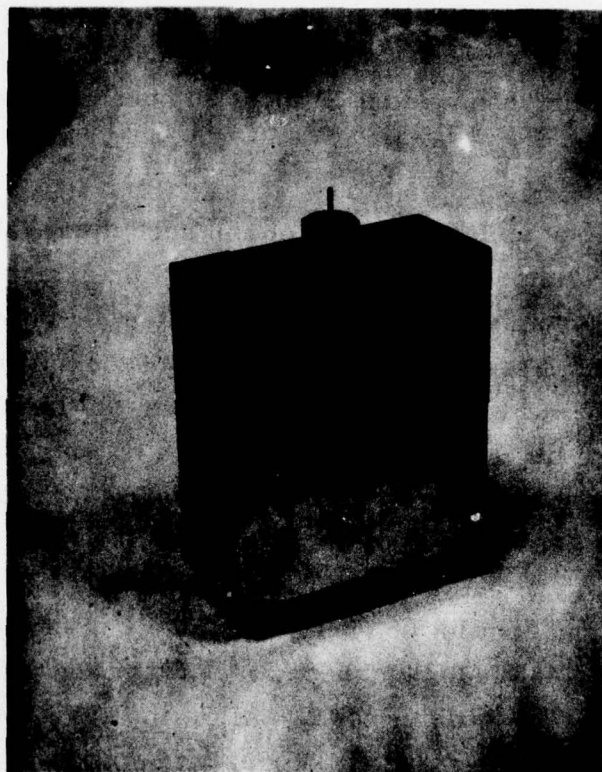
Figure 7   C-Band Top-Hat Oscillator.

The test results indicate that the basic design of the 15 W 5 GHz diode is well in hand. Ten of the twelve wafers meeting the growth specifications in use produced units which reached or exceeded the 15-W (nominal) power output level. The efficiencies obtained from the 15 W units all fell in the 25 - 30 percent range. Wafers grown in the first series tended to produce diodes with optimum operating frequencies above 5 GHz. Only three of the first six wafers produced units with optimum frequencies in the 4.8 - 5.2 GHz range. After the profile modifications were implemented, six of eight wafers in the second series produced units in this range. Individual diodes usually have - 1 dB operating bandwidths of about 20 percent centered on the optimum frequency.

Given proper epitaxial material and good diode fabrication techniques, the yield of "15 W" diodes can be quite high. For example, of one group of 26 diodes fabricated from wafer 81910 (Lot 907) toward the end of the program, 25 units survived RF testing. Power outputs of the survivors ranged from 17 to 19 watts. More typically, about 50 percent of the diodes received for evaluation survive basic RF tests. There was no exceptional problem in producing sufficient quantities of 15 W diodes with similar characteristics for use in the transmitter output stage.

The results from lot 909 are particularly interesting. Through the end of September, 46 diodes had been made from the wafer. Of these, sixteen survived CW oscillator tests. All of the survivors produced more than 18-W CW output. Also, eight diodes of the sixteen produced more than 20-W CW output. Thus, while the 20-W diode must still be regarded as an experimental device, it is more than a one-of-a-kind accident.

The fabrication of substantial quantities of diodes with power outputs in excess of 20 W CW at 5 GHz now appears to be possible. This is demonstrated by the the test results from lot 951. This lot of diodes was fabricated with four 12-mil-diameter mesas on each 50×50-mil PHS chip. Typical thermal resistances were 3.0 - 3.5°C/W. The total junction area was too large for efficient operation at the 6.2-GHz frequency characteristic of the doping profile in this particular wafer. Junction area was reduced

by in-package etching, and the tabulated performance was finally obtained from a diode having a junction capacitance of 5 pF at breakdown. Scaling this result to 5 GHz, one finds that it should be possible to tolerate a junction capacitance of at least 6.2 pF before the diode impedance becomes too low for efficient operation. Since the best 5 GHz result (~ 21.9 W CW output) from diodes in lot 909 was obtained with a junction capacitance of only 3.4 pF, a substantial increase in the area of the 5-GHz diodes should be possible. If efficiency is maintained, a total junction area sufficient to produce 35 - 40 W CW output from a single package should be useable. This would permit design of a two-diode 40-W transmitter output stage that would operate very conservatively. However, the present four-mesa structure would be thermally limited before 35 - 40 W could be obtained from one package. A larger diode package with a larger number of mesas would be required to achieve the maximum potential power output.

3.2.2 The power-combining circuit

3.2.2.1 General circuit types and operating modes

While circuits for combining the power outputs of microwave diodes may take a number of different forms, they usually belong to one of two general classes, the tandem and parallel power combiners. These two types are illustrated in Fig. 8. The tandem power-combining circuit is a succession of low-gain amplifier or injection-locked oscillator stages containing equivalent IMPATT diodes. The earlier stages in the chain are adjusted for higher gain and the later stages for lower gain so that each stage contributes to the ongoing signal the maximum power which its diode can produce. This type of combiner tends to be severely limited by circuit losses, particularly in the later stages, where the power consumed by a fraction of a decibel of loss can approach the power contribution of the diode. Because of this loss limitation, the tandem power combiner was not selected for use in the deliverable transmitter. The parallel power combiner is a single reflection amplifier or injection-locked oscillator stage

31

Tandem Combiner
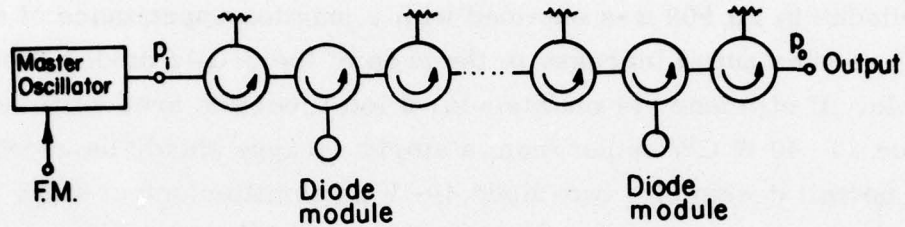
Parallel Combiner
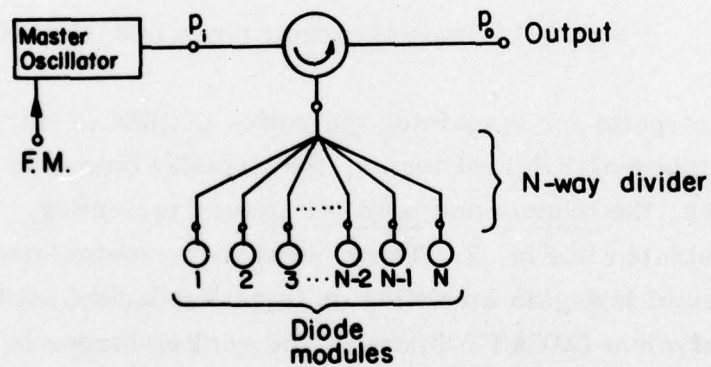
Figure 8   Two Basic Types of Power Combiner. Each
            is shown in conjunction with a low-power
            master oscillator having FM capability to
            produce a complete transmitter.

32

with multiple active elements. Circuit losses tend to accumulate less rapidly in this type of circuit than they do in the tandem power combiner. The power-combining circuits considered for use in the deliverable transmitter were all of the parallel type.

There are two general types among the parallel power combiners. In the resonant power combiner, there is a single resonator to which an ensemble of diodes is coupled and from which the output power is extracted. In the nonresonant power combiner, an ensemble of oscillators, each with its own resonator, is locked to a common reference signal and coupled to a single output port through a broad-bandwidth multiport hybrid circuit. Both resonant and nonresonant power combiners were considered for use in the deliverable transmitter.

3.2.2.2 Circuit requirements and performance limitations

There are two principal factors which limit the performance of a power-combining circuit. The first is circuit loss which tends to reduce overall efficiency. The second is the presence of undesired modes of oscillation in the circuit which may be caused by insufficient diode-to-diode isolation in a nonresonant power combiner or by the presence of multiple resonances in a resonant power combiner. These limiting factors can be described in terms of the model shown in Fig. 9.

The circuit efficiency is a useful quantity for comparing the relative performance of different power combiners. This is defined as the net power contributed by the power combiner divided by the total power available from the diodes. With reference to Fig. 9, one can write $\eta = (P_o - P_i) / (NP_D)$. The circuit efficiency depends on the circuit loss and on the gain at which the power-combined stage operates. The special case of a power-combined, free-running oscillator is treated by allowing the stage gain to become arbitrarily large. Circuit efficiency as a function of loss with diode gain as a parameter is shown in Fig. 10.

33
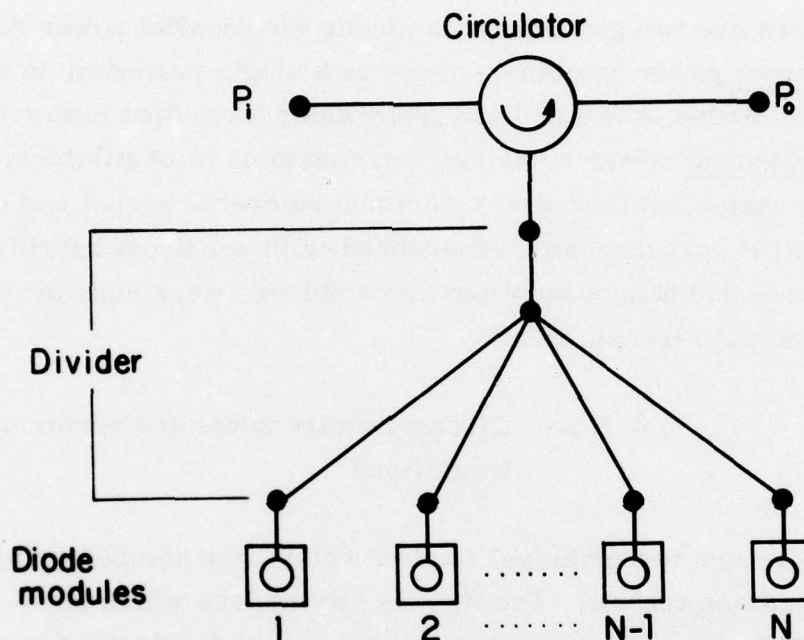
Figure 9   Model Used for Analyzing the Limitations of the Microwave Power Combiner. N identical diode modules, each capable of producing a power output P_D, are combined in a single stage.

$$\eta = \frac{G \cdot 10^{-a/10} - 10^{a/10}}{G - 1}$$

G value in ( )
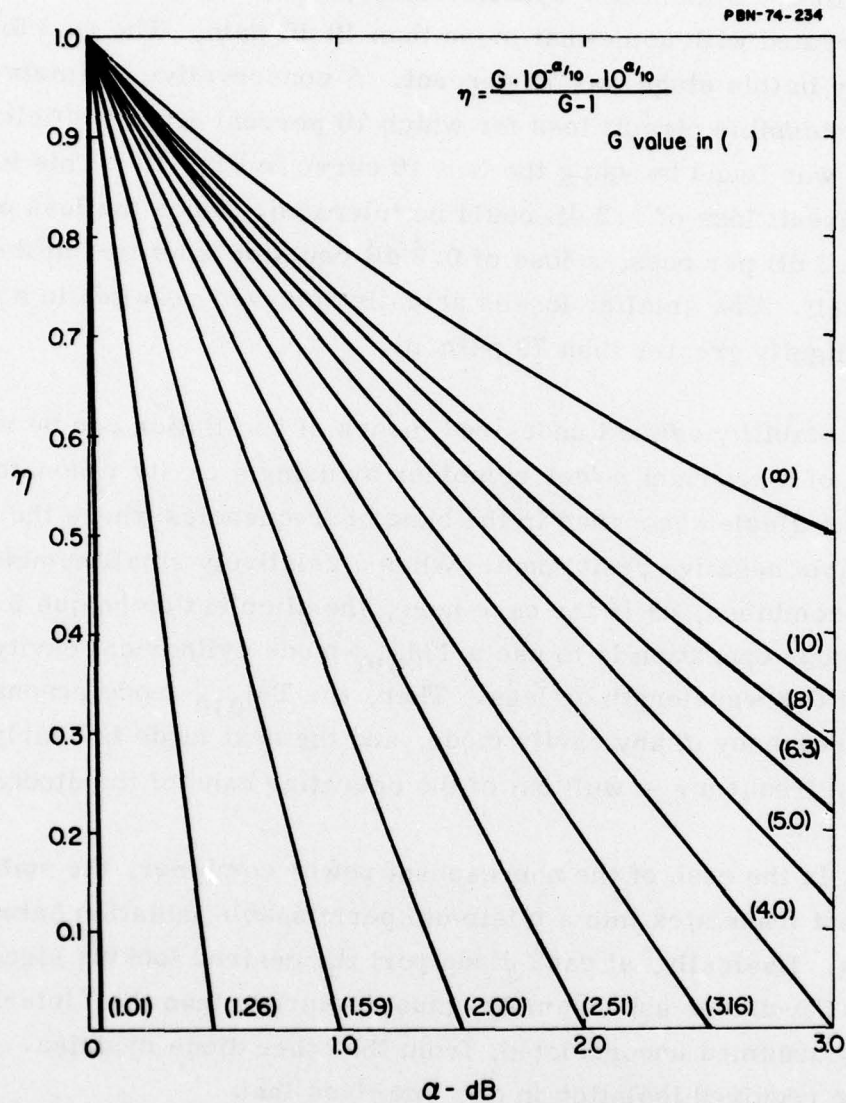
Figure 10   Circuit Efficiency as a Function of Circuit Loss with
Diode Gain as a Parameter. α is the total power loss,
expressed in dB, between the output port and the diode
ports. The diode gain G is the square of the magnitude
of the reflection coefficient at the diode ports.

35

In the transmitter system description presented in Sec. 2, the output stage operated with somewhat more than 10 dB gain. The goal for the circuit efficiency in this stage was 70 percent. A conservative estimate of the maximum permissible circuit loss for which 70 percent circuit efficiency could be achieved was found by using the G = 10 curve in Fig. 10. This indicated that a total circuit loss of 1.2 dB could be tolerated. Since the loss of the circulator was ~ 0.3 dB per pass, a loss of 0.9 dB could be tolerated in the power combiner itself. The smaller losses actually achieved resulted in a circuit efficiency slightly greater than 70 percent.

Stability against undesired modes of oscillation can be assured in the case of a resonant power combiner by using a cavity resonator which has only a single resonance in the band of frequencies where the diodes have appreciable negative resistance. When a relatively small number of diodes is to be combined, as is the case here, the simplest technique for realizing single-mode operation is to use a TM_{010}-mode cylindrical cavity with a height of 0.3 wavelength or less. Then, the TM_{010}-mode resonance has the lowest frequency of any cavity mode, and the next mode is nearly 40 percent higher in frequency — well out of the operating band of the diodes.

In the case of the nonresonant power combiner, the stability requirement translates into a minimum permissable isolation between diode modules. Basically, at each diode port the desired locking signal, supplied by the VCO-driver subassembly, must be larger than the "interfering" signals, assumed uncorrelated, from the other diode modules. Defining α_i as the required isolation in dB, one finds that:

$$(P_i / N) \ 10^{-(\alpha \ / \ 10)} > (N - 1) P_D \cdot 10^{-(\alpha_i / \ 10)}$$

is the condition for locking in the correct mode.

For the conditions in the deliverable transmitter, P_i = 3.2 W (accounting for loss in the interstage isolator), N = 4, α ~ 1, P_D = 12.5 W, and the minimum required isolation is ~ 17 dB. Measured isolation, to be

36

reported later in Sec. 3, was typically 24 - 28 dB at 5 GHz. This provided an ample margin of stability against locking in the incorrect mode.

3.2.2.3 Circuit designs for the transmitter output stage

3.2.2.3.1 Dielectrically loaded cavity – background, design, and supporting experiments

During the previous program, six high-power GaAs IMPATT diodes were successfully combined in a resonant cavity circuit. When operated as a free-running oscillator, the circuit produced 62-W CW output at 5.120 GHz with 20.9 percent DC-to-RF conversion efficiency. It was successfully operated as an injection-locked oscillator with nearly 23 dB of locking gain.[3]

This previous cavity circuit design was too large and heavy to use in the deliverable transmitter. One way to reduce the size of the circuit while retaining its high efficiency and single-mode characteristics would be to fill the cavity with dielectric material. When material of dielectric constant $K \sim 4$ is used, the complete cavity circuit can be reduced to a cylindrical volume 1.7 inches in diameter and 3 inches long. The dielectrically loaded cavity is thus one form in which the new transmitter output stage could have been realized.

Figure 11 is a schematic representation of the transmitter output stage using the dielectrically loaded cavity. Four high-power GaAs Read IMPATT diodes are coupled to a common TM_{010}-mode cavity. Except for a small hole on axis and the cutouts required to pass the coaxial lines, the cavity is filled with dielectric. STYCAST 36 DA, manufactured by Emerson and Cuming, Inc., appears to be a suitable dielectric. This material has a dielectric constant of 3.7 and a loss tangent of 0.0007. The cavity frequency is controlled by the dielectric rod tuner, and output coupling is adjusted by

Top section

Cavity shell

Diode line

Tuner/Output

Cavity I.D. ~ 0.8"

Coaxial output

Bias input

Termination

Cavity shell

Output coupling probe

Diode line

Dieletric loading K ~ 4

Slug transformer

Diode

Cavity height ~0.4"

Diode mounting plug

Dielectric rod tuner K ~ 10

Front section
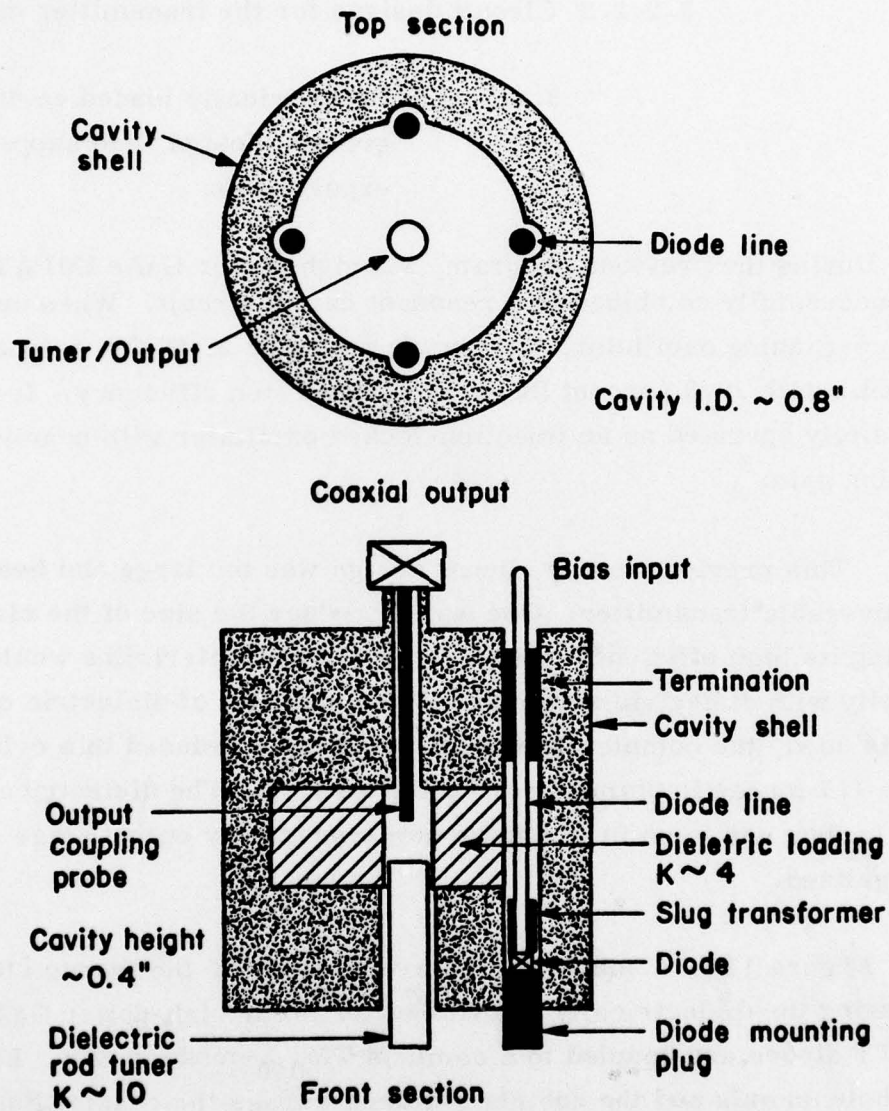
Figure 11   Schematic Representation of a Power Output Stage Using a Dielectrically-Loaded Cavity-Type Power Combiner.

moving the coaxial probe axially. Coupling of the diodes to the cavity is adjusted by changing the slug transformers and by moving the diodes axially. The required DC bias is supplied to the individual diodes along the coaxial center conductors which pass through lossy terminations in the top of the cavity structure. Cooling of the cavity can be provided either by including an appropriate water jacket or by mounting the cavity against a cold plate.

The operating principles for the resonant cavity power combiner are now fairly well understood and have been described elsewhere.[3] The chief difference which will occur with the dielectric-filled cavity is a reduction in unloaded Q from ~5000 to ~1400 because of the losses in the STYCAST material. This will result in somewhat lower circuit efficiency and less freedom in the choise of cavity-coupling adjustments. However, the previous circuit operated with a loaded Q of ~100, less than 10 percent of the reduced unloaded Q, so less than 10 percent of the available power should be consumed in dielectric losses. This should still permit a circuit efficiency of at least 80 percent, since the full-size unfilled cavity had a circuit efficiency of ~90 percent.

The cavity circuit could have met the needs of this program and had a high probability of initial success based on our previous experience. However, it involved complicated machining and would have been more expensive in production than the microstrip circuits to be described in the following section. For this reason, it was considered a back-up design to be pursued only if the microstrip circuit development encountered severe difficulties.

During the current program, diodes from lots 907, 909, 910, and 946 were operated in the original resonant cavity circuit, which is shown in Fig. 17. Both single-diode and multiple-diode (power combined) tests were included. In single-diode qualification tests, diodes typically produced power outputs within 0.5 dB of those originally obtained in the top-hat oscillator circuit. The multiple-diode tests achieved what was at the time the highest CW power reported from an IMPATT diode source in the 5 GHz region. There were two reasons for these tests. First, they provided a demonstration that the circuit conditions necessary for efficient operation

39
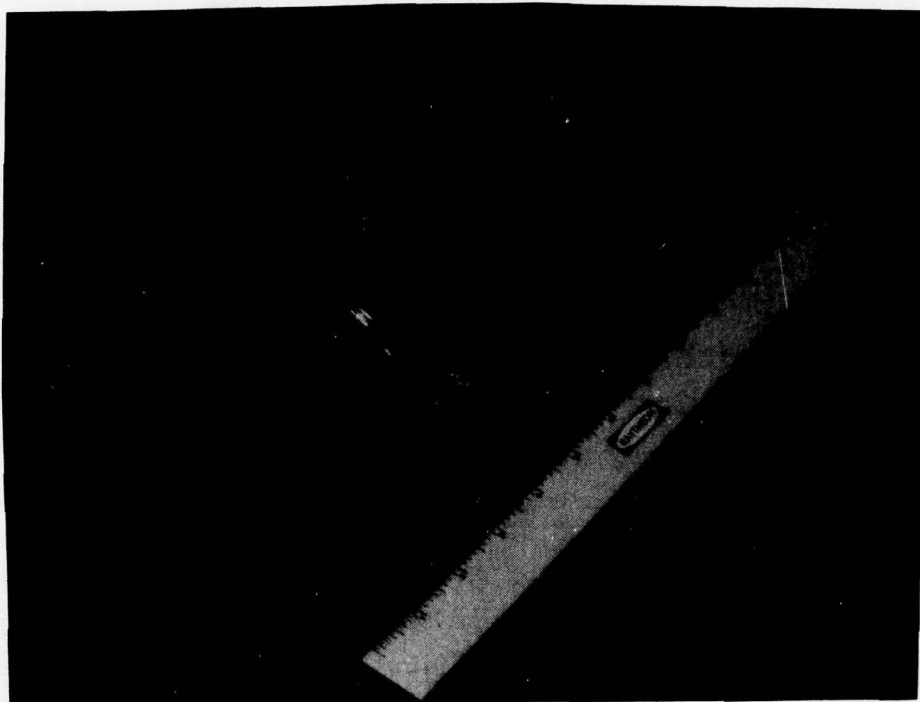
Figure 12   Photograph of Resonant Cavity Power Combiner.

of the new large-area diodes, both singly and in combination, could be achieved within the range of adjustments possible in a cavity circuit. Second, the cavity circuit provided a vehicle in which large-signal impedance measurements of the diodes could be made. The data obtained in these measurements were necessary for the design of the oscillator modules described later in this report.

Successful operation of the multiple-diode cavity circuit requires an organized tuning procedure. One such procedure was described in the final report of the previous program.[3] The operating voltages of the diodes and their variation with changes in the resonant frequency of the cavity provide a good indicator for the approach to correct tuning. This is shown in Figs. 13 through 15. First, the "correct" operating voltage for maximum efficiency at a given operating current is determined by independent tests in the top-hat oscillator. The diode is then operated in the cavity circuit. The diode voltage, during operation from a constant-current bias source, varies as shown in Fig. 13 when the resonant frequency of the cavity is changed by moving the dielectric rod tuner. If the voltage at the frequency of maximum power output is higher than the "correct" value, the real part of the impedance being presented to the diode is too large, and the coupling between the cavity and the external load must be reduced or the slug transformer diameter increased. Too low a voltage requires the opposite action. The frequency at which maximum power occurs is controlled primarily by the imaginary part of the impedance presented to the diode. This frequency is raised or lowered as required by shortening or lengthening, respectively, the slug transformer or the coaxial line between the cavity and the diode.

When six diodes are installed in the cavity, the individual diode operating voltages vary with cavity tuning in the same general fashion as shown in Fig. 13. Proper tuning has each diode operating at its "correct" voltage at the frequency of maximum output for the ensemble, and all voltage minima will occur together. Figure 14 shows a nonoptimum tuning condition where the spread of operating voltages and center frequencies for the

41
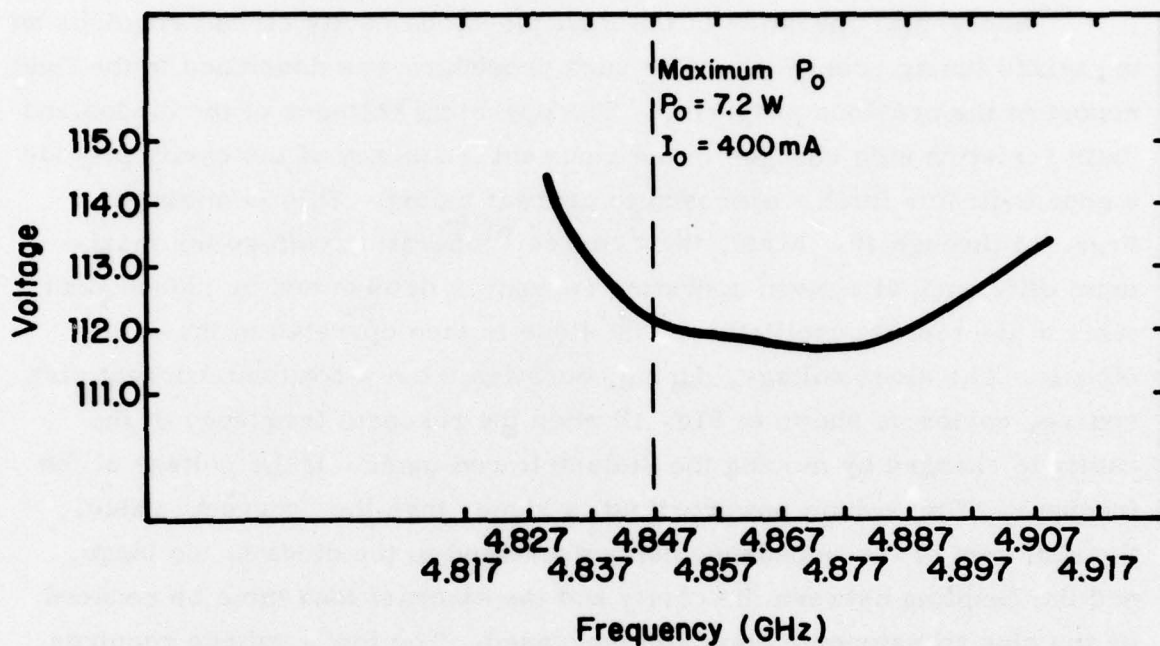
Figure 13   Operating Voltage as a Function of Frequency under Constant Bias Current Conditions for a Single Diode in the Resonant Cavity Power Combiner. Frequency adjustment was made using only the dielectric rod tuner.

42
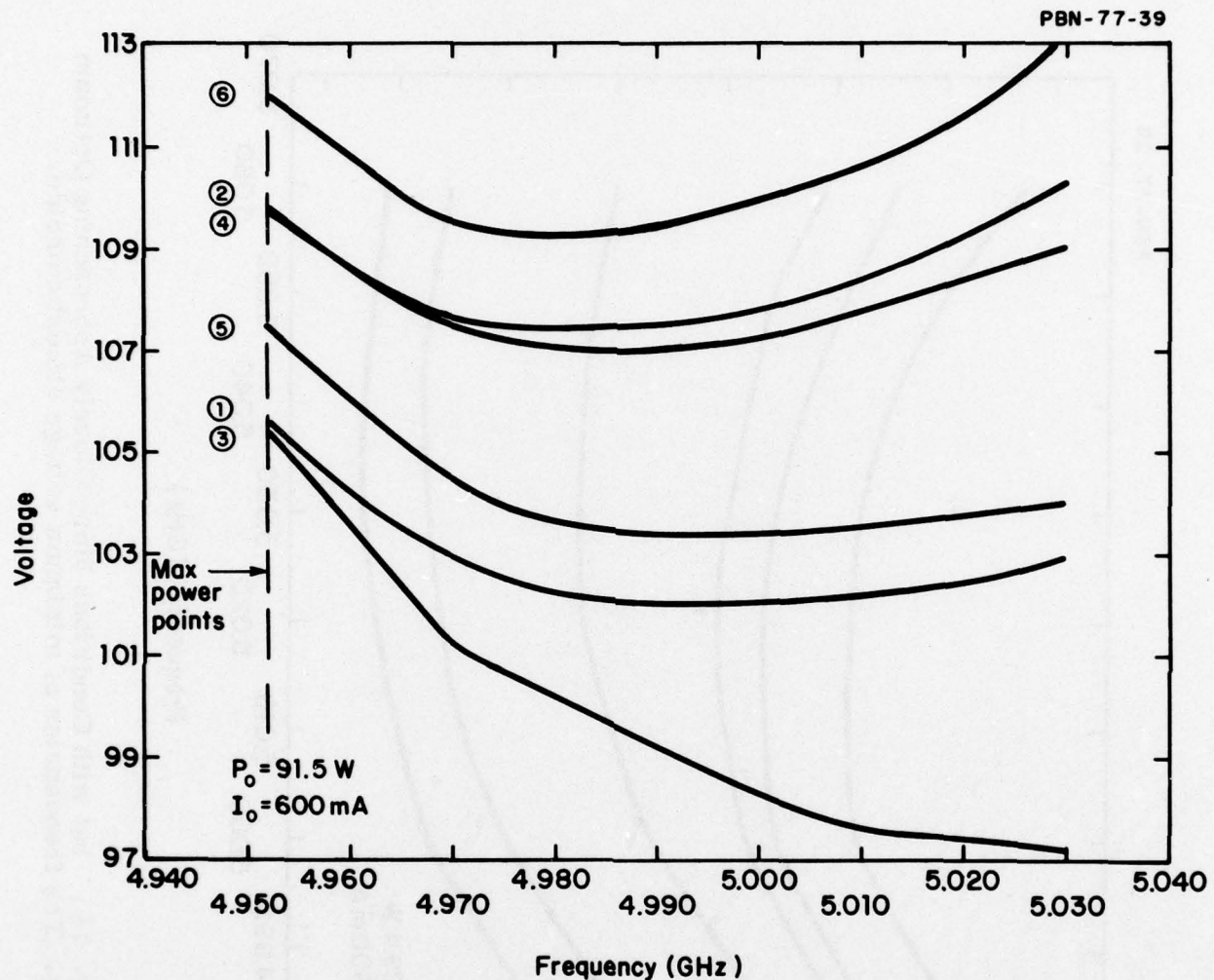
Figure 14   Operating Voltages as Functions of Frequency for Six Diodes in the Resonant Cavity Power Combiner under Conditions of Constant Bias Current. Only the dielectric rod tuner was adjusted to obtain the curves. Divergence of operating voltages and of the frequencies for minimum voltage indicates improper tuning.
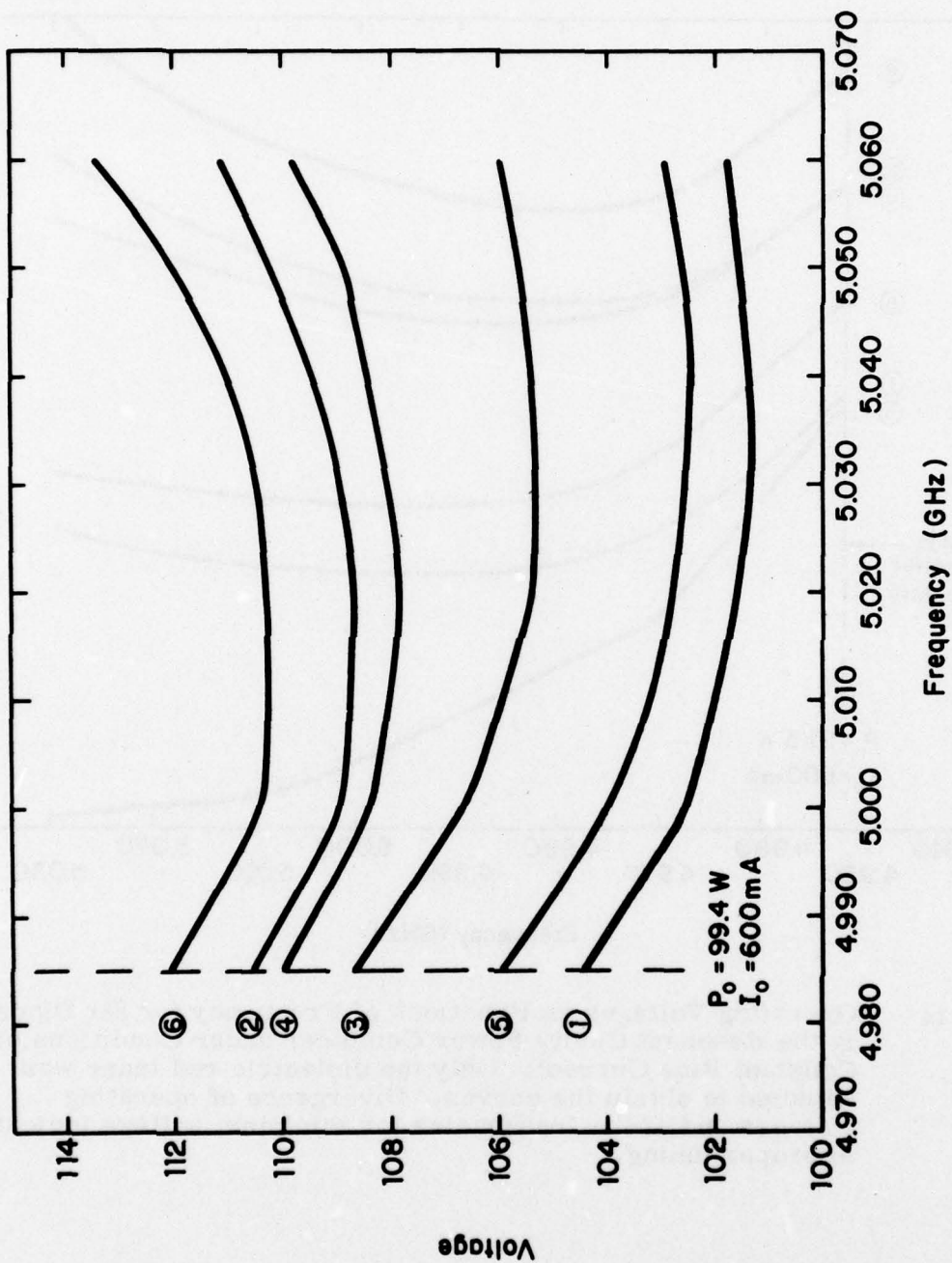
Figure 15   As Fig. 14 , but with Conditions More Closely Approaching Optimum Tuning. The frequencies of minimum voltage almost coincide.

44

individual diodes is excessive. A power output of 91.5 W was obtained in this case with the nominal 600 mA (per diode) operating current. Retuning produced the behavior shown in Fig. 15. Here the voltage minima for the six diodes coincide, and tracking of the voltages across the tuning range is improved. Power output with 600 mA bias current per diode was 99.4 W, a significant improvement. Still further refinement of the tuning could increase this power output slightly.

Figure 16 shows output power versus input power for 5 GHz (nominal) operation of the six-diode cavity under optimum tuning conditions. Six diodes from lot 909 were used, and the maximum bias current applied was ~ 750 mA per diode. Best CW power output was 120.6 W with 25.2 percent DC-to-RF conversion efficiency at 4.997 GHz. Best efficiency was 25.8 percent with 110.3 W CW output at 5.002 GHz. Operating junction temperatures were typically 220 - 240° at a maximum power output. However, since the overall efficiency of the circuit was virtually constant at 25 percent from 80 to 120 W CW output, power could be reduced to lower the junction temperature and enhance diode life with no sacrifice in overall efficiency. The combining efficiency of the cavity circuit in these tests was 87 percent.

3.2.2.3.2   Nonresonant power combiners

3.2.2.3.2.1 Circuit types

Nonresonant power combiners can take one of several forms. These forms can usually be divided into two broad classes. In the first, the division of RF power from the output port back to the diode modules is accomplished by cascading dividers, each of which has a relatively small number of ports. In the second class, the division is accomplished in a single multiport power divider/combiner. These classes are illustrated in Fig. 17.
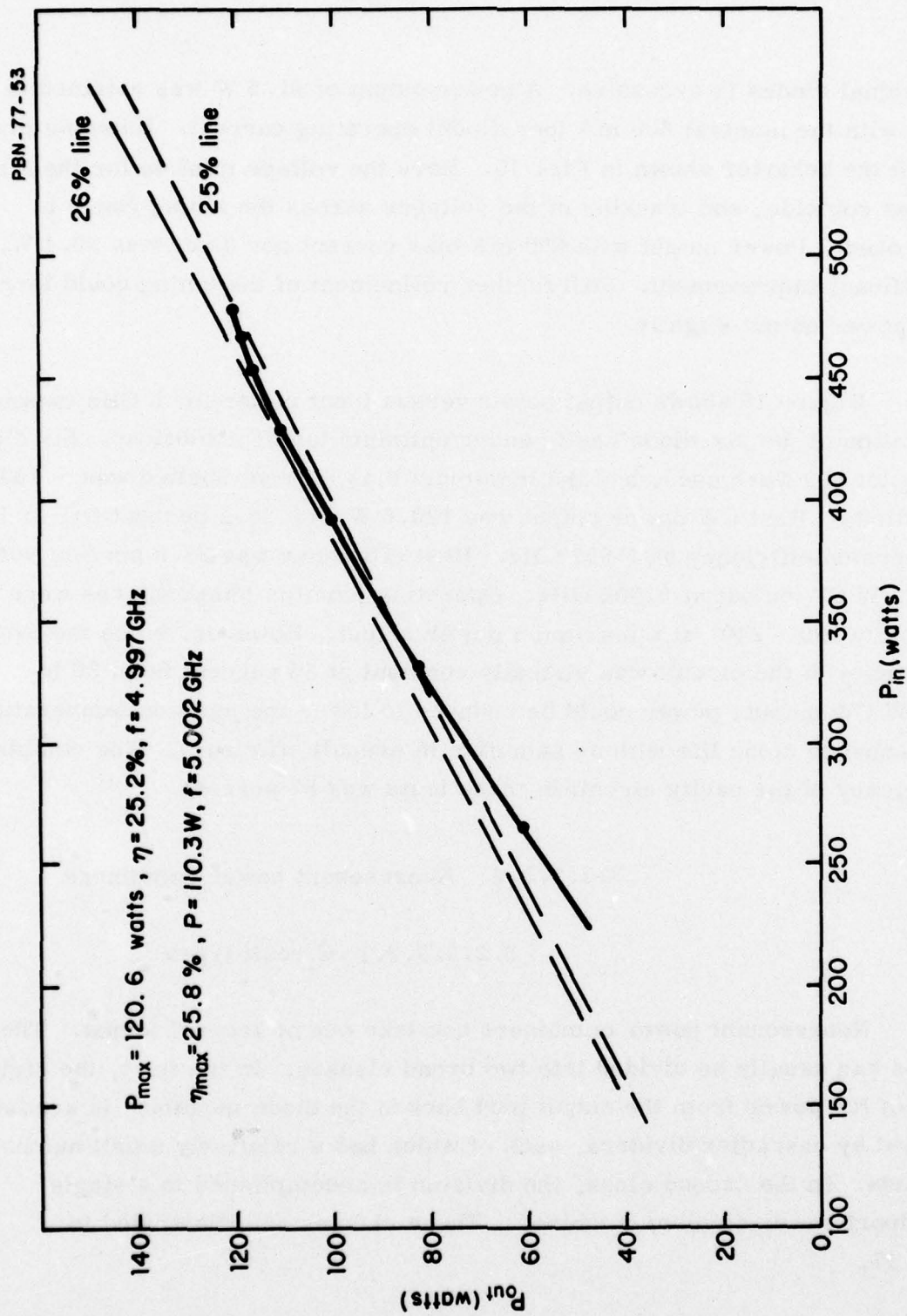
Figure 16   RF Power Output as a Function of DC Power Input for the 6-Diode Resonant Cavity Power Combiner. Efficiency is relatively constant from 80 to 120 W output.

OUTPUT

DIODE
MODULES

CASCADE OF 3-dB HYBRIDS

OUTPUT

DIODE
MODULES

SINGLE-LEVEL N-WAY POWER DIVIDER/COMBINER
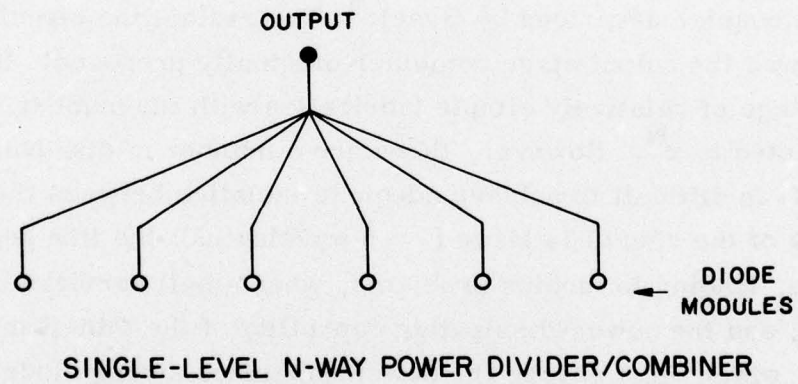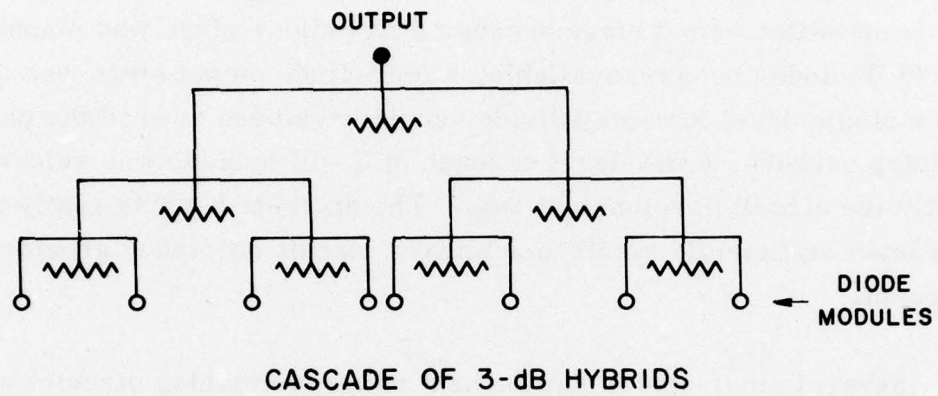
Figure 17   The Original Cavity-Type Power Combiner.

The cascade of 3-dB hybrids allows the combination of 2^N diodes, where N is the number of levels in the cascade. Circuit losses tend to accumulate rapidly as the number of levels is increased. The practical limit for this type of circuit is reached when 8 or perhaps 16 diodes are combined. Initially, cascades of 3-dB hybrids were not considered for use in the transmitter output stage because a five-diode stage was planned. After 15 W diodes became available, a four-diode output stage was designed. While a single-level four-way divider could have been used in the power-combining network, a two-level cascade of 3-dB hybrids was selected to simplify the circuit development task. The discrete hybrids easily reached a loss level sufficiently small to achieve a circuit efficiency greater than 70 percent.

Several single-level nonresonant power-combining circuits were considered for use in the transmitter output stage. These include the radial line, or "rising sun," combiner, the Wilkinson coupler,[4] and a modified Wilkinson coupler described by Gysel.[5] The radial-line circuit, shown in Fig. 18, was the output stage combiner originally proposed. It has the advantage of relatively simple fabrication with the number of diode ports not restricted to 2^N. However, there are a number of disadvantages of the circuit. It is difficult to achieve adequate isolation between the diode ports; the radius of the circuit is large (~ 6 wavelenths); the line segments become quite wide, leading to moding problems, when small numbers of diodes are combined; and the power-dissipating capability of the thin-film resistive material, which must absorb the power unbalance among diode modules, is limited.

The Wilkinson and Gysel circuits are potentially more compact than the radial-line circuit, since they are composed of quarter-wavelength line segments. The arrangement of each circuit for the case of two output ports is shown in Fig. 19. Both can give adequate performance in terms of loss and isolation. However, the Gysel circuit offers one particular advantage where high-power diodes are to be combined. The terminating resistors, Z_T, which must dissipate any power unbalance between the

48
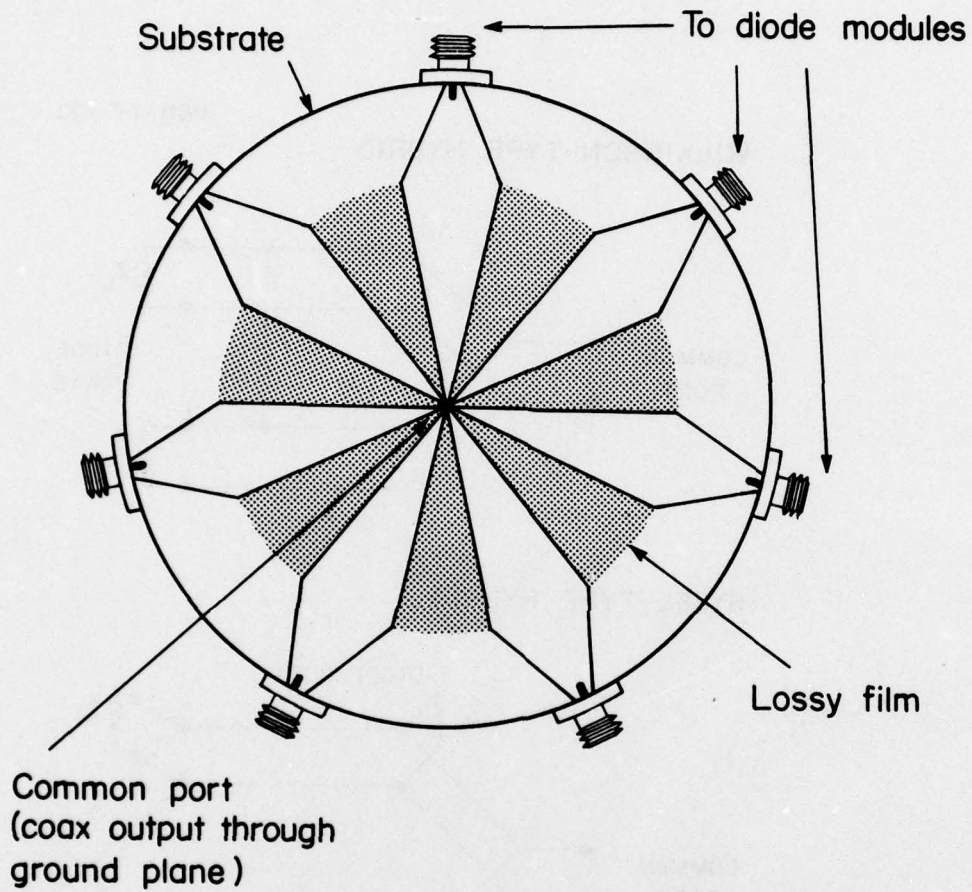
Figure 18   Microstrip N-Way Power Divider of the "Radial
             Line" Type.

WILKINSON-TYPE HYBRID
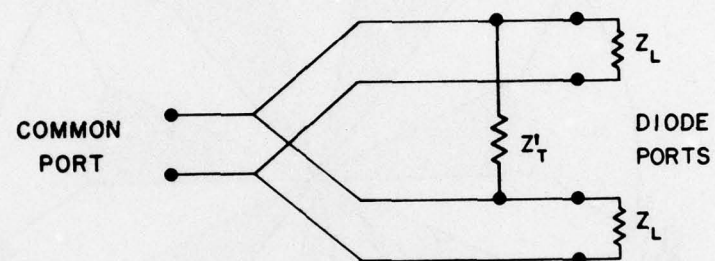
GYSEL-TYPE HYBRID
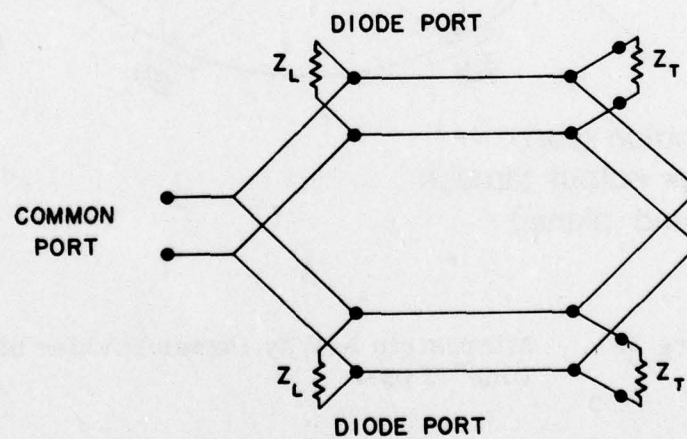
Figure 19   Transmission Line Configurations for
            Wilkinson and Gysel Hybrids with Two
            Output Ports.

diodes, are connected from line to ground. They can be high-power loads placed at the end of transmission line segments of characteristic impedance Z_T, thus removing them from the center of the circuit. Since power unbalances of several watts can occur in the event of a diode failure, high power loads are required in the present application. In the Wilkinson circuit, the termination is connected from line to line. Small chip resistors are commonly used for this purpose in microstrip circuits. These resistors have limited power-dissipating capability and would be unsuitable for the present application. Actual circuits of the Wilkinson and Gysel types are shown in Figs. 20 and 21 to demonstrate this difference in the terminations.

3.2.2.3.2.2 Transmission line types

The nonresonant power-combining circuits can be realized in any one of several different transmission line media. Those considered for use in the present program include ordinary microstrip line, suspended microstrip line, balanced stripline, and trapped inverted microstrip (TIM) line. Each has some particular advantages and disadvantages.

Conventional microstrip is the most commonly used of the transmission line types. There is a great deal of experience in its use, and fabrication costs are relatively low. The circuit is accessible for adjustment after fabrication. Microstrip has a number of disadvantages: losses are the highest of any of the types of line; fringing fields are fairly strong, making a high level of isolation difficult to obtain; and techniques normally used for tuning the circuit are inconvenient.

Suspended microstrip offers lower losses than conventional microstrip, and the air gap between the circuit and the ground plane permits convenient tuning, either with dielectric slugs or tuning screws inserted through the ground plane. Fabrication costs are similar to those of conventional microstrip, but fringing fields are greater, making good isolation more difficult to obtain.

51
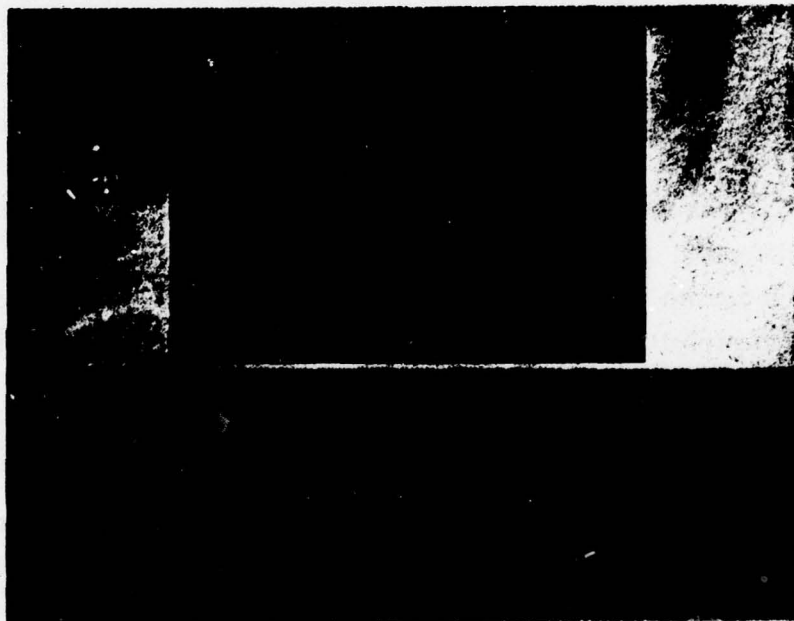
Figure 20   Wideband Two-Port Wilkinson Hybrid
in Microstrip Configuration. In this
double-section circuit, the terminations
are small chip resistors connected from
line to line.
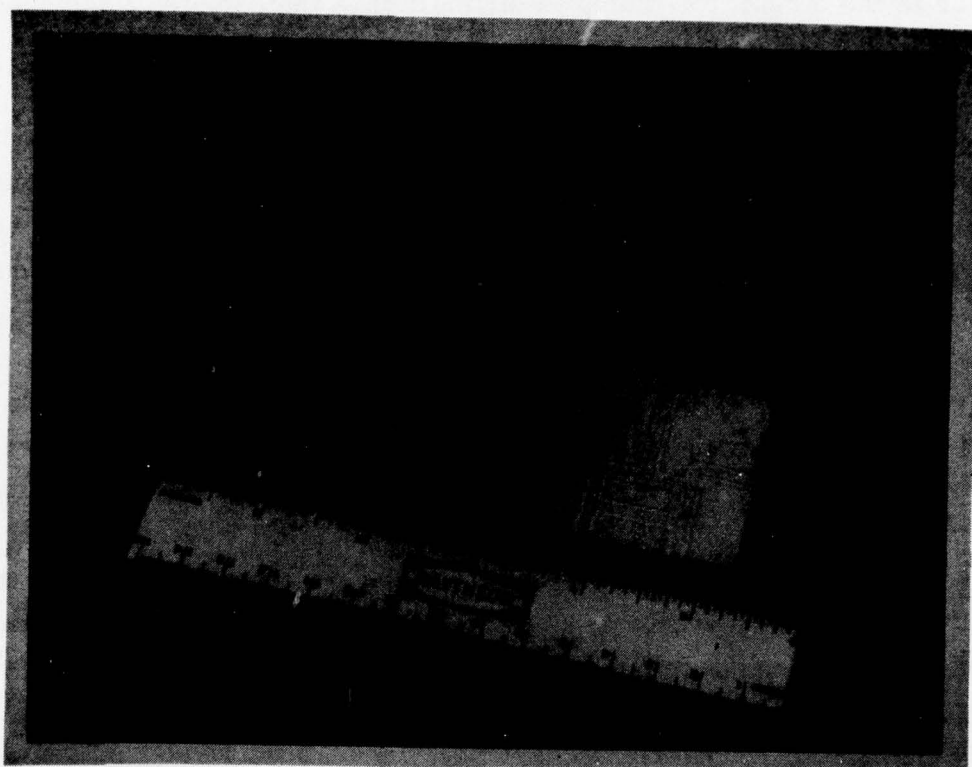
Figure 21   Photograph of Two-Port Gysel Circuit. Low-power
loads have been used for the internal terminations.

Balanced stripline with air dielectric offers the lowest loss and highest isolation of any of the transmission lines. Fabrication costs are relatively high because two ground plane structures are required. The access to the circuit for tuning is difficult once the assembly has been completed.

Trapped inverted microstrip (TIM) line, recently described by Buntschuh,[6] appeared to offer a number of advantages for the present program. Figure 22 shows the TIM line structure. This is basically a trough line with a dielectric overlay. Compared with conventional microstrip, dielectric losses are reduced because most of the wave energy propagates in the air gap. Conductor losses are reduced because line widths are greater at a given impedance level, thus reducing current density. Isolation is improved because fringing fields tend to be confined within the dielectri overlay near the channel. Tuning can be accomplished by inserting tuning screws into the channel through the ground plane or by sliding dielectric slugs along inside the channel. Fabrication costs are higher than those for conventional microstrip. The substrate processing is similar, but the ground plane is more difficult to produce because the channel must be formed under the circuit.

Results reported by Buntschuh show effective dielectric constants of about 3 - 3.5 for TIM lines using alumina substrates, which confirms that much of the wave energy propagates in the channel. Loss per wavelength is about 0.05 dB, approximately 60 to 70 percent of that present in conventional microstrip. Much of this loss is conductor loss. A further reduction could be achieved by using a Cr-Cu-Au metallization instead of the simpler Cr-Au system used in Buntschuh's tests.
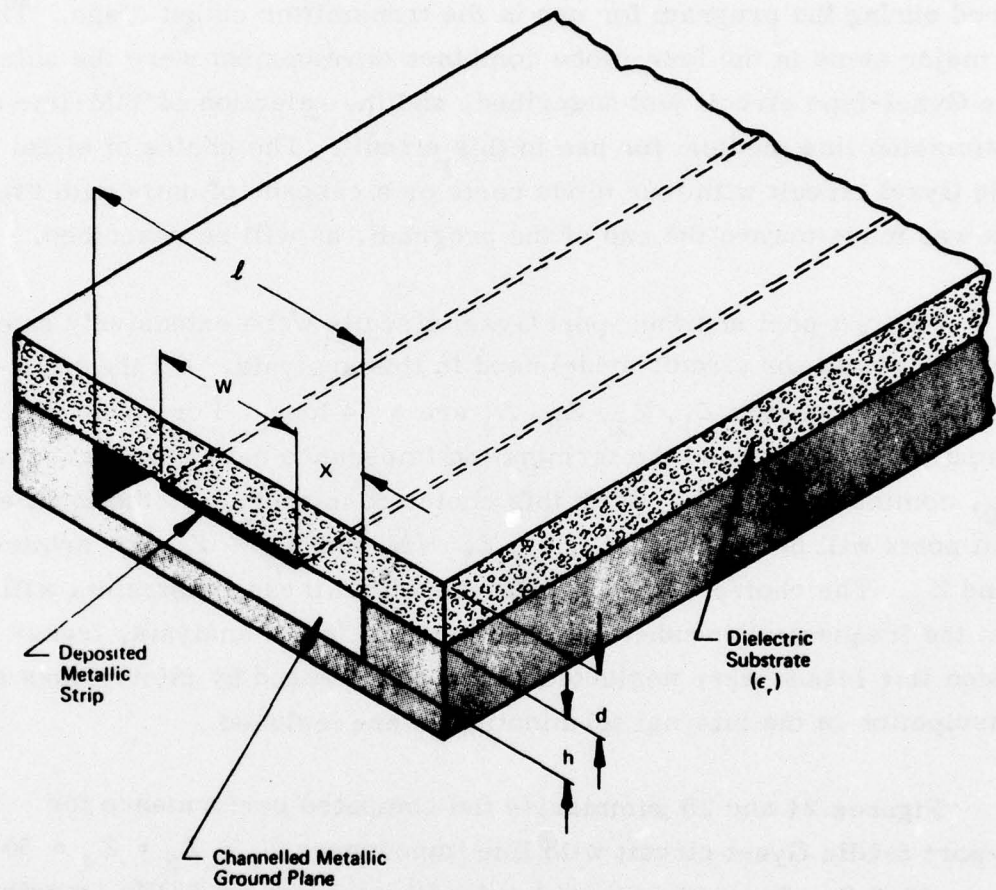
Figure 22   Trapped Inverted Microstrip (TIM) Line Structure.

3.2.2.3.2.3 Progress in nonresonant power-combiner development

The nonresonant power combiner was the principal circuit type considered during the program for use in the transmitter output stage. The first major steps in the four-diode combiner development were the selection of the Gysel-type circuit just described, and the selection of TIM-line as the transmission line medium for use in this circuit. The choice of either a single Gysel circuit with four diode ports or a cascade of units with two diode ports was made toward the end of the program, as will be described.

The two-port and four-port Gysel circuits were extensively analyzed. Figure 23 shows the circuit model used in this analysis. All the transmission line segments Z_1, Z_2, Z_3, Z_4 are $\lambda/4$ long. For convenience, the input, the output, and the termination impedance have been set equal to Z_0, nominally 50 ohms. With this choice of impedances, the input and output ports will be matched if $Z_2 = Z_1 \sqrt{N}$ and $Z_3 = Z_0$ for arbitrary Z_1 and Z_4. The choice of the impedances within these constraints will affect the frequency dependence of the circuit. In the analysis, transmission line losses were neglected, but losses caused by mismatches and by dissipation in the internal terminations were included.

Figures 24 and 25 summarize the computed performance for a two-port 5-GHz Gysel circuit with line impedances $Z_1 = Z_3 = Z_4 = 50\,\Omega$, and $Z_2 = 70.7\,\Omega$. In an 18 percent bandwidth centered on 5 GHz, maximum input VSWR is 1.2, maximum output VSWR is 1.1, maximum loss is 0.2 dB, and minimum isolation between outputs is 25 dB.

Figures 26 through 29 summarize the computed performance for a four-port 5-GHz Gysel circuit. Results for three different cases are shown: (1) $Z_1 = Z_3 = Z_4 = 50\,\Omega$, $Z_2 = 100\,\Omega$; (2) $Z_1 = 25\,\Omega$, $Z_2 = Z_3 = Z_4 = 50\,\Omega$; and (3) $Z_1 = Z_3 = 50\,\Omega$, $Z_2 = 100\,\Omega$, $Z_4 = 25\,\Omega$. The best overall performance was found in the first case. There, for a

56
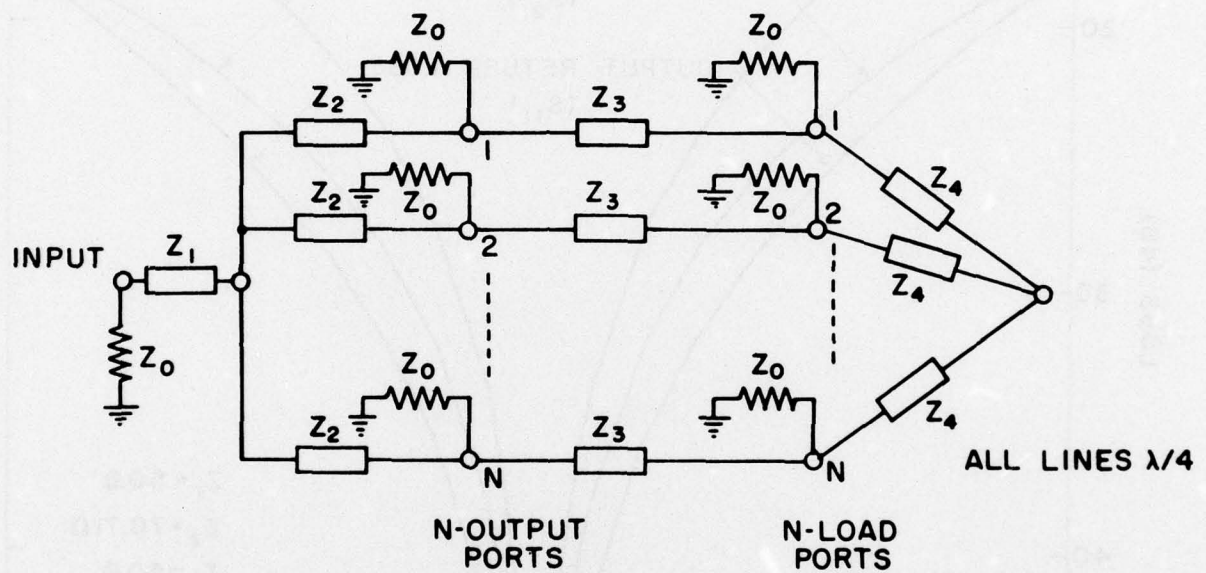
Figure 23   Model for a Generalized N-Port Gysel Circuit.
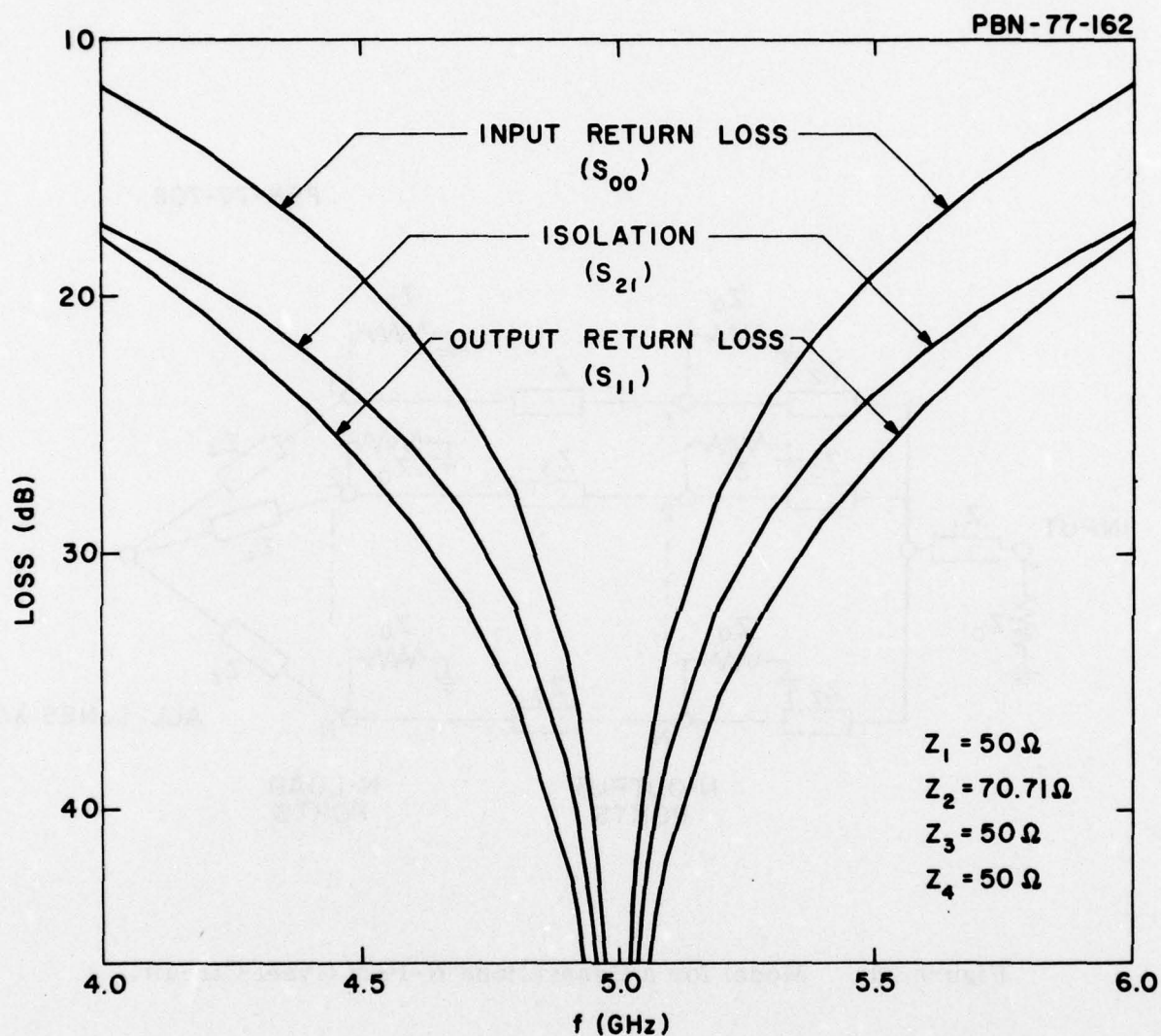
Figure 24   Composite Plot Showing Computed Input Return Loss,
Output Return Loss, and Isolation Between Outputs
for a Two-Port Gysel Hybrid.
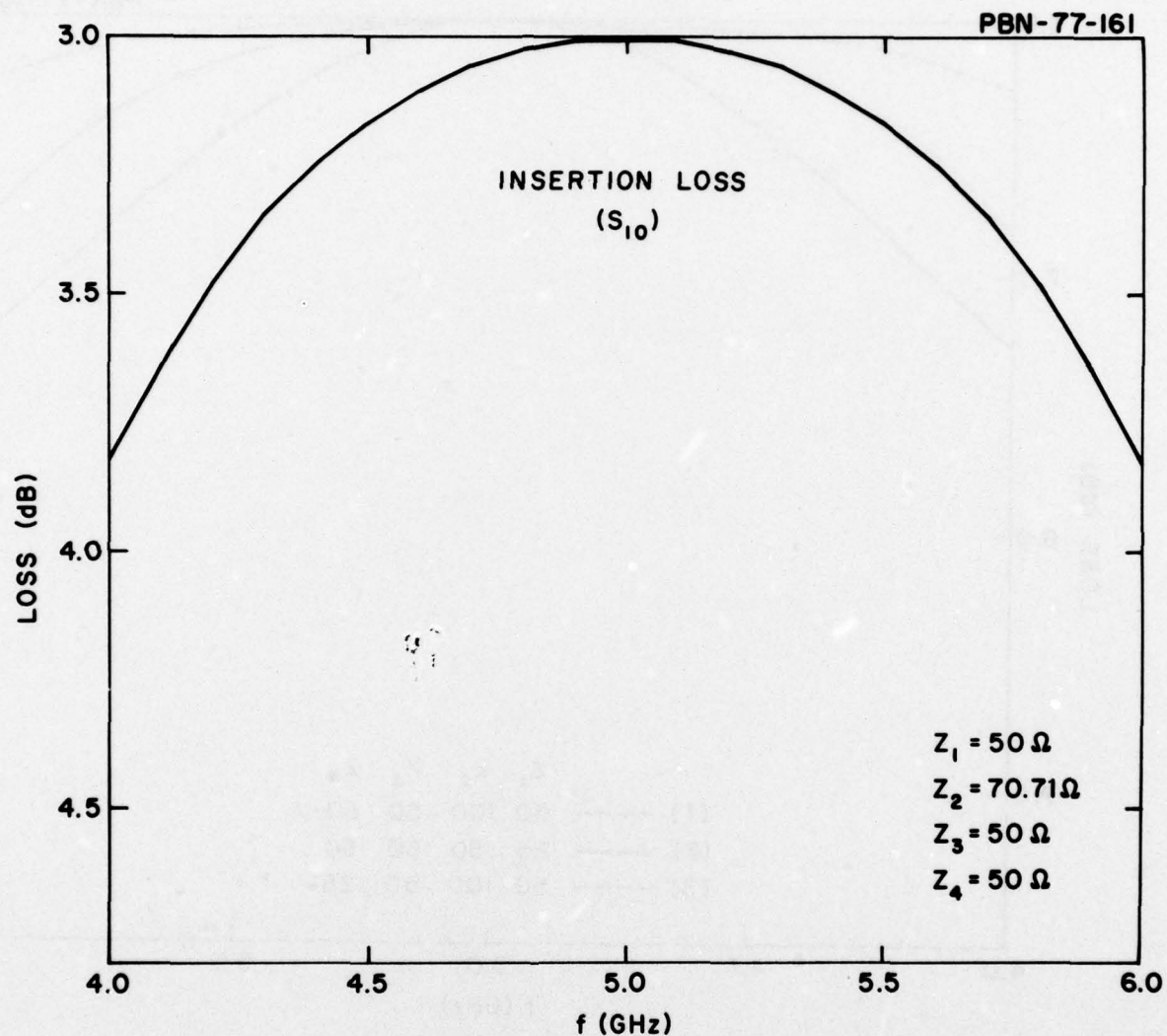
Figure 25   Computed Loss from the Common Port to One
Diode Port of a Two-Port Gysel Circuit. The
nominal power division results in 3 dB loss; loss
above 3 dB represents unrecoverable dissipated power.

59
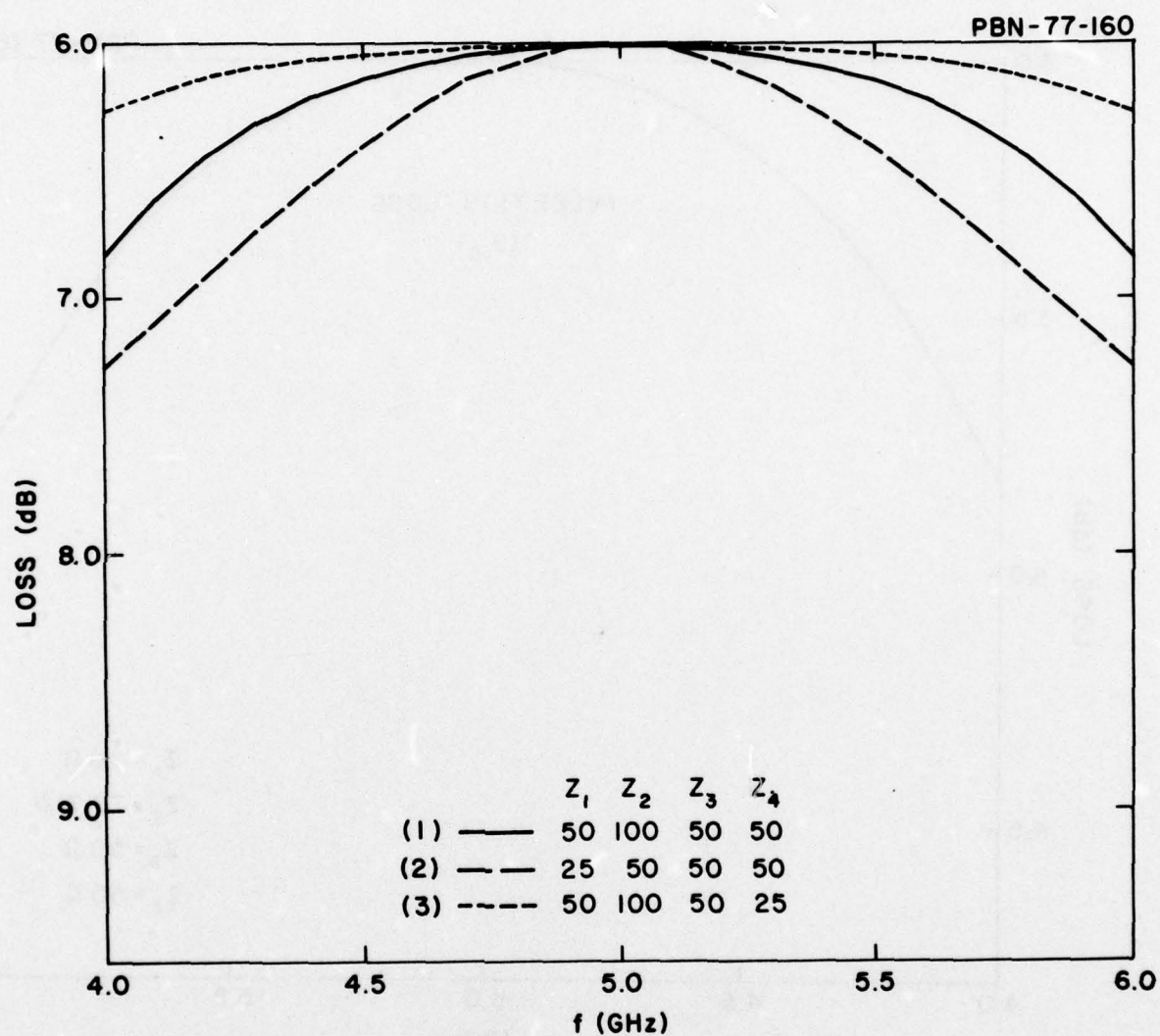
Figure 26   Computed Loss from the Common Port to One Diode Port of a Four-Port Gysel Circuit for Three Different Sets of Internal Line Impedances. The nominal power division results in 6 dB loss; loss above 6 dB represents unrecoverable dissipated power.
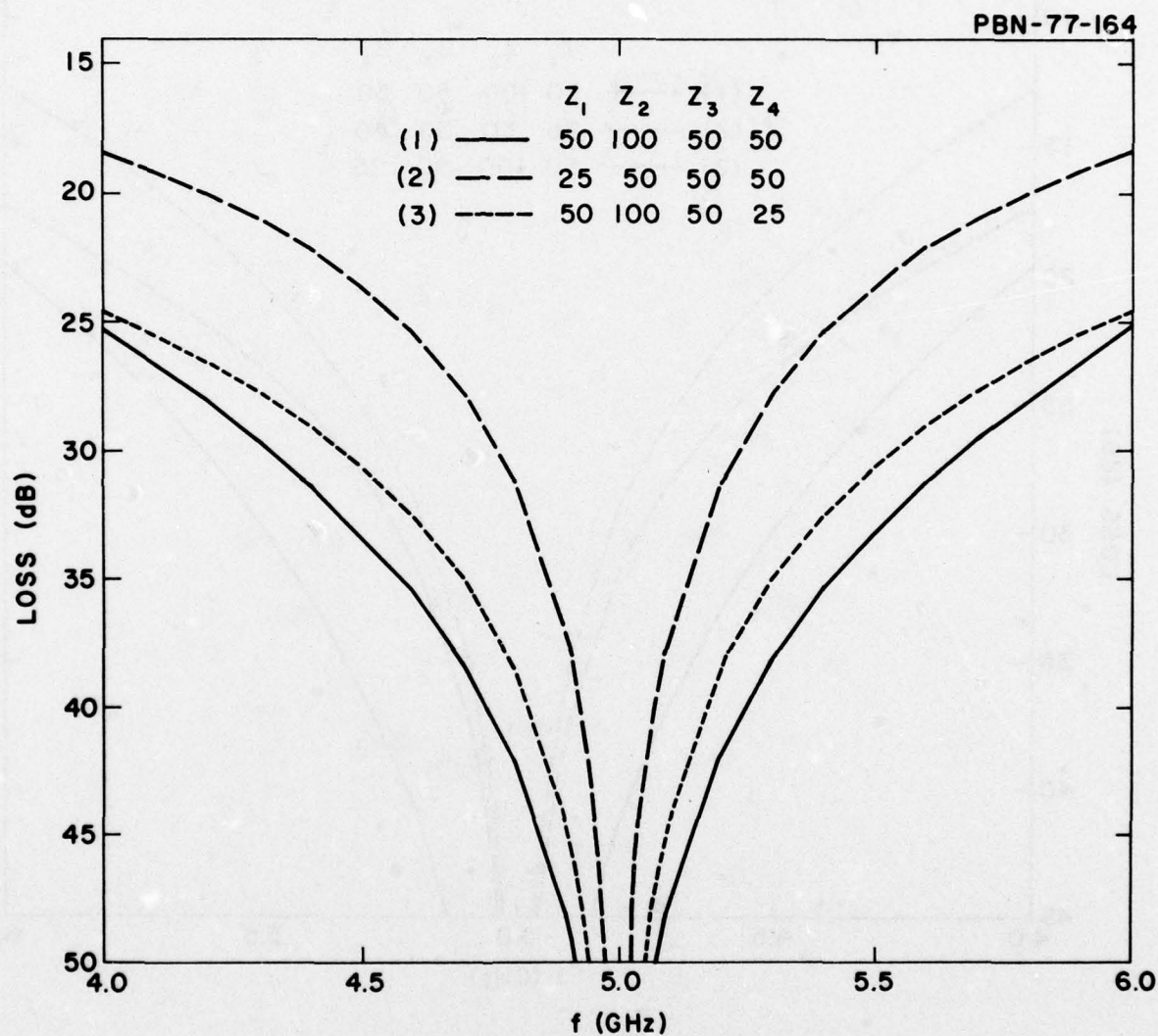
Figure 27   Computed Isolation Between Two Diode Ports in a
Four-Port Gysel Circuit for Three Different Sets
of Internal Impedances.
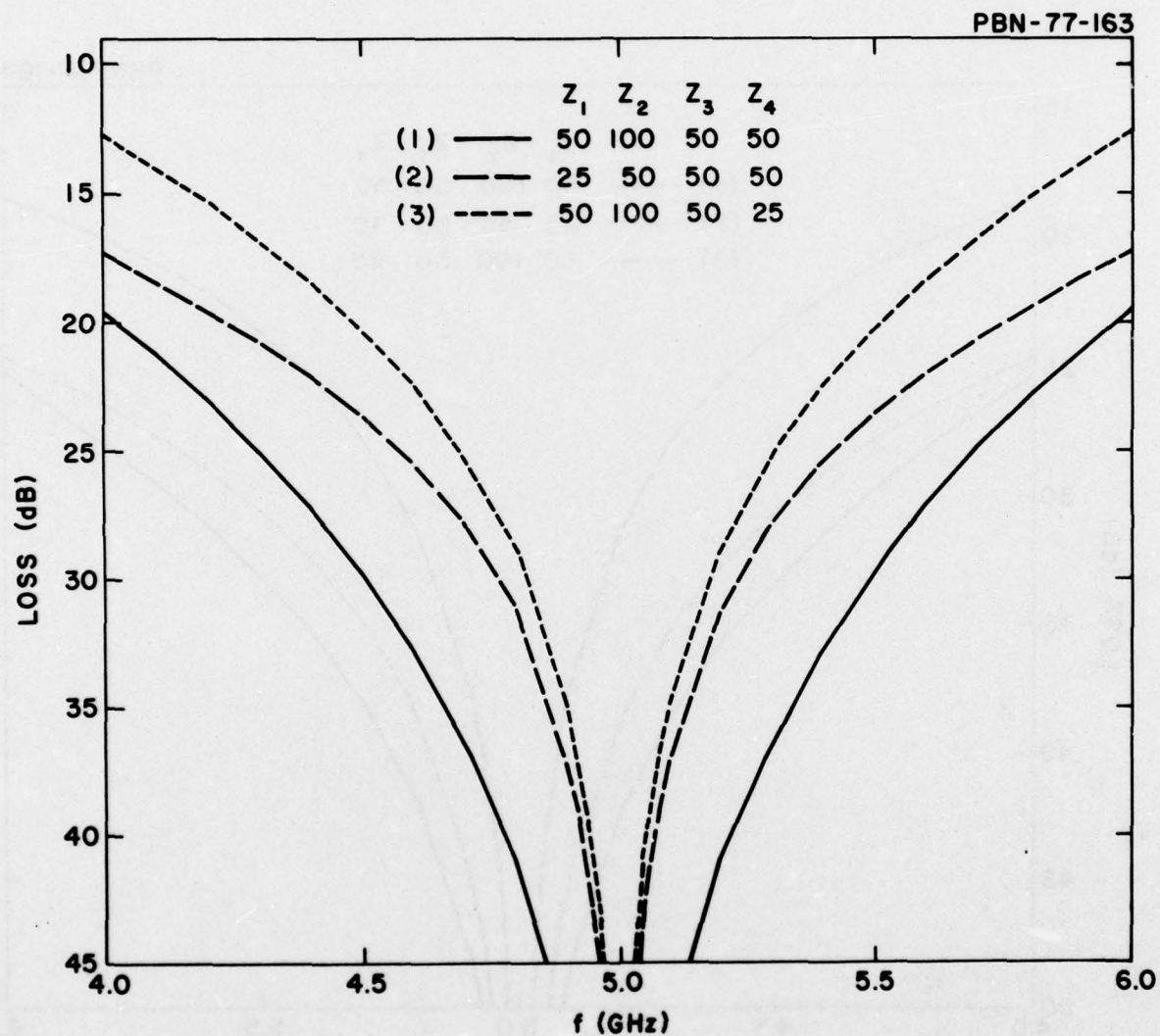
Figure 28   Computed Return Loss at One Diode Port in a
Four-Port Gysel Circuit for Three Different
Sets of Internal Impedances.
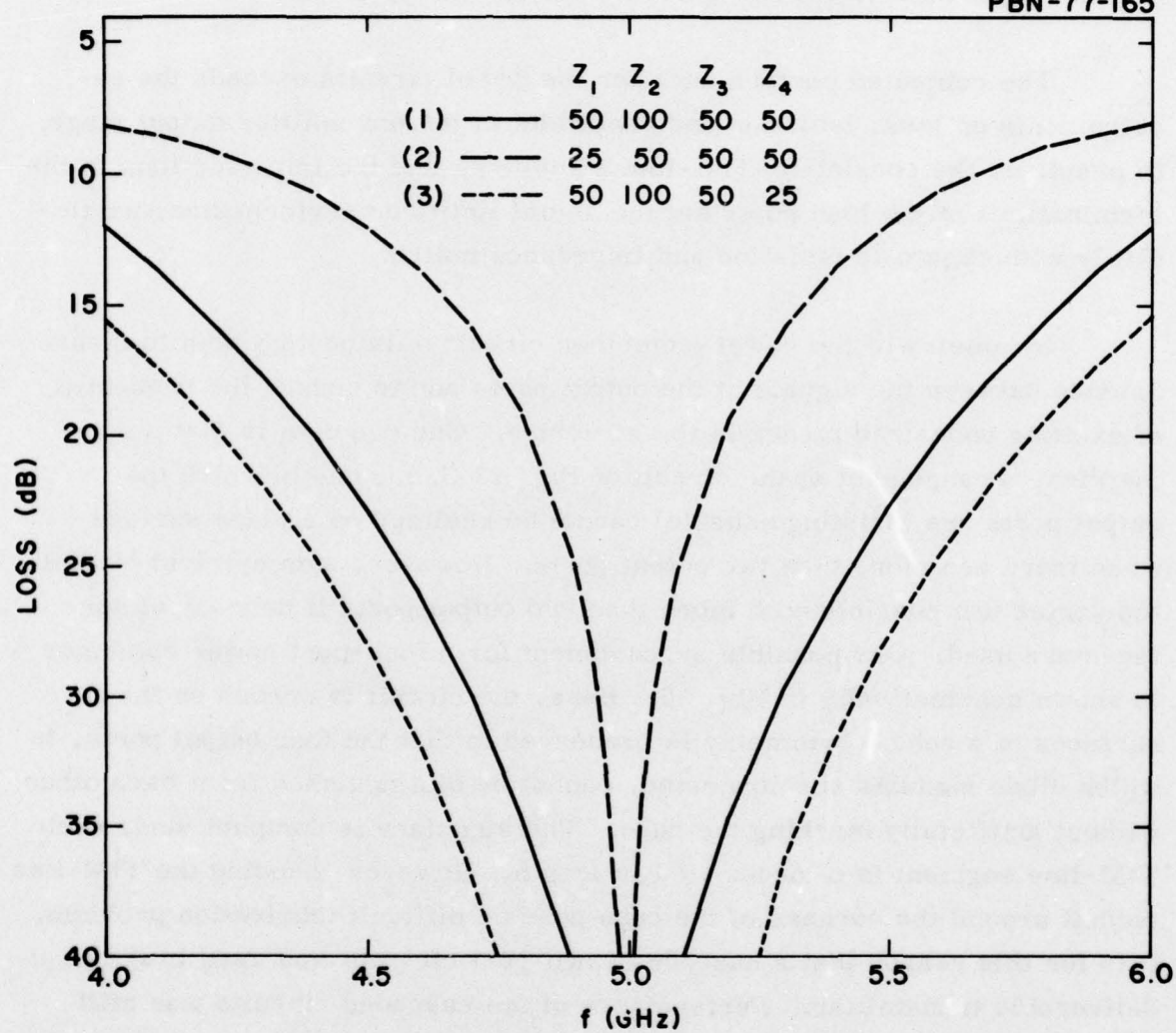
Figure 29   Computed Return Loss at the Common Port of a Four-Port
Gysel Circuit for Three Different Sets of Internal Impedances.

25 percent bandwidth centered on 5 GHz, maximum input VSWR was 1.2, maximum output VSWR was 1.1, maximum loss was 0.2 dB, and minimum isolation between output ports was 30 dB. Case (3) offered lower loss and a better input match, but had poorer isolation and output match.

The computed performance for the Gysel circuits exceeds the requirements on loss, isolation and bandwidth in the transmitter output stage. In practice, the coaxial-to-TIM-line transitions and the imperfections in the terminations at the load ports set the actual limits on performance, particularly with regard to isolation and impedance match.

Symmetry of the power-combiner circuit is important both to insure balance between the signals at the output ports and to reduce the probability of exciting undesired modes in the structure. One problem is that a symmetrical arrangement of the circuit of Fig. 23 (i.e., one in which the output ports are indistinguishable) cannot be realized on a plane surface when there are more than two output ports. However, symmetrical circuit topologies are possible with more than two output ports if polyhedral surfaces are used. One possible arrangement for a four-port power combiner is shown schematically in Fig. 30. Here, the circuit is spread on the surfaces of a cube. Symmetry is preserved in that the four output ports, to which diode modules are connected, cannot be distinguished from each other without artificially marking the cube. The structure is compact since each TIM-line segment is of order $\lambda/4$ in length. However, bending the TIM-line circuit around the corners of the cube poses a difficult fabrication problem. It is for this reason that a cascade of two-port circuits was used in the first deliverable transmitter. Performance of the cascaded circuits was still good enough to provide more than 70 percent combining efficiency in the output stage.

Hardware for the TIM-line power combining circuit was developed in a series of stages. First, one-inch and two-inch lengths of 50-ohm line were prepared to test design data, and to determine whether a satisfactory SMA to TIM-line transition could be constructed. The transition shown in

64
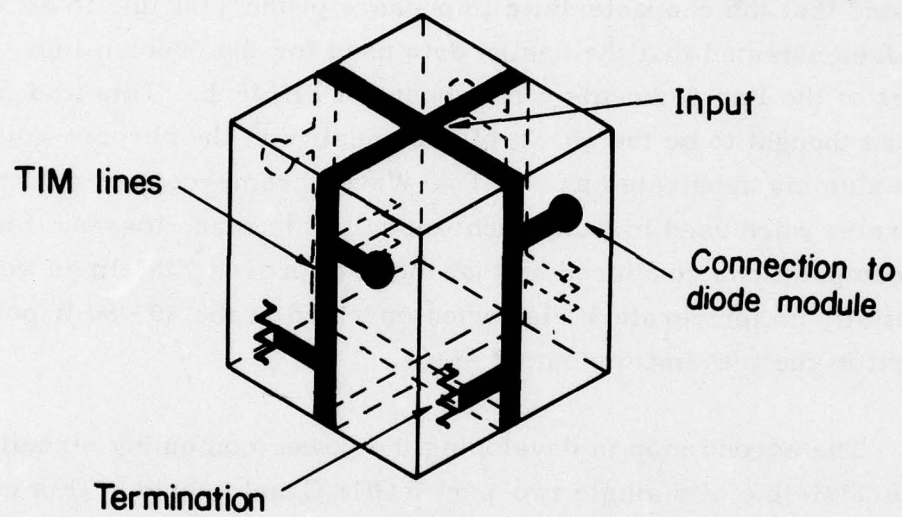
Figure 30   Topology for a Symmetrical Gysel Circuit with
Four Diode Ports.

Fig. 31 was used in these and subsequent tests. The measured VSWR looking into the terminated 50-ohm line segments was typically 1.1:1 across the 4 - 6 GHz range. Some of this mismatch was contributed by the termination itself, and by the transition from the APC-7 connectors of the network analyzer to the SMA connectors on the test fixture. However, the VSWR was low enough to indicate that a reasonably good transition to the TIM-line had been achieved. Separate time-domain reflectometer (TDR) measurements indicated that the characteristic impedance of the TIM line itself was 49 ohms. This demonstrated that the design data used for the 50-ohm line were correct. Losses of the line segments were about 0.1 dB/inch. This was judged excessive, and was thought to be the result of poor quality in the chrome-gold metallization of the alumina substrates used. Tek-Wave chrome-copper-gold metallized substrates were used in subsequent circuits to reduce losses. Simple heat flow computations convinced us that these improved TIM-lines would experience essentially no temperature rise when operated at the 40 - 50 W power levels present in the transmitter output stage.

The second step in developing the power combining circuit was fabrication in TIM-line of a single two-port 5 GHz Gysel hybrid. This circuit, constructed on a 2×2 in^2 substrate, was shown in Fig. 21. The initial testing was carried out using low-power 50-ohm loads for the internal terminations. The circuit was designed, assembled, and tested without making any adjustments to improve performance.

The actual band center for this first hybrid occurred at 5.2 GHz rather than at the 5 GHz design value. Within a 500 MHz band around 5.2 GHz, however, the performance of the hybrid was excellent. Excess loss between the input port and the two output ports was only 0.2 - 0.3 dB. The two output ports were balanced within 0.1 dB in amplitude and 3° in phase. Isolation between the two output ports was at least 30 dB and reached 38 dB at band center. The maximum VSWR at the input port was 1.2, and VSWR at the output ports was less than 1.1. Band-center VSWR's were less than 1.04 at input and output ports.

Figures 32 through 35 compare the measured and computed

66

PBN-77-104
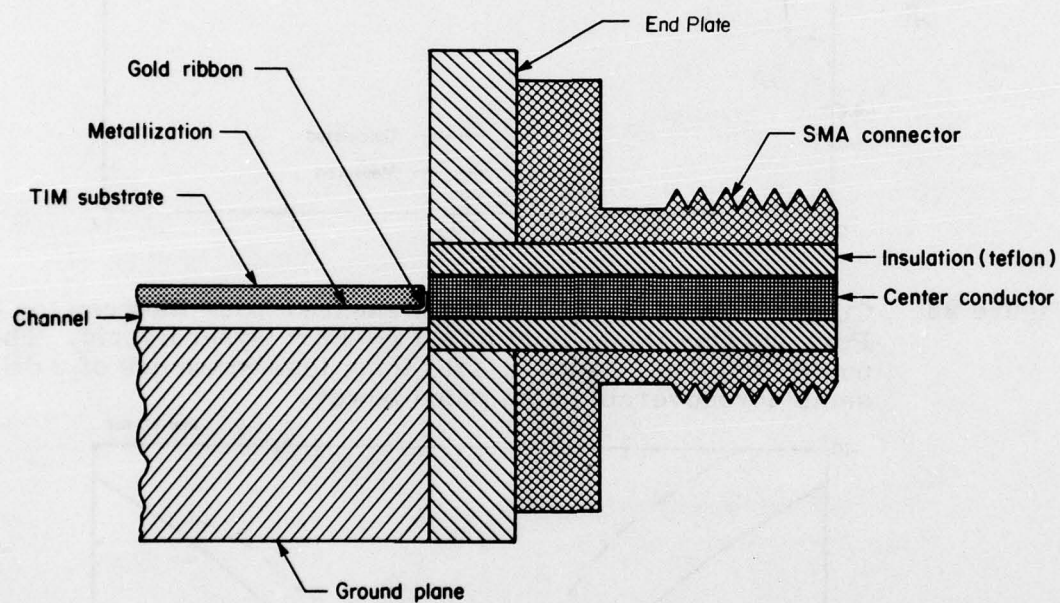
Figure 31   TIM Line to SMA Transition. The gold ribbon is thermo-
compression bonded to the TIM-line circuit metallization,
and soldered to the center conductor of the SMA connector
using a hot-gas gun.
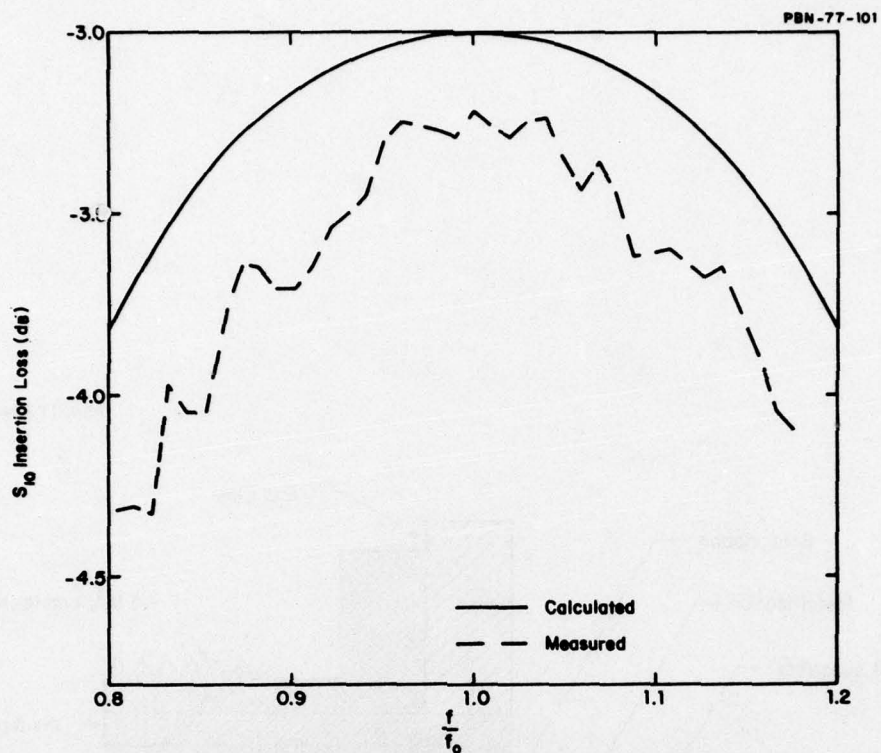
Figure 32   Comparison of Computed and Measured Loss Between the Common Port and One Diode Port of a Two-Port Gysel Hybrid. The nominal power division results in 3 dB loss; loss in excess of 3 dB represents unrecoverable dissipated power.
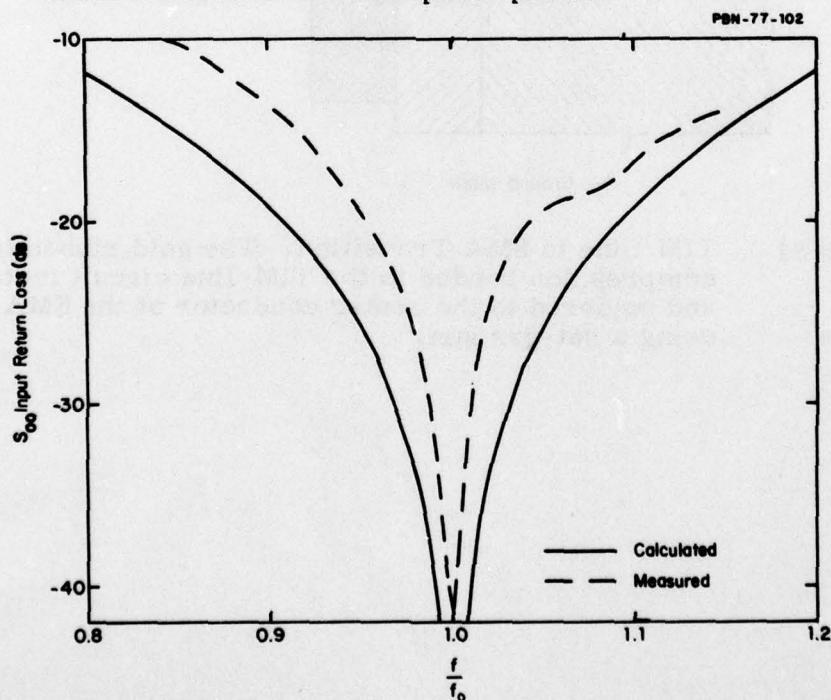
Figure 33   Comparison Between Computed and Measured Return Loss at the Common Port of a Two-Port Gysel Hybrid.
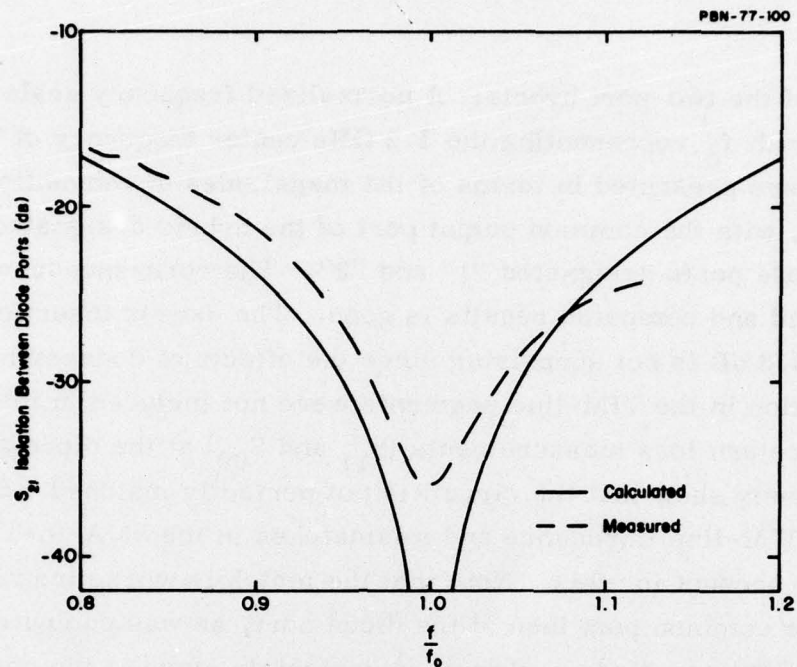
Figure 34   Comparison of Computed and Measured Isolation Between the
Output Ports of a Two-Port Gysel Hybrid.
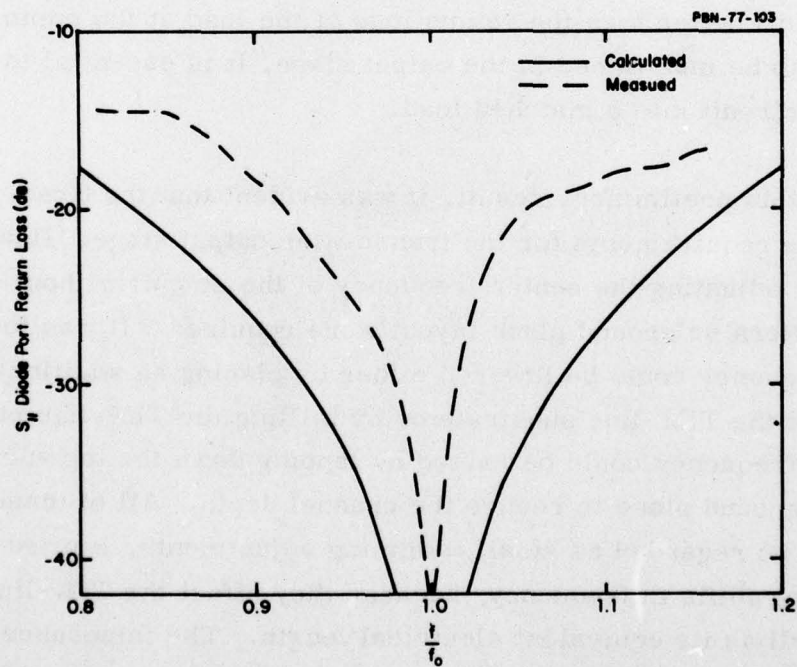
Figure 35   Comparison Between Computed and Measured Return Loss at
One Output Port of a Two-Port Gysel Hybrid.

performance of the two-port hybrid. A normalized frequency scale is used in all cases, with f_o representing the 5.2 GHz center frequency of the actual hybrid. Data are presented in terms of the magnitudes of conventional S-parameters, with the common output port of the hybrid designated "0" and the two diode ports designated "1" and "2". The correspondence between measured and computed results is good. The excess insertion loss (S_{10}) of 0.2 - 0.3 dB is not surprising since the effects of connector mismatch and of dissipation in the TIM-line segments were not included in the computations. The return loss measurements $(S_{11}$ and $S_{00})$ at the diode and output ports respectively show that the circuit is not perfectly matched. Slight errors in the TIM-line impedance and mismatches in the SMA-to-TIM transitions probably account for this. Note that the match is worse (return loss is smaller) at the common port than at the diode port, as was computed. The isolation (S_{21}) between diode ports was surprisingly close to the computed values. Isolation depends strongly on the termination placed at the common "0" port during operation of the hybrid. Even with a perfect circuit, isolation will be only 6 dB better than the return loss of the load at the common port. If stability is to be maintained in the output stage, it is essential to operate the combiner circuit into a matched load.

From this preliminary result, it was evident that the Gysel hybrid would meet the requirements for the transmitter output stage. However, techniques for adjusting the center frequency of the circuit without changing the circuit pattern or ground plane layout were required. It was found that the center frequency could be lowered either by placing an additional dielectric layer on top of the TIM-line substrate or by milling the TIM-line channels deeper. The frequency could be raised by lapping down the top surface of the TIM-line ground plane to reduce the channel depth. All of these techniques should be regarded as small trimming adjustments, limited to less than 10 percent shifts in frequency, because they affect the TIM-line impedance as well as its equivalent electrical length. The impedance match at the input and output ports will become progressively worse as larger changes in operating frequency are made.

The final step in the development of the power combining circuit was the fabrication of three two-port hybrids which could be combined in cascade to form the four-port circuit to be used in the output stage. To save time, the circuit mask and ground plane designs of the original prototype were retained. The only design change was to increase the depth of the TIM-line channels slightly to bring the band center of the circuit down to 5 GHz. The three hybrids are shown connected together in the output stage in Fig. 64 (p. 129). High power loads, OSM 2069-6005-00, capable of dissipating 5 W each were used as internal terminations to permit operating output stage diodes singly during tuning.

In the future, the power combining circuit could be fabricated on a single substrate approximately 4×1.5 in^2, instead of on three 2×2 in^2 substrates. This change would probably reduce the overall losses of the four port circuit by $0.2 - 0.3$ dB by reducing line lengths and eliminating the connectors and transitions joining the separate hybrids.

The four-port power combiner was subjected to an extensive series of tests to evaluate its performance. As with the original prototype circuit, no adjustments were made to improve the performance. The layout of the combiner and the port designations used in the tests are shown in Fig. 36. Representative test results are shown in Figs. 37 through 38. Except for the phase tracking data, all results are presented as magnitudes of conventional S-parameters.

The impedance matches at all ports are quite good. At the common port, S_{00} is set by the circulator, and indicates a VSWR better than 1.22:1 across the entire $4 - 6$ GHz range. The VSWR at 5 GHz is 1.1:1. The VSWR's at all of the diode ports showed a stagger-tuned doubly resonant behavior. There were different spacings between the two resonances, giving a more or less pronounced double minimum in VSWR near 5 GHz. The plots of S_{11} and S_{33} represent the extreme cases. For port 3, VSWR at 5 GHz is 1.027 and remains below 1.12 from 4.82 to 5.30 GHz. At port 1, VSWR at 5 GHz is larger, 1.09, but remains below 1.12 from 4.81 to 5.34 GHz.

71

Port 0 for
$S_{01} - S_{04}$ → 3 | 1 ← Teledyne microwave
Circulator C-4S63T-10
S/N 182
Port 0 for S_{00}

1

Unit
1

2

Unit
3

Unit
2

4

3

OSM 2069-6005-00
Terminations (6)
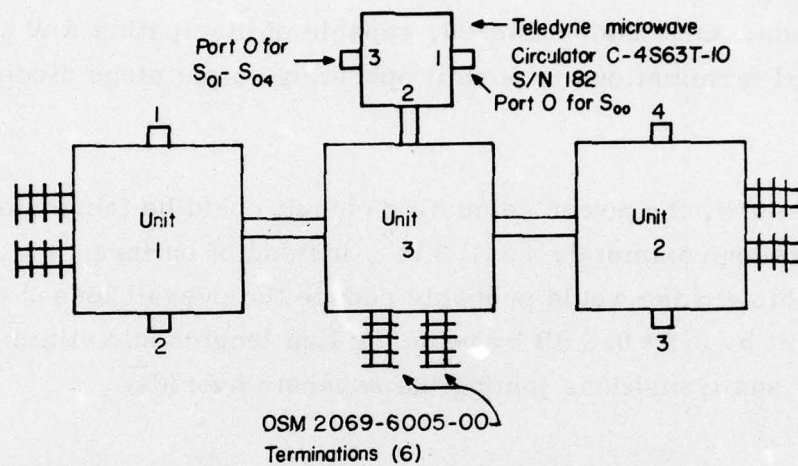
Figure 36   Arrangement of Two-Port Gysel Hybrids in
Cascade to Produce a Four-Port Hybrid. Port
designations are determined while looking down
on the open tops of the TIM-line circuits.

72

S_{oo} 4 - Port with circulator
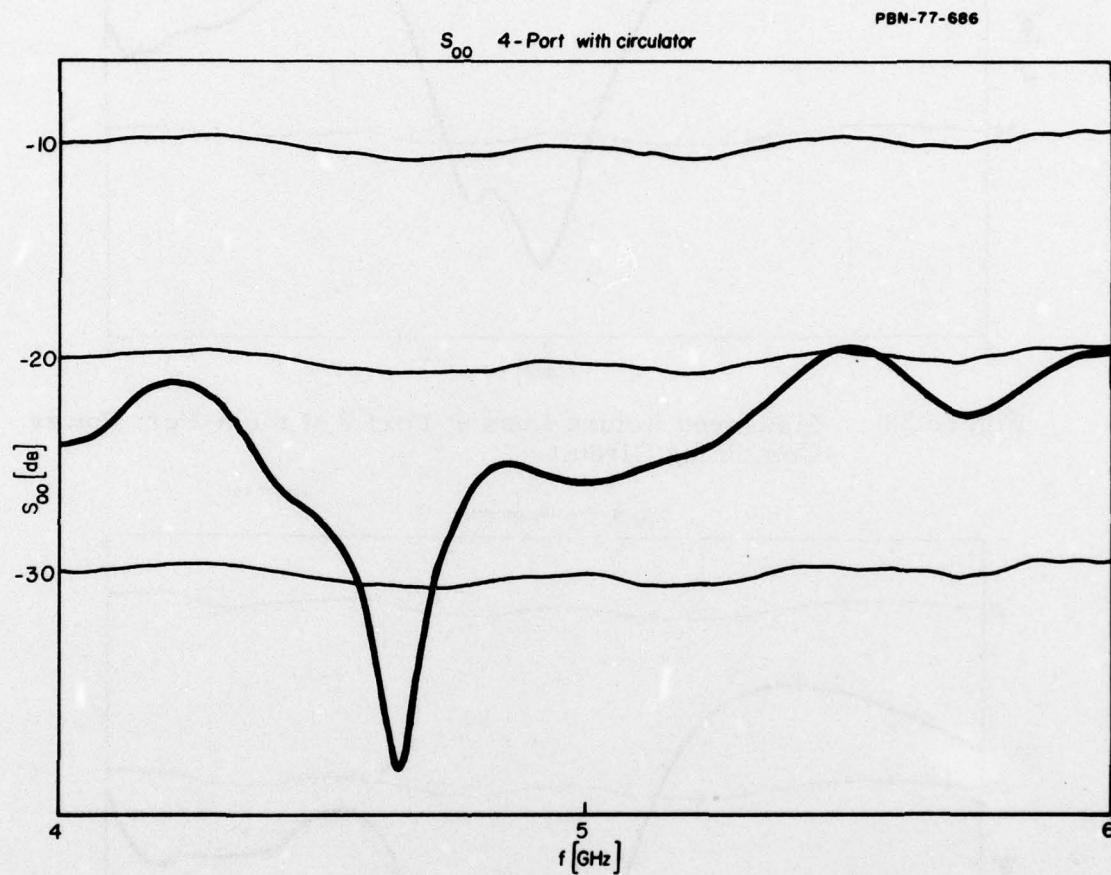
Figure 37   Measured Return Loss at the Common Port ("0")
of the Four-Port Power Combining Circuit.

73
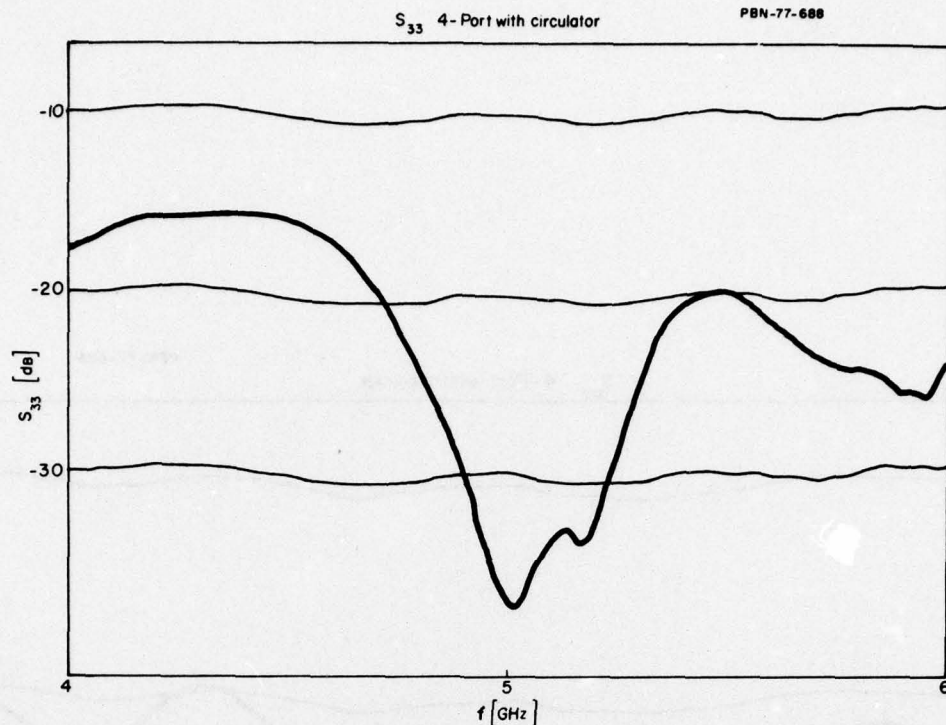
Figure 38   Measured Return Loss at Port 3 of the 4-Port Power
              Combining Circuit.
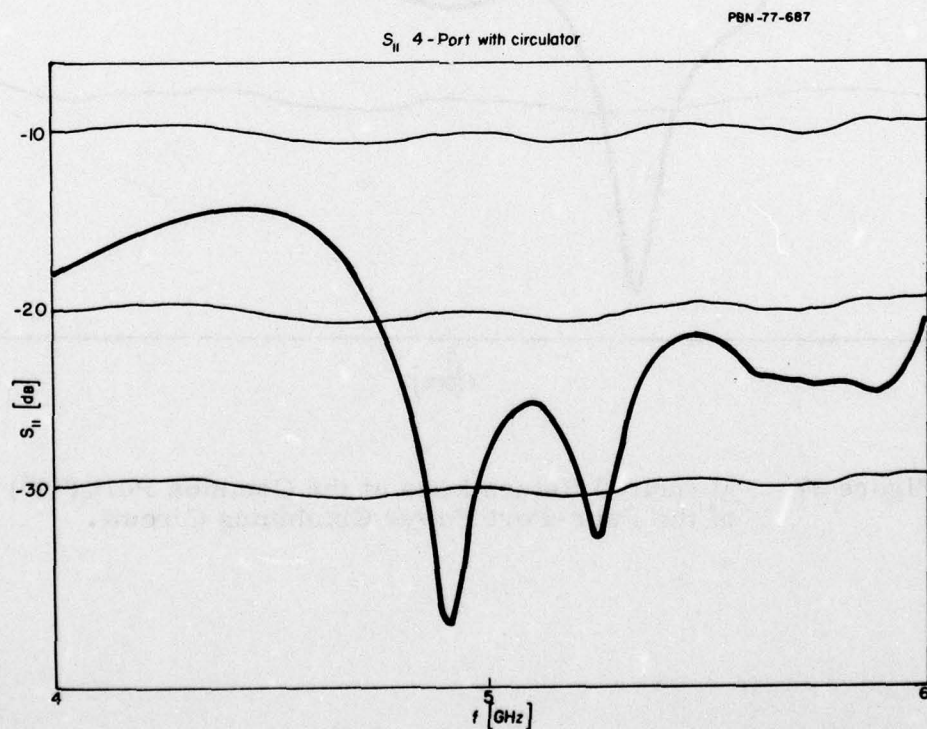
Figure 39   Measured Return Loss at Port 1 of the 4-Port Power
              Combining Circuit. The double resonance is more
              strongly developed here than in Fig. 38.
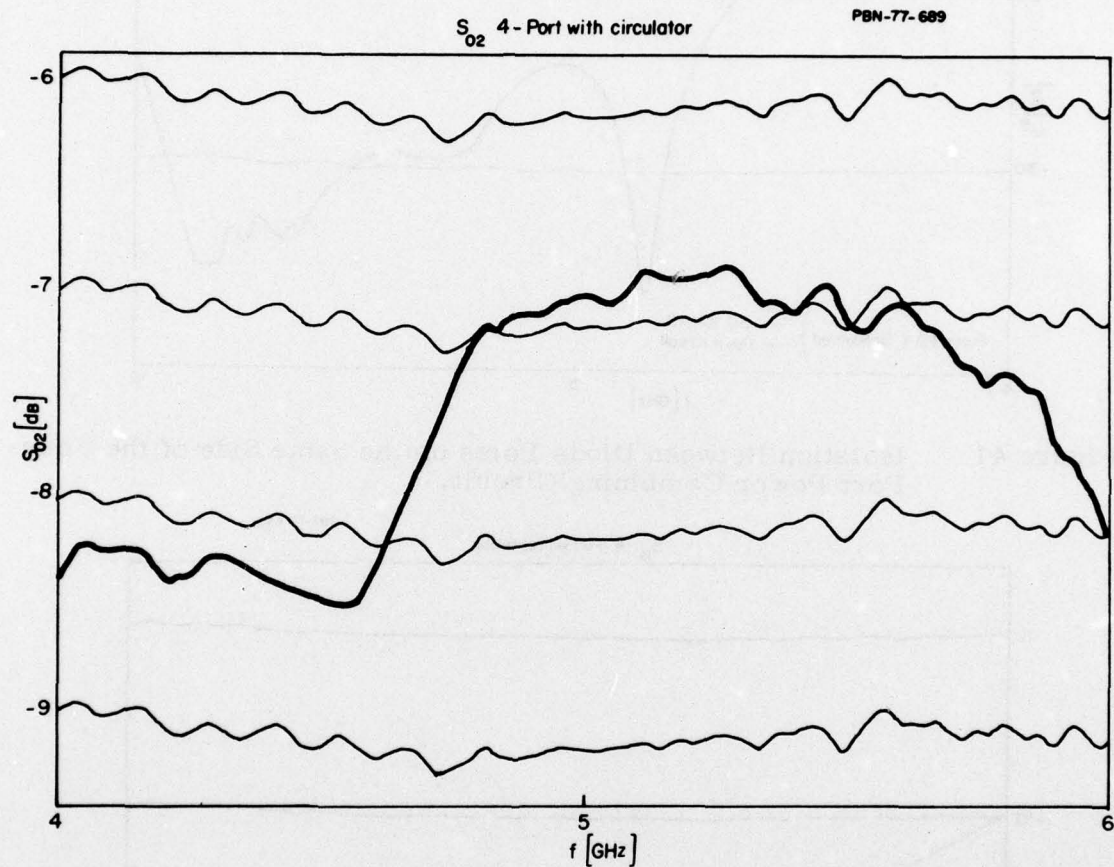
Figure 40   Measured Loss Between the Common Port and One
Output Port of the Four-Port Power Combining
Circuit, Including the Circulator. The nominal
power division results in 6 dB loss; loss in excess
of 6 dB represents unrecoverable dissipated power.
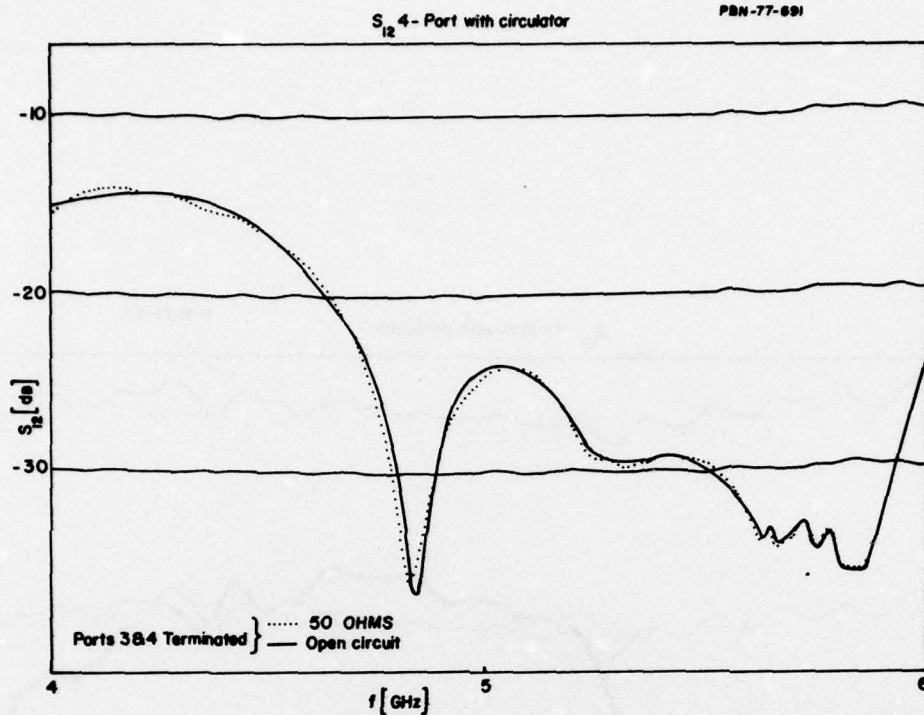
Figure 41   Isolation Between Diode Ports on the Same Side of the Four-
                Port Power Combining Circuit.
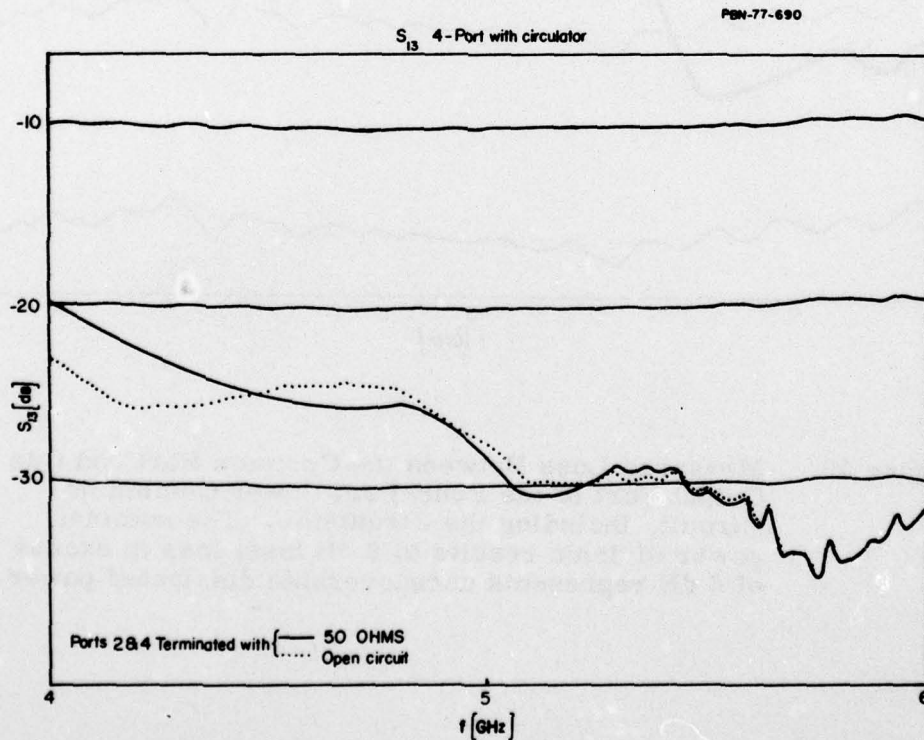
Figure 42   Isolation Between Diode Ports on Opposite Sides of the Four-
                Port Power Combining Circuit.

Relative Phase (S_{01}, S_{02}, S_{03}, S_{04}) 4 - Port with circulator
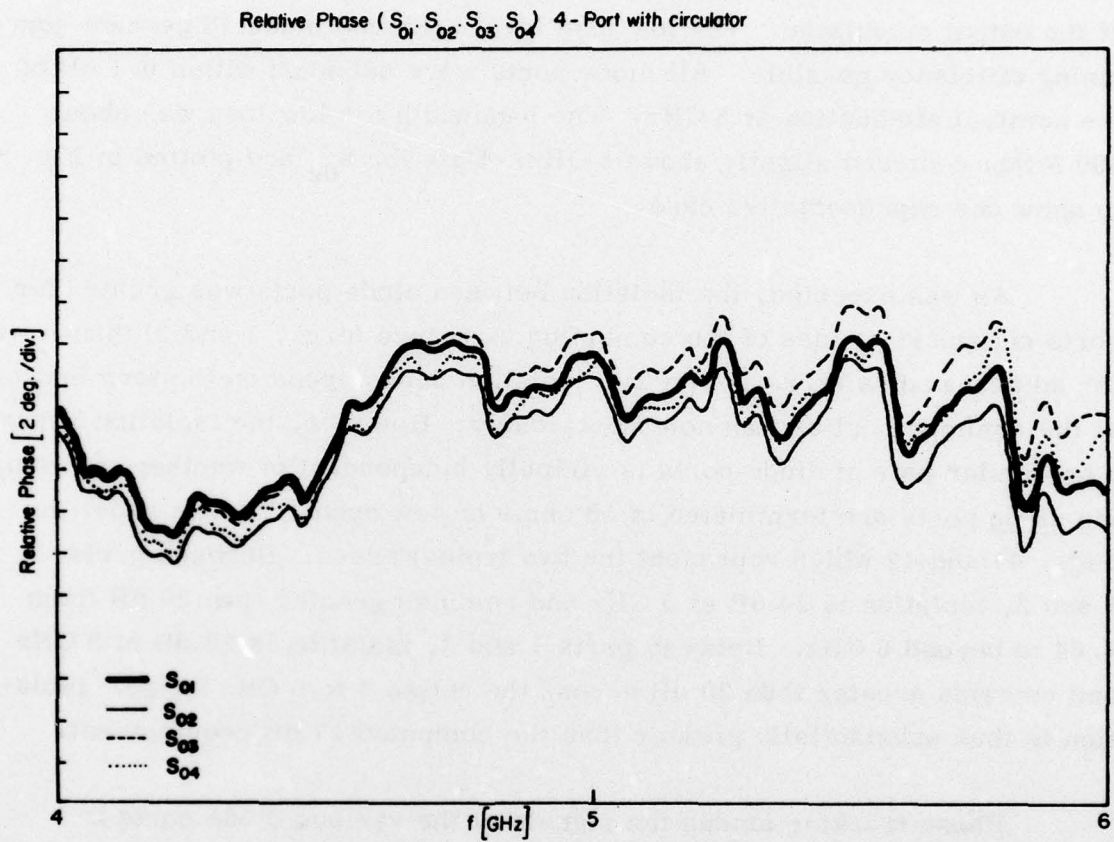
Figure 43 Relative Transmission Phase as a Function of Frequency Between the Common Port and Each Output Port of the Four-Port Power Combining Circuit. All phases are within 2° at 5 GHz.

77

Thus, low VSWR is maintained well beyond the operating band (4.97 - 5.03 GHz) of the transmitter.

Losses between the common port and the diode ports were typically 1 dB above the nominal 6 dB power division at 5 GHz. This included the loss of the output circulator. The low loss level achieved made 75 percent combining efficiency possible. All diode ports were balanced within 0.1 dB of the nominal attenuation at 5 GHz. The bandwidth for low loss was about 800 MHz, centered slightly above 5 GHz. Data for S_{02} are plotted in Fig. 40 to show one representative case.

As was expected, the isolation between diode ports was greater for ports on opposite sides of the combining structure (e.g., 1 and 3) than it was for adjacent ports (e.g., 1 and 2). Isolation does depend on the termination at the common port as was noted previously. However, the isolation between a particular pair of diode ports is virtually independent of whether the remaining diode ports are terminated in 50 ohms or left open. This is shown in Figs. 41 and 42 which represent the two typical cases. Between ports 1 and 2, isolation is 24 dB at 5 GHz and remains greater than 20 dB from 4.64 to beyond 6 GHz. Between ports 1 and 3, isolation is 28 dB at 5 GHz and remains greater than 20 dB across the entire 4 to 6 GHz range. Isolation is thus substantially greater than the computed 17 dB requirement.

Phase tracking among the signals at the various diode ports is important if the powers from the individual diode modules are to add directly. For two signals offset in phase by the angle θ, the power of their sum will be reduced by $\cos^2(\theta/2)$ from what it would be under in-phase conditions. Fortunately, the measured phase tracking in the four-port combiner is excellent. Signals at all ports have relative phases lying within a range 2° wide at 5 GHz. At worst, near 6 GHz, the relative phases are still confined to a range 5° wide. This implies essentially no loss in power combining efficiency because of phase offsets imposed by the combining circuit.

3.2.3 Diode modules

3.2.3.1 Introduction

In the resonant cavity power combiner (Section 3.2.2.3.1), the IMPATT diodes are mounted in coaxial line assemblies which are an integral part of the cavity structure. The nonresonant power combiner, in contrast, uses discrete oscillator modules which are coupled to the power combining network.

The idea of using a completely integrated nonresonant power combiner in which the oscillator modules and the combining network have a common type of transmission line is very attractive. Such construction would simplify fabrication of the output stage in the transmitter, allowing the entire circuit to be printed on a single substrate. Because TIM line was used in the power combining network, we attempted to develop a TIM line oscillator module which could be used in an integrated output stage. To simplify the initial development work, however, the power combining network and the TIM-line oscillators were designed as separate units.

The work with high-power TIM-line oscillators was not successful. While power outputs in the 10-15 W range were ultimately achieved, tuning remained erratic and discontinuous. The performance obtained was not acceptable for a prototype transmitter representing a practical unit. Two other oscillator modules, a double slug coaxial circuit and a coaxial cavity circuit were evaluated for possible use in the transmitter, and the latter was finally selected. The work on all three circuits will be described in the following subsections.

3.2.3.2 TIM-line oscillator modules

3.2.3.2.1 Impedance measurements

An attempt was made to follow an organized design and development

79
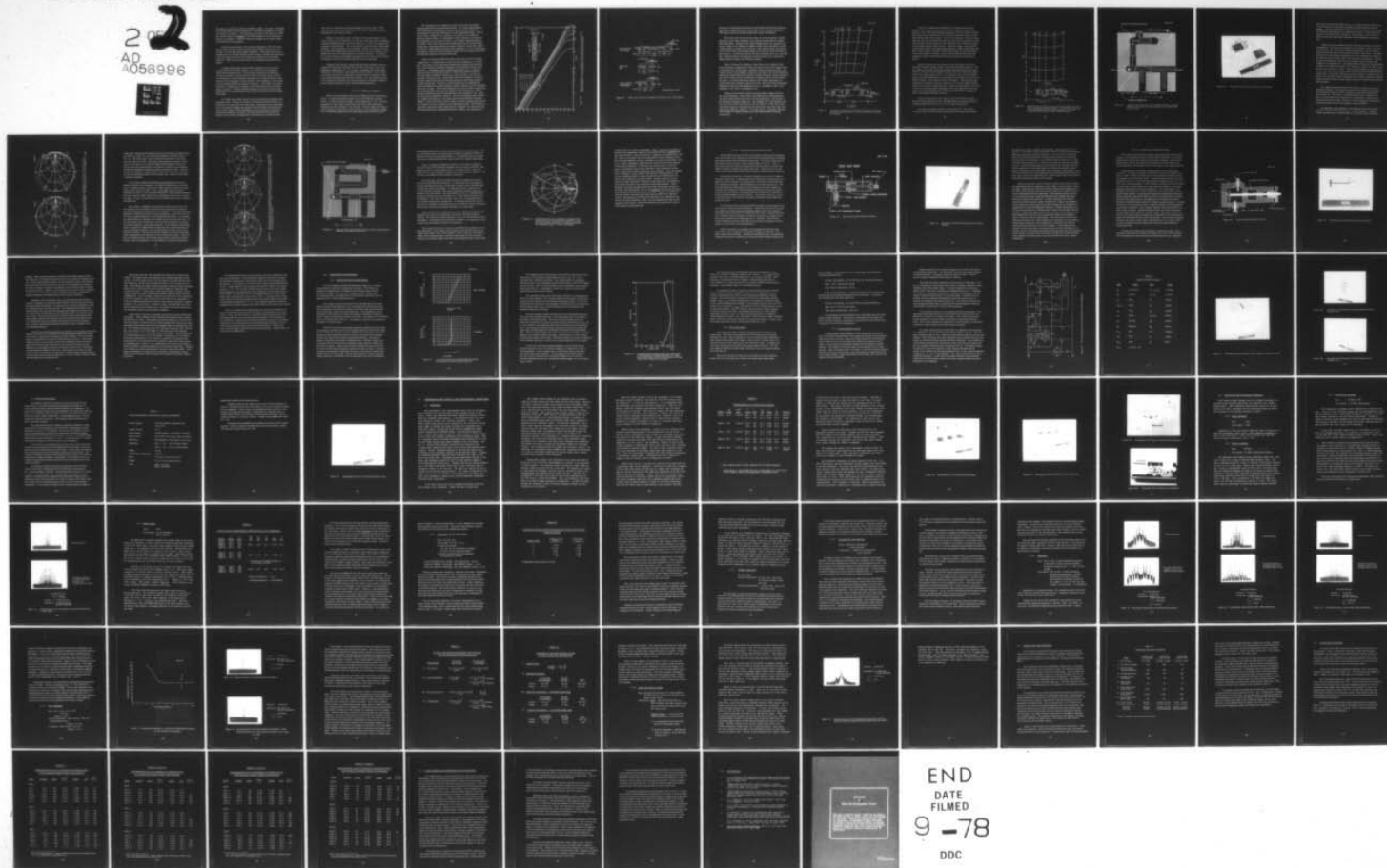
procedure to produce the TIM-line oscillator module. For this, a knowledge of the large-signal terminal impedances of the IMPATT diodes to be used in the module was required. The impedance presented to the diode in the TIM-line circuit must be the <u>negative</u> of the diode impedance at the desired frequency of oscillation. Standard transformer designs can be used to obtain the required circuit impedance.

Limited measurements of the terminal impedances of the four-mesa diodes produced in the previous program[3] gave typical values near -0.8 + j6 ohms at 5 GHz under large-signal conditions. This value was used as a starting point for the TIM oscillator module design, although the impedances of the new large-area four-mesa diodes were expected to be somewhat different. Efforts were then directed toward obtaining data from the new diodes.

A simple single-slug coaxial circuit, analogous to one of several possible TIM-line oscillator designs, was used in the first attempts to obtain diode impedance data. The procedure planned was to adjust the circuit for optimum 5 GHz performance with a particular diode, and then to determine the circuit impedance presented to the diode terminals, from which the diode impedance could be deduced. The impedance is very small, and consequently difficult to measure accurately. Fortunately, the characteristics of a single slug in precision 7 mm coaxial line can be calculated quite accurately. A simple computer program was prepared which would quickly give the circuit impedance from data on the dimensions and position of the slug.

The single slug coaxial circuit was not successful in producing useful impedance data. In tests of a variety of C-band GaAs IMPATT diodes, including the new large-area four-mesa types, strong bias circuit oscillations were encountered as tuning was adjusted toward conditions producing maximum power output. These oscillations occurred because the relatively large shunt capacitance (~46 pF) of the bias network and the 50 ohm impedance of the external coaxial system both appeared in parallel with the

bias source, reducing its equivalent impedance to a low value. [1] The tendency toward bias circuit oscillations was further enhanced by the low operating Q of the coaxial circuit.

Rather than attempt a major redesign of the coaxial system to overcome the bias circuit oscillations, we used the cavity-type power combining circuit developed during the previous program as a vehicle for making diode impedance measurements. The circuit could be operated with a single diode installed. The environment in the immediate vicinity of the diode was similar to that in the single-slug coaxial circuit, and the same technique of computing the effect of the slug transformer could be employed. The smaller bias circuit capacitance and higher operating Q of the cavity circuit combined to eliminate most of the problems with bias circuit oscillations.

Using the cavity circuit, large-signal terminal impedance data were gathered on diodes from lots 909, 910, and 946. Real parts of the diode impedance ranged from -0.7 to -1.0 ohms. Imaginary parts of the diode impedance were inductive, and ranged from j4 to j8 ohms. These values were of the same order as impedances measured for the small-area four-mesa diodes produced in the previous program. For an oscillator module to use the diodes effectively, its range of impedance adjustment should extend somewhat beyond the range of expected diode impedance.

3.2.3.2.2 Module development

Before precise impedance data were available for the new four-mesa diodes, we began preliminary design work for the TIM-line oscillator module. In this preliminary design, a diode impedance of -0.8 + j6 ohms, appropriate to the smaller (7-mil-mesa) four-mesa diodes fabricated during the previous program[3], was assumed. This was within the range of diode impedances measured for the new diodes, so the preliminary design work was directly applicable to the diodes ultimately used in the circuit.

81

The advantages of the TIM-line in terms of low loss and reduced fringing field have been described previously. One shortcoming which became evident when designing the oscillator module was the difficulty of fabricating low-impedance TIM-lines in a well-controlled fashion. This is shown in Fig. 44 which gives impedance as a function of line width for different channel widths. For impedances below ~20 ohms, the characteristic impedance Z_o of the line becomes a very rapidly varying function of line width. This occurs when the line width approaches the channel width, leaving only a small gap between the printed conductor and the side walls of the channel. Maintaining a particular (low) impedance requires a high degree of precision, both in the line and channel widths and in the alignment between the dielectric substrate and the ground plane.

Figure 45 shows the difficulty which arises when one tries to design a single-step $\lambda/4$ transformer to match the diode impedance to a 50-ohm line. Also given are two alternative transformer designs which should require less precision in substrate alignment and dimensional control of the conductors. The single-section transformer requires use of a 198-mil-wide line with a 200-mil-wide channel. Besides the obvious problem of extremely tight mechanical tolerances in such a structure, one will also encounter excessive losses, and possibly electrical breakdown, because of the high electric field in the narrow gap between the microstrip conductor and the channel wall. The three-section transformer accomplishes the desired matching to the diode impedance without requiring any line impedance lower than 25 ohms. The overall bandwidth of the three-section transformer can be made greater than that of the single-section transformer, and the precision required for the 176-mil-wide lines will certainly be less. Some price is paid in overall size, however. The series capacitive gap, followed by a length of 50-ohm line, is in many ways the most attractive matching network. Only 50-ohm lines need be printed, and the capacitive gap provides DC isolation from the remainder of the microstrip circuit. This isolation is important, because the diodes which will be connected to the ends of the 50-ohm stub lines must be independently biased. Further, the capacitance of
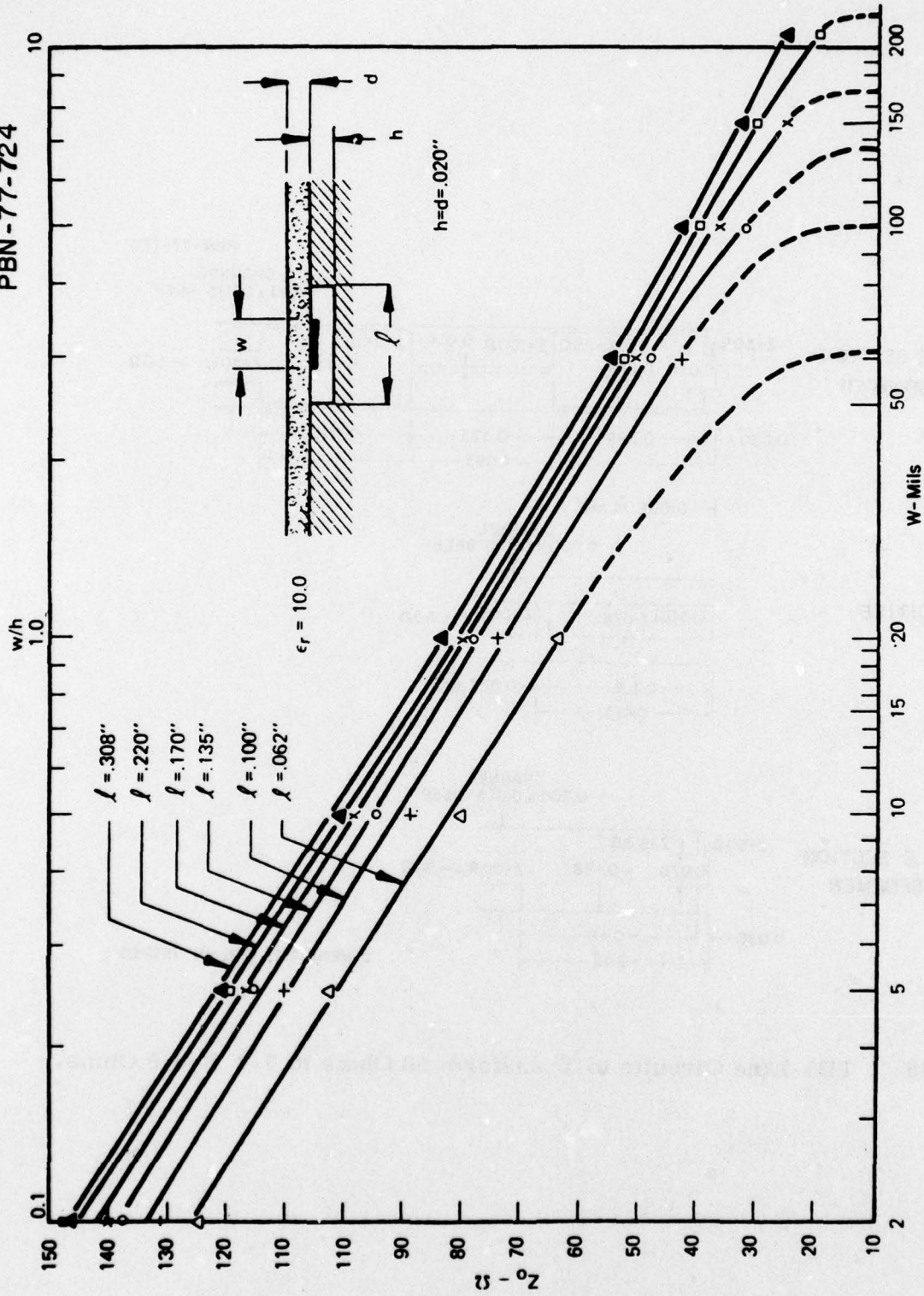
82

Figure 44   TIM Line Impedance as a Function of Line Width for Several Different
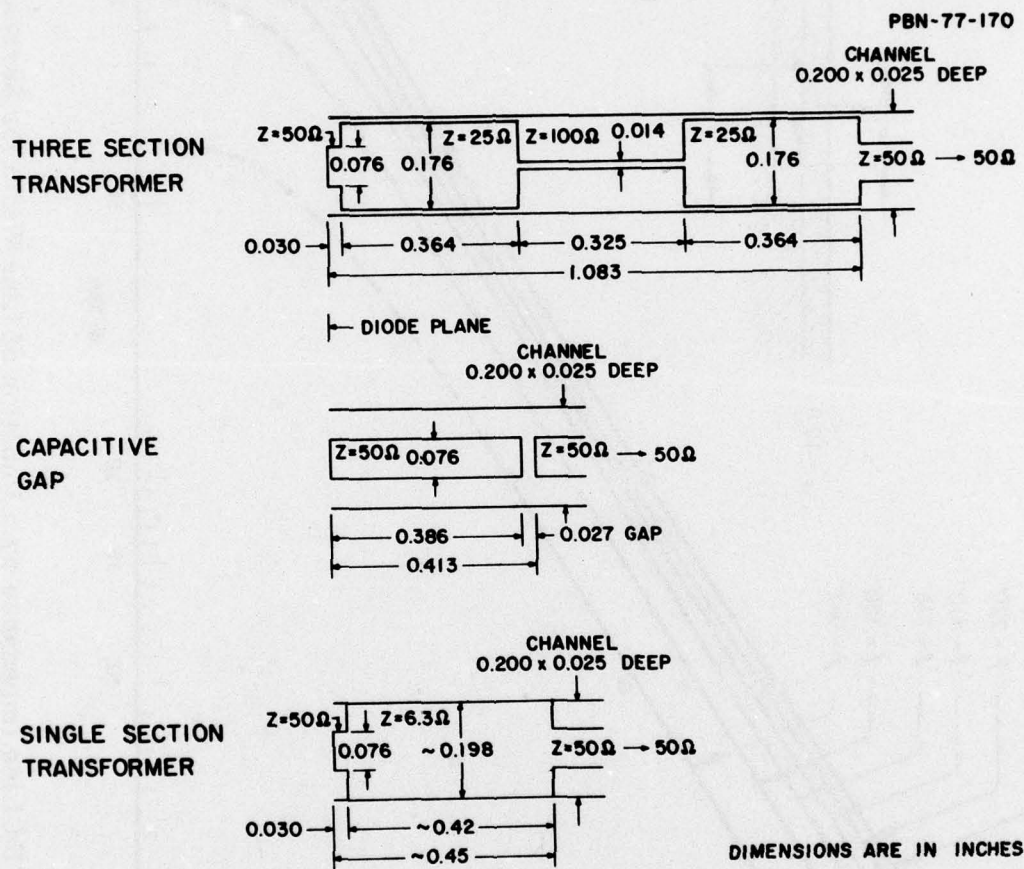Channel Widths. A channel depth of 20 mils has been assumed.

83

Figure 45   TIM-Line Circuits to Transform 50 Ohms to 0.8 + j6.0 Ohms.

the gap is so small that it prevents the external RF circuit from having any appreciable loading effect which would lower the bias circuit impedance. This helps to promote stability against bias circuit oscillations.

While any of the circuits shown in Fig. 45 could provide the required impedance at the diode terminals, none includes any provision for tuning after fabrication. Tuning is most easily implemented in the capacitive gap circuit, which can be adjusted by adding variable shunt capacitances spaced a finite distance on either side of the gap. The required shunt capacitances can be formed either by inserting tuning screws into the channel through the ground plane, or by adding variable stub lines perpendicular to the main TIM line. Smooth control of the stub line electrical length can be achieved by sliding dielectric slugs in the TIM-line channel.

Figure 46 shows the impedance range which can be obtained at the diode terminals by adjusting the shunt capacitors (formed with tuning screws or stub lines) in a "series-gap" oscillator circuit operating at 5 GHz. The nominal center of the impedance range is $0.8-j6$ ohms, the circuit impedance required by typical high-power diodes developed during the previous program. The circuit model used for obtaining the impedance values is also shown in the figure. For this preliminary analysis, line lengths appropriate to a relative dielectric constant of unity were used. Note that nearly independent adjustment of the real and imaginary parts of Z is possible, with C_2 controlling Im $[Z]$ and C_1 controlling Re $[Z]$.

Tuning screws would be likely to provide rather erratic control of the circuit impedance, both because of the difficulty in maintaining good electrical contact between the screw and the ground plane, and because of the extremely nonlinear tuning rate. For example, if a 0-80 machine screw is used for the tuning element in the circuit of Fig. 46, most of the available tuning range is compressed into the last quarter turn before the screw contacts the TIM-line conductor. For these reasons, adjustable stub lines were selected as tuning elements in the TIM-line oscillators actually constructed.
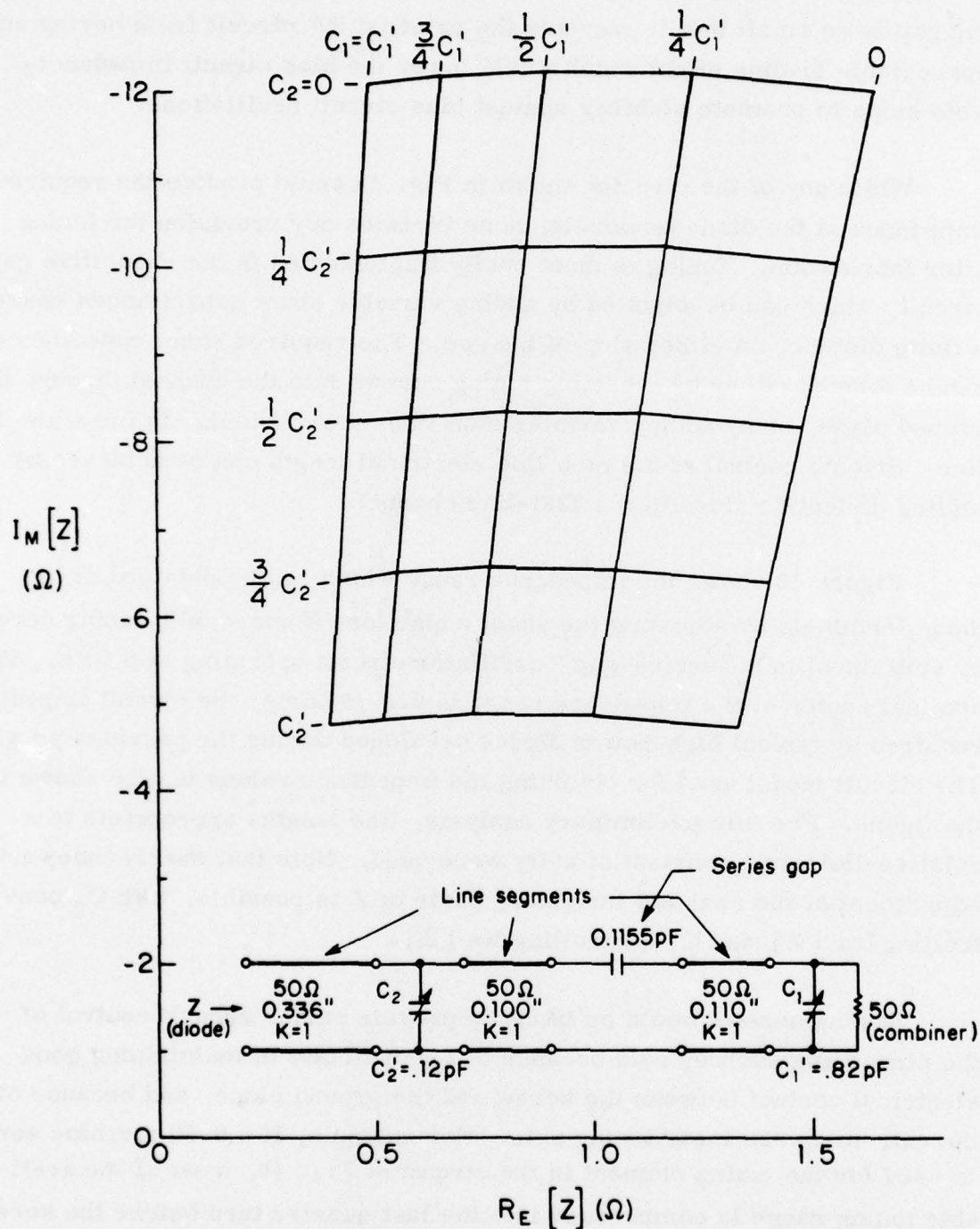
Figure 46   Impedances Presented to the Diode Terminals in a Series Gap TIM-Line Oscillator Circuit Having Shunt Capacitors for Tuning.

86

A number of changes and additions were required in the circuit design of Fig. 46 before a practicable TIM-line oscillator could be constructed. First, the characteristic impedance of the line segment containing the diode was reduced from 50 to 25 ohms to lower the losses in this high-VSWR portion of the circuit. Second, the stub lines serving as tuning elements had to be moved farther apart because it was not possible to place 200-mil-wide TIM-line channels at the center-to-center spacing called for in the original design without overlap. After this change, both capacitive and inductive values of the shunt tuning elements, easily realized with stub lines, were required to achieve the necessary range of circuit impedance at the diode location. Finally, a three-section TIM-line bias choke was designed to isolate the RF portion of the circuit from the external bias source.

Figure 47 shows the circuit model for the RF portion of the first TIM-line oscillator module actually constructed during the program. The line lengths and relative dielectric constants indicated apply to the actual circuit. Also shown is the impedance range that can be covered by adjustment of the shunt tuning elements. The available range of circuit adjustment is more than sufficient to accommodate the new large-area four-mesa IMPATT diodes. The adjustable shunt "capacitors", which assume both capacitive and inductive values of reactance, are made by sliding alumina slugs in the channels of TIM-line stubs. There is a step change, from 50 Ω to 25 Ω, in the characteristic impedance of the main TIM-line on the load side of the series capacitive gap. This is accomplished by changing the width of the printed TIM-line conductor.

Figure 48 shows the circuit layout for the first TIM-line module. The basic series-gap RF circuit, adjustable stubs for tuning and bias decoupling network are formed on a 2 x 2 in^2 alumina substrate.

The actual oscillator module is shown in Fig. 49. The diode is connected to the circuit through a gold strap thermocompression bonded

87
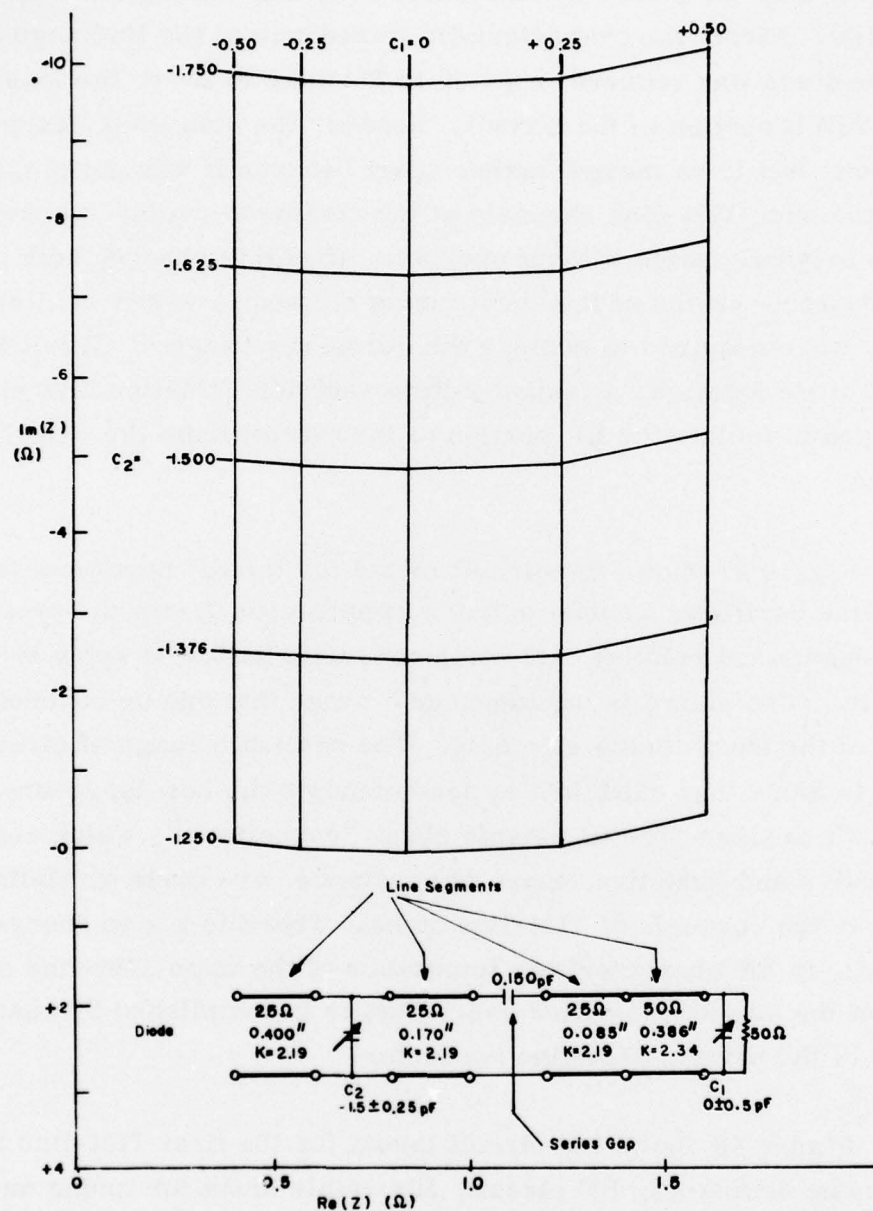
Figure 47   Model for the RF Portion of the Circuit Actually Used in the First TIM-Line Oscillator Module. Also shown are the different impedances which can be presented to the diode terminals by adjusting the shunt tuning elements.

88

Oscillator ground Plane Channels ☐

Oscillator Ground Plane Land ▨

Bias Input

Diode

RF Output

TIM Conductor ▨

Tuning Stubs

|← 1" →|

Gap used in modified circuit

Figure 48   Layout of the First TIM-Line Oscillator Module. The gap
adjacent to the diode was later inserted as a modification
of the circuit.

89
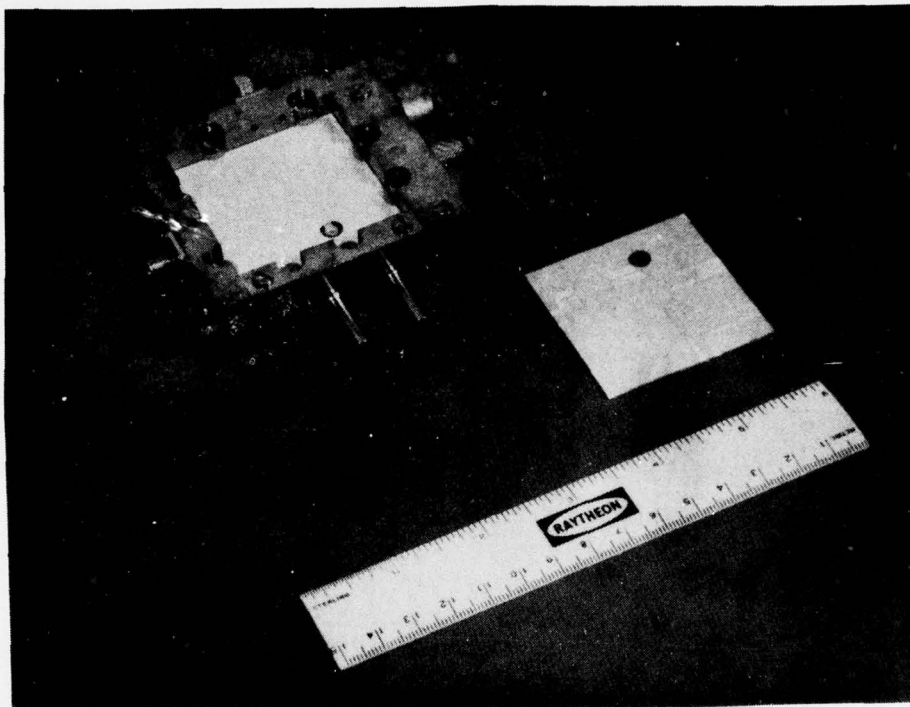
Figure 49   Picture of the First TIM-Line Oscillator Module.

both to the circuit and the diode top cap. An alumina disc (not shown) can be inserted into the diode hole to minimize the discontinuity in line impedance. The two knurled knobs operate the drive mechanism which moves the dielectric slugs that serve to adjust the stub lines. Bias input and RF output are through the SMA connectors. The module is water-cooled to allow for long-term laboratory operation without significant temperature rise.

Initial test results obtained from the TIM-line oscillator circuit were disappointing. The circuit was designed for operation at 5 GHz, but oscillated between 3 and 4 GHz in its original configuration. The two built-in tuning elements did not have the expected effects on the circuit. The adjustable stub line controlling the imaginary part of the impedance presented to the diode did exert a strong effect on the frequency of oscillation. However, the line controlling the real part of the impedance did not change output coupl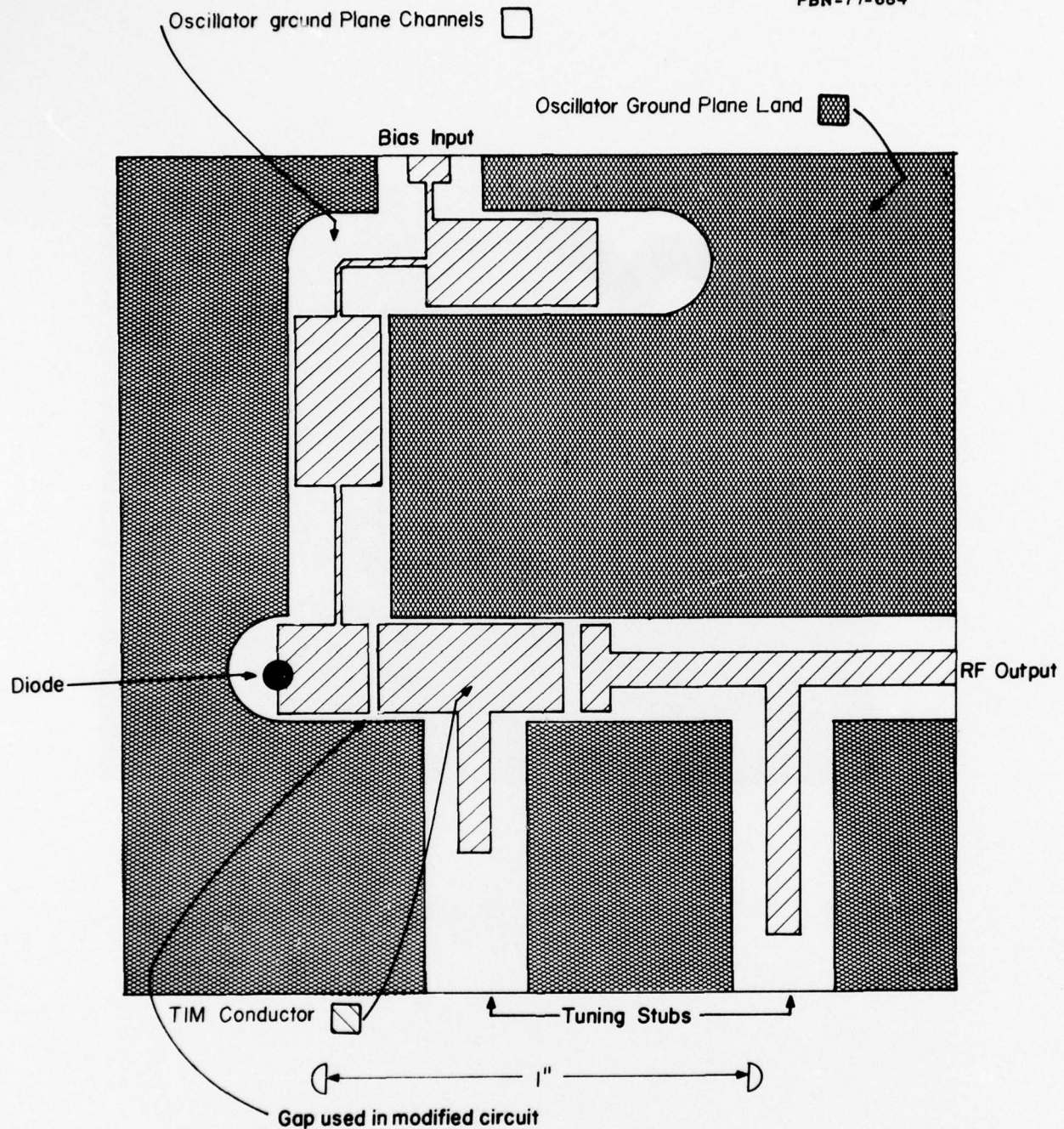ing in a systematic way. By adding additional tuning elements (metallic overlays on the TIM-line circuit), it was possible to obtain over 6W CW output from one oscillator at 5 GHz. This was substantially less than the 14-15 W CW output which the GaAs Read IMPATT diodes used had demonstrated in earlier tests. One positive feature was that the TIM-line oscillator was relatively free from bias circuit oscillations such as those which had limited the simple coaxial oscillator circuit in which impedance measurements had first been attempted.

In an effort to find the reason for the 3-GHz oscillation in the first TIM-line oscillator, the impedance presented to the diode was computed for frequencies from 2 to 8 GHz. Results are shown in the Smith-chart plots of Fig. 50. These show a substantial region of low impedance in the 2 to 3 GHz range which could produce an oscillation. Except for the desired reasonance at 5 GHz, there are no other frequencies at which the circuit impedance becomes low enough to cause oscillation.

By additional circuit analysis, it was found that the low-frequency behavior of the first TIM-line oscillator could be modified. Adding a second capacitive gap as shown in Fig. 48, and using a short-circuited
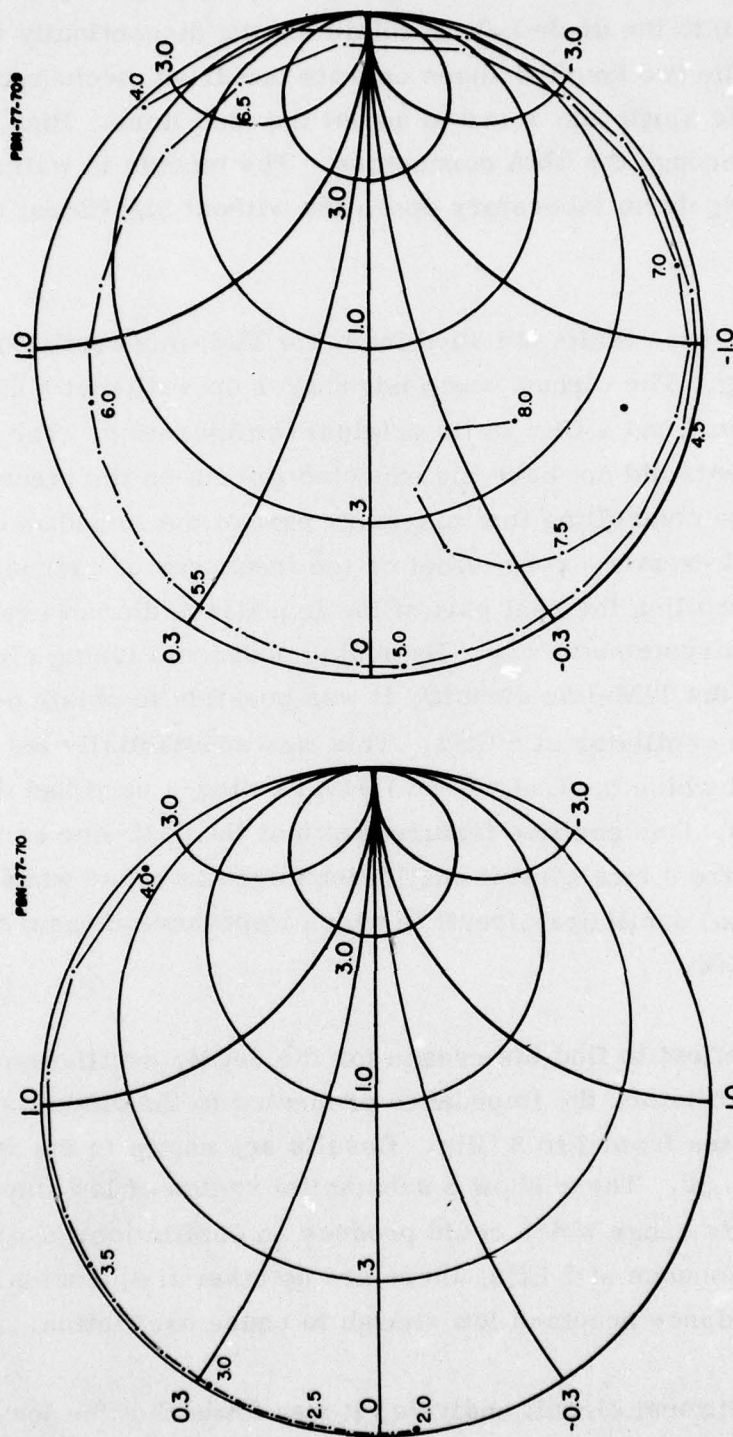
PBM-77-709

PBM-77-710

Figure 50   Smith Chart Plots of the Impedance Presented to the Diode Terminals in the First TIM-Line Oscillator Module. The separate charts cover the ranges 2 - 4 and 4 - 8 GHz.

92

rather than a dielectrically-loaded stub line for the tuning element nearest the diode (C_2 in Fig. 47), one obtains the impedance behavior shown in Fig. 51. The Smith charts show the impedance presented to the diode over the range 1 to 10 GHz. The broad, low-frequency resonance of Fig. 50 has been replaced by a relatively high-Q high-impedance resonance. This provides less opportunity for the diode to oscillate at low frequency. The desired impedance is still presented to the diode at 5 GHz. There is another low impedance region between 7 and 8 GHz, but this is well above the normal operating frequency for the diodes used, and does not produce a spurious oscillation.

Tests of the modified TIM oscillator showed that there was less tendency toward the low-frequency (3-4 GHz) oscillation found in the first tests. Additional tuning elements were still required to produce any substantial power output at 5 GHz. Also, a substantial amount of direct radiation was found to occur from the TIM circuit. The strongest radiation was from regions of high electric field, particularly those near the capacitive gaps. Overall, the performance of the modified circuit was considered unsatisfactory.

The complex, multiply-resonant behavior of the series gap circuit was thought to be one possible reason why such discontinuous tuning and generally unsatisfactory performance were obtained. A smoother impedance function is available in the three-section transformer circuit (see Fig. 45), and better results should have been possible with that design. Accordingly, the original TIM-line oscillator was modified to the form shown in Fig. 52. The RF portion of the circuit used a three-section transformer to produce the desired impedance at the diode terminals. Some impedance adjustment could be obtained by sliding dielectric slugs into the main line through the two perpendicular channels, or by moving metallic overlays on top of the TIM-line substrate. The bias circuit was modified to make its decoupling action independent of the impedance of the external bias system. This was done by feeding bias into a two-section choke along a 50-ohm line segment having a built-in termination. The termination was frequency-dependent,
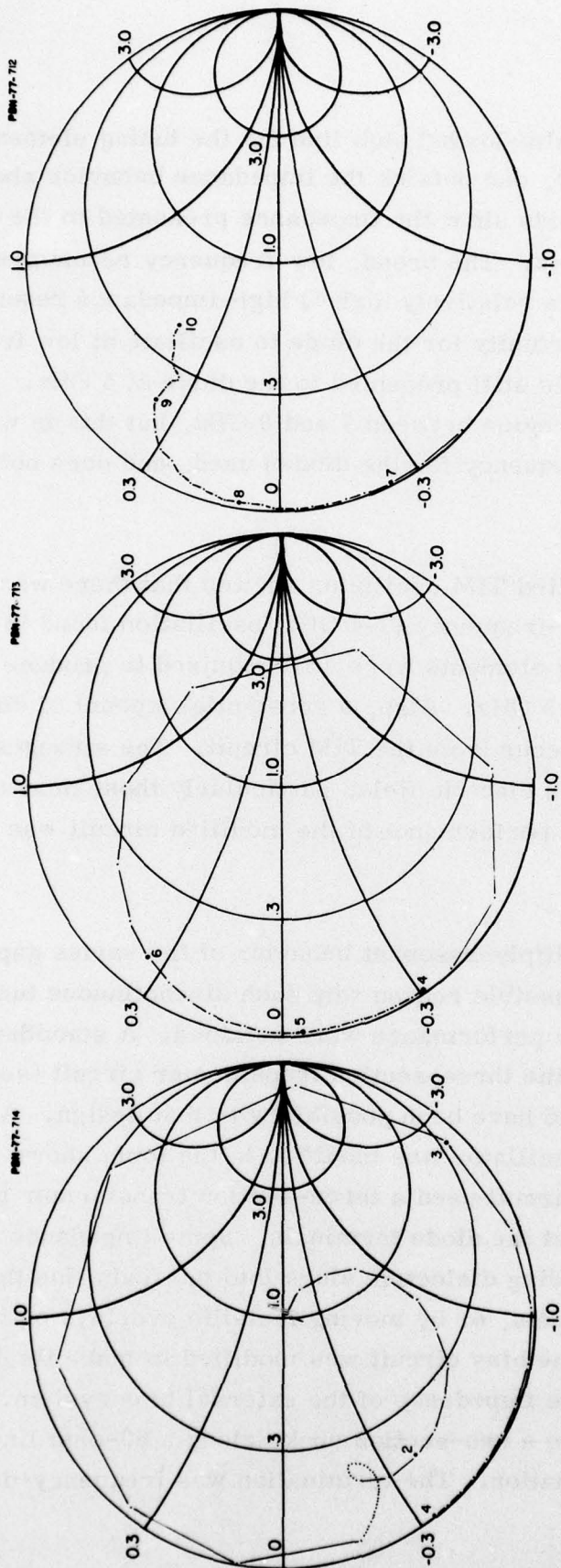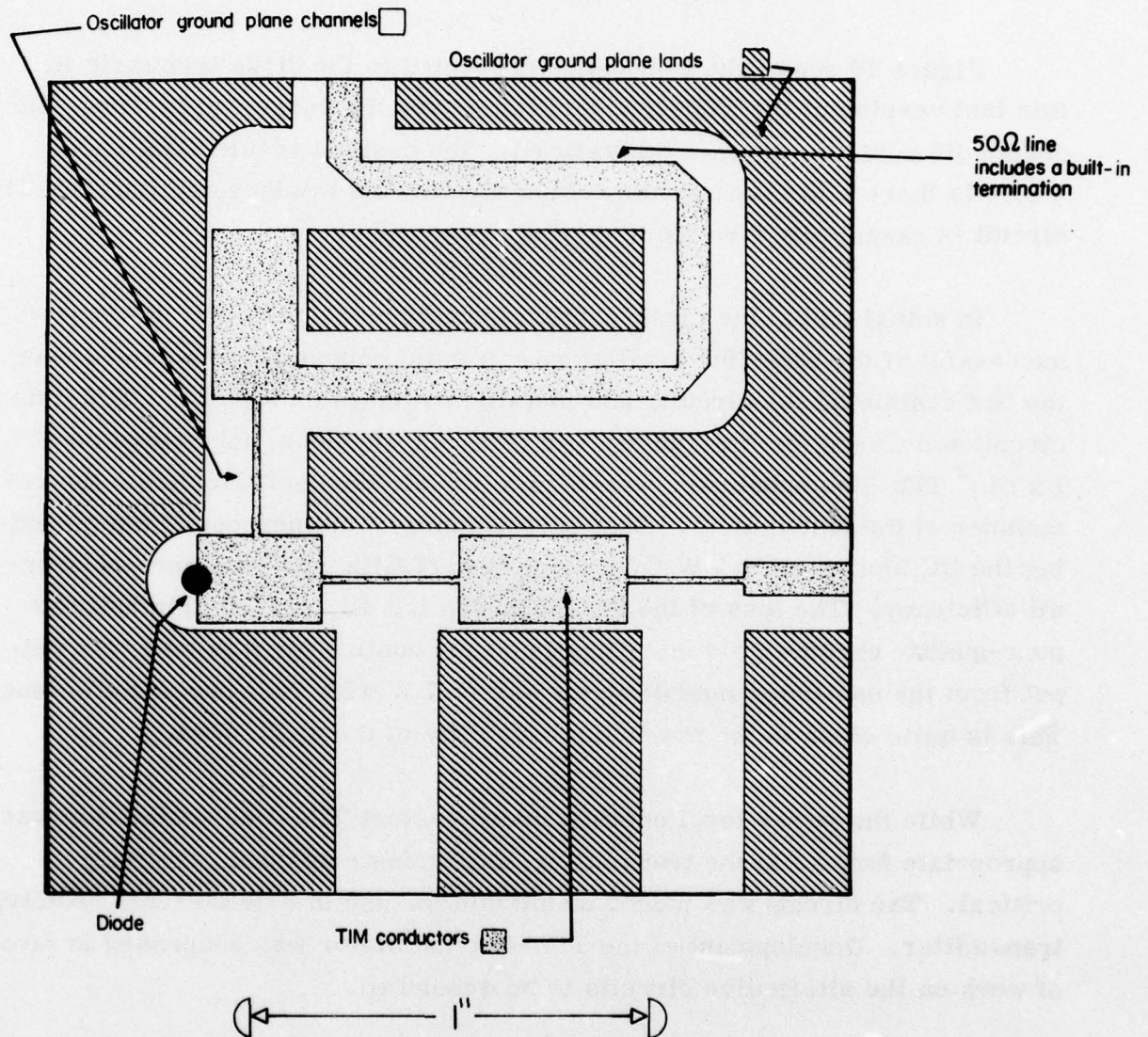
Figure 51   Smith Chart Plots of the Impedance Presented to the Diode Terminals in the Modified (Two-gap) TIM-Line Oscillator Module. The separate charts cover the ranges 1 - 4, 4 - 6.8, and 6.8 - 10 GHz.

Figure 52　Layout of TIM-Line Oscillator Circuit Using a Three-Section Impedance Transforming Network.

and gradually approached an open-circuit condition at low frequencies. The new circuit did not have the series gap to provide DC isolation from the remainder of the power-combining structure. Consequently it was necessary to provide an external DC block in series with the RF output during testing.

Figure 53 shows the impedance presented to the diode terminals in this last version of the TIM-line oscillator over the range 1 to 10 GHz. The design did achieve, at least theoretically, the desired result. Only near 5 GHz is there a low-impedance region which could produce oscillation. The circuit is essentially free from spurious resonances.

In actual tests, the three-section transformer design was the most successful of the TIM-line oscillators. A solid copper lid was placed over the box containing the circuit, and metallic overlays on top of the TIM-line circuit were used for fine tuning. An external DC block, fabricated on a $1 \times 1 \text{ in}^2$ TIM-line substrate, was used to isolate the oscillator from the remainder of the test system. Best performance of the new oscillator including the DC block was 11.7 W CW output at 4.77 GHz with 18.4 percent overall efficiency. The loss of the DC block was 1.3 dB, caused primarily by poor-quality chrome-gold metallization. Accounting for this loss, the output from the oscillator module itself was 15.7 W with 24.8 percent efficiency. This is quite close to the maximum capability of the diode used.

While the power level obtained from the last TIM-line osciallator was appropriate for use in the transmitter, the tuning remained extremely critical. The circuit was judged unsuitable for use in a deliverable prototype transmitter. Development of the TIM-line oscillator was suspended in favor of work on the alternative circuits to be described.

The reasons for the lack of success of the TIM-line oscillator are not fully understood. Some further effort should be directed toward the identification and solution of the actual problems, since it would be worthwhile to obtain a fully integrated power-combined output stage for the transmitter. A number of possible problem areas have been identified which could provide
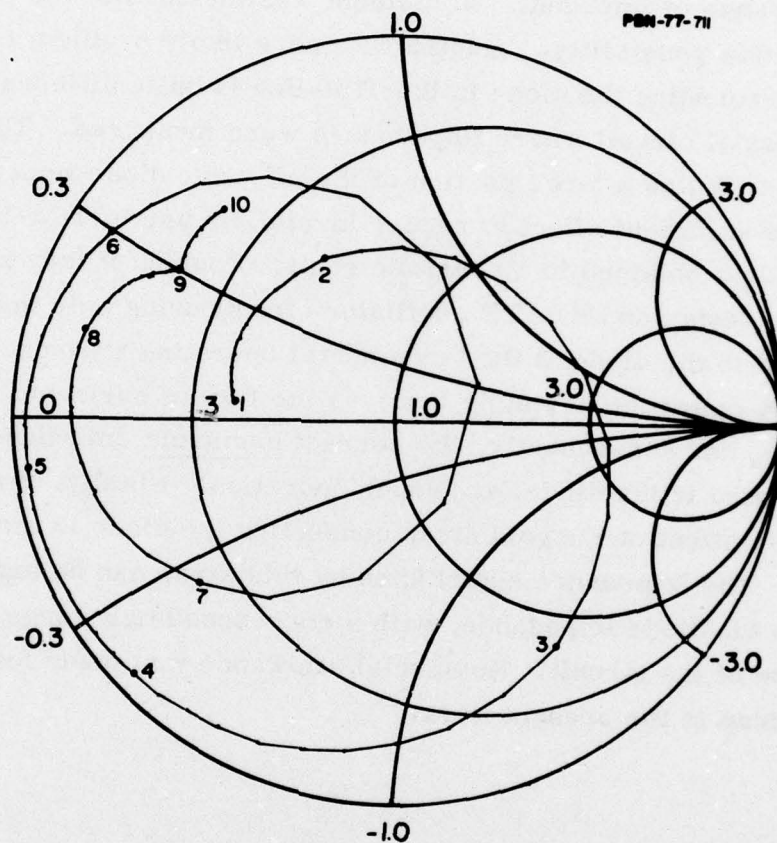
Figure 53   Smith Chart Plot of the Impedance Presented to the
             Diode Terminals in the TIM-Line Oscillator Using
             the Three-Section Impedance-Transforming Network.
             The frequency range 1 - 10 GHz is included.

97

starting points for a future investigation. First, it may not be possible to obtain the low impedances required by the diodes through an <u>efficient</u> TIM-line transformation. This could provide a limitation on available power output. Next, it is possible that the measurements of diode impedance were not made with sufficient accuracy to produce a correct circuit design. However, a range of impedance adjustment was included in the early designs to offset this possibility. A third and more likely problem is that the space surrounding the diode in the TIM-line is quite different from that in the coaxial circuit where impedances were measured. This surrounding space contributes a large portion of the effective diode impedance, and may have sufficient effect to render invalid for use in TIM-line the impedance data obtained in a coaxial circuit. Fourth, it may not be sufficient to design an IMPATT oscillator circuit using only the impedances presented to the diode at the fundamental operating frequency. High-efficiency operation certainly involves the flow of harmonic currents in the diode, and consequently, the correct <u>harmonic</u> impedances must also be presented to the diode for proper operation. Finally, it is difficult to model the effect of the gold strap connecting the diode to the TIM-line circuit. The impedance contributed by this strap can be significant compared to the diode impedance, with a correspondingly large effect on the operation of the circuit. No special allowance was made for the effects of the strap in the present work.

3.2.3.3   Slug-tuned coaxial oscillator module

As the difficulties with the TIM-line oscillator module became apparent, work was started on two alternative circuits which showed promise of meeting the requirements for the transmitter output stage. The first of these was the slug-tuned coaxial oscillator, shown schematically in Fig. 54. This circuit was derived from similar circuits which had been used with small-area IMPATT diodes at frequencies higher than 5 GHz. Development of the new 5-GHz circuit operating with four-mesa diodes was almost entirely empirical.

In the circuit of Fig. 54, the diode is mounted at one end of a 0.290 in. diameter coaxial line. A fixed quarter wave transformer incorporating an integral DC block is placed on top of the diode. Bias is fed to the diode along this transformer through a high-impedance ferrite-loaded coaxial line. The principal adjustable tuning element is the sliding two-section transformer. Once the fixed transformer and the depth of the recess in which the diode is mounted have been chosen, the sliding transformer provides an adjustment of the operating frequency of the oscillator. The circuit, pictured in Fig. 55, is water-cooled to allow long-term laboratory operation without significant temperature rise.

In initial tests of the slug-tuned coaxial oscillator, some problems with bias circuit oscillations were encountered. These were overcome by the use of an additional lumped-element decoupling network which was mounted in the small Pomona box bolted to the side of the RF circuit. Observations with a low-frequency network analyzer verified that there were no regions of low bias circuit impedance for frequencies out to ∼ 500 MHz. With the bias circuit problems corrected, first tests of the oscillator produced 5.6 W CW output at 4.4 GHz with 14 percent efficiency.

Several iterations of the design of the transformers followed these initial tests, with the objective of raising the frequency, efficiency, and power output of the oscillator. During this development work, the operating voltage of the diode at a specific bias current provided a useful indication of
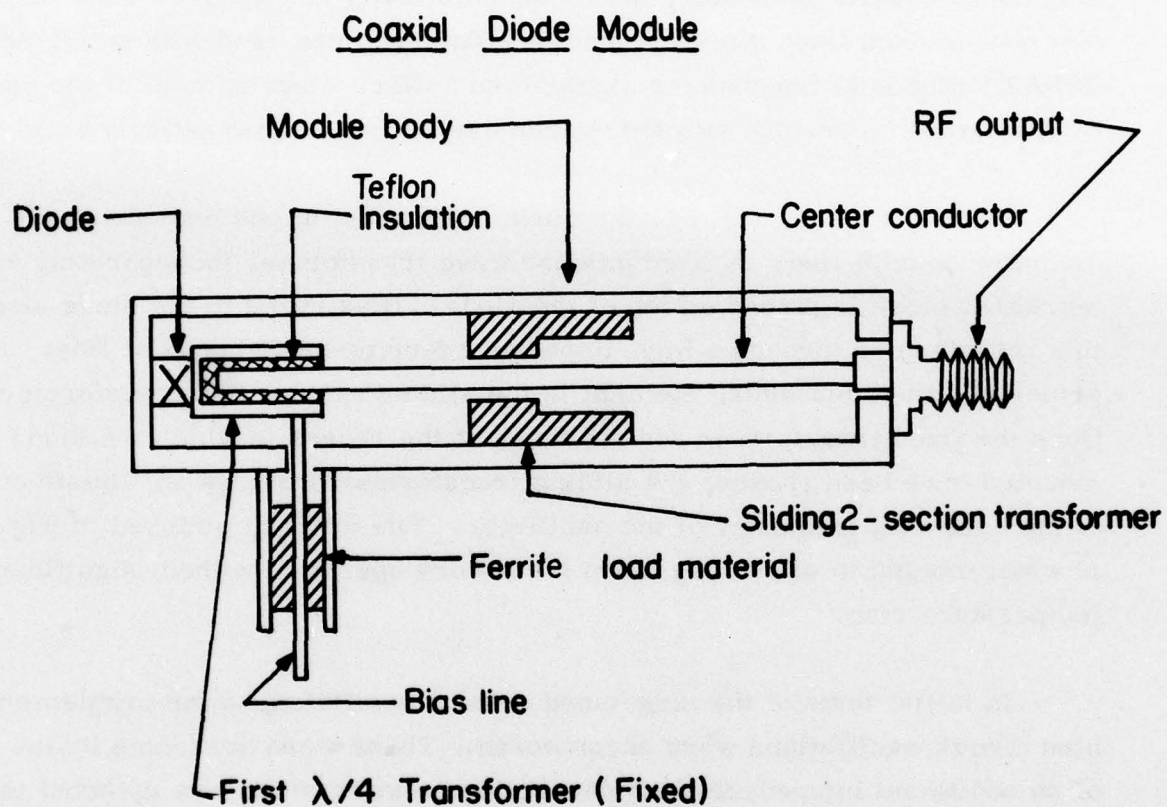
99

Coaxial Diode Module

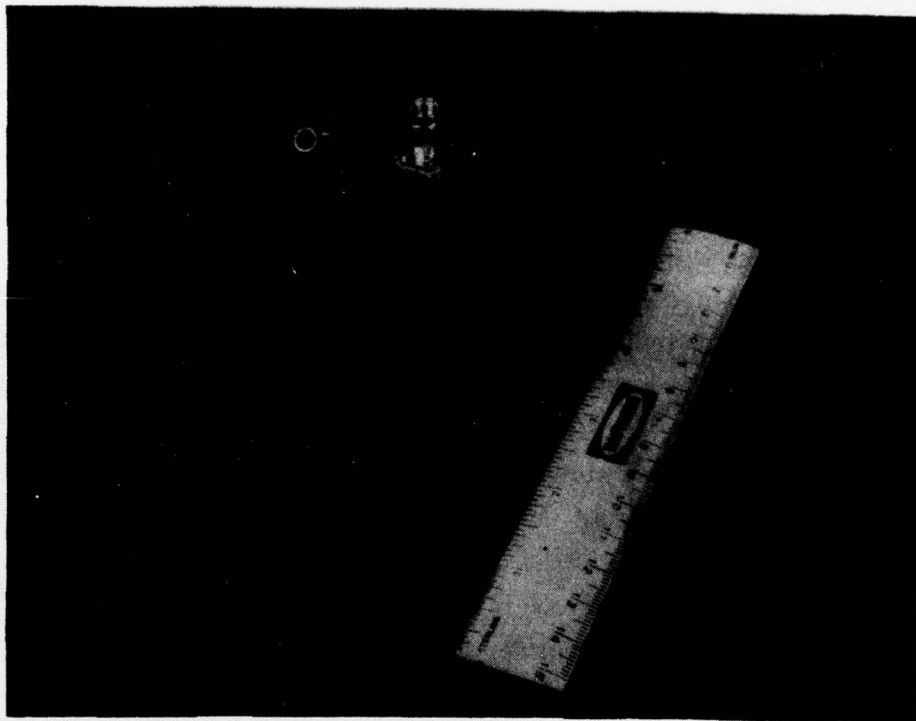Figure 54   Slug-Tuned Coaxial Oscillator Module.

Figure 55   Photograph of Multiple-Slug Coaxial Oscillator
Module.

the approach to correct tuning of the oscillator. (See Sections 3.2.2.3.1 and 3.3.) Ultimately, a power output of 9.5 W CW at 5 GHz with 20 percent efficiency was obtained from the oscillator. This was about 0.9 dB less power than had been produced by the same diode in the top-hat oscillator with the same bias conditions. The oscillator could be tuned over a range ~400 MHz wide centered on 4.95 GHz by moving the two-section slug transformer. Injection-locking experiments showed that the oscillator operated with an external Q of ~35, sufficiently low to allow an electronic tuning range of somewhat more than 60 MHz in the transmitter output stage. Turn-on of the oscillator was accomplished simply by bringing the bias current up from zero to the normal operating level. There were no bias circuit oscillations during ordinary operation of the module.

While the slug-tuned coaxial oscillator module came close to meeting the requirements for the transmitter output stage, it had a number of short-comings. These led us to hold the circuit as a back-up for possible use in the transmitter while development work proceeded on the coaxial cavity oscillator described in the next subsection. The greatest problem with the circuit was that its power output and efficiency were significantly lower than those of the top-hat oscillator. Losses in the bias line, which is coupled to the RF circuit at a point of nonzero RF voltage, and dissipation in the dielectric of the DC block in the first transformer are probably responsible for most of this efficiency reduction. Further refinement of the circuit with the objective of reducing these losses would probably raise efficiency. Another limitation of the circuit was that the dimensions of the first transformer often had to be changed when diodes were changed in order to maintain optimum performance. This could be tolerated in the laboratory situation, but would probably not be acceptable in cost-sensitive large-volume production, where diodes with a relatively wide range of characteristics might have to be accommodated. A final feature of the circuit, one that might prove a drawback where low-cost fabrication is required, is that a very smooth and precise outer diameter must be maintained in the coaxial line to permit the two-section transformer to slide smoothly. This requires machining which is more precise and costly than a simple drilled hole.

102

3.2.3.4 Coaxial cavity oscillator module

The coaxial cavity oscillator module, developed toward the end of the program, was selected for use in the deliverable transmitter. Its overall performance was the best among the oscillators evaluated. Like the slug-tuned coaxial circuit, the design for this oscillator was derived from an X-band prototype. Development of the 5-GHz version was largely empirical.

Figure 56 gives a schematic representation of the coaxial cavity oscillator. The diode is mounted at the end of a coaxial line slightly less than $\lambda/2$ long. Neither the length nor the characteristic impedance of this line appears to be extremely critical. During development work, electrical lengths from 0.29λ to $.45\lambda$ and characteristic impedances from 87 to 116 ohms were used successfully. A disc resonator is placed on top of the diode. This provides a coarse adjustment of the operating frequency, with larger diameters being used at the lower frequencies. Fine adjustments of the frequency are made with a metallic tuning screw placed $\lambda/4$ from the end of the coaxial section. In this position, maximum tuning effect is obtained. Output coupling is obtained through an electric field probe placed $\lambda/8$ from the end of the coaxial section, and adjustments in coupling are made by turning the threaded output connector to change the probe position. Locating the probe at the $\lambda/8$ position causes a minimum change in cavity frequency as the probe is adjusted. Bias voltage is applied to the diode along the co-axial center conductor. Isolation between the RF circuit and the external DC bias supply is provided by a 3-section choke. The choke, which is effective over a wide range of frequencies, is designed for low capacitance to reduce the possibility of bias circuit oscillations. Like the other oscillator modules, the coaxial cavity circuit, pictured in Fig. 57, is water-cooled to permit extended periods of laboratory operation without significant temperature rise.

Tuning of the coaxial cavity oscillator is relatively simple. With a particular diode and disc resonator installed, the circuit is first operated with the tuning screw removed and the coupling probe set near minimum
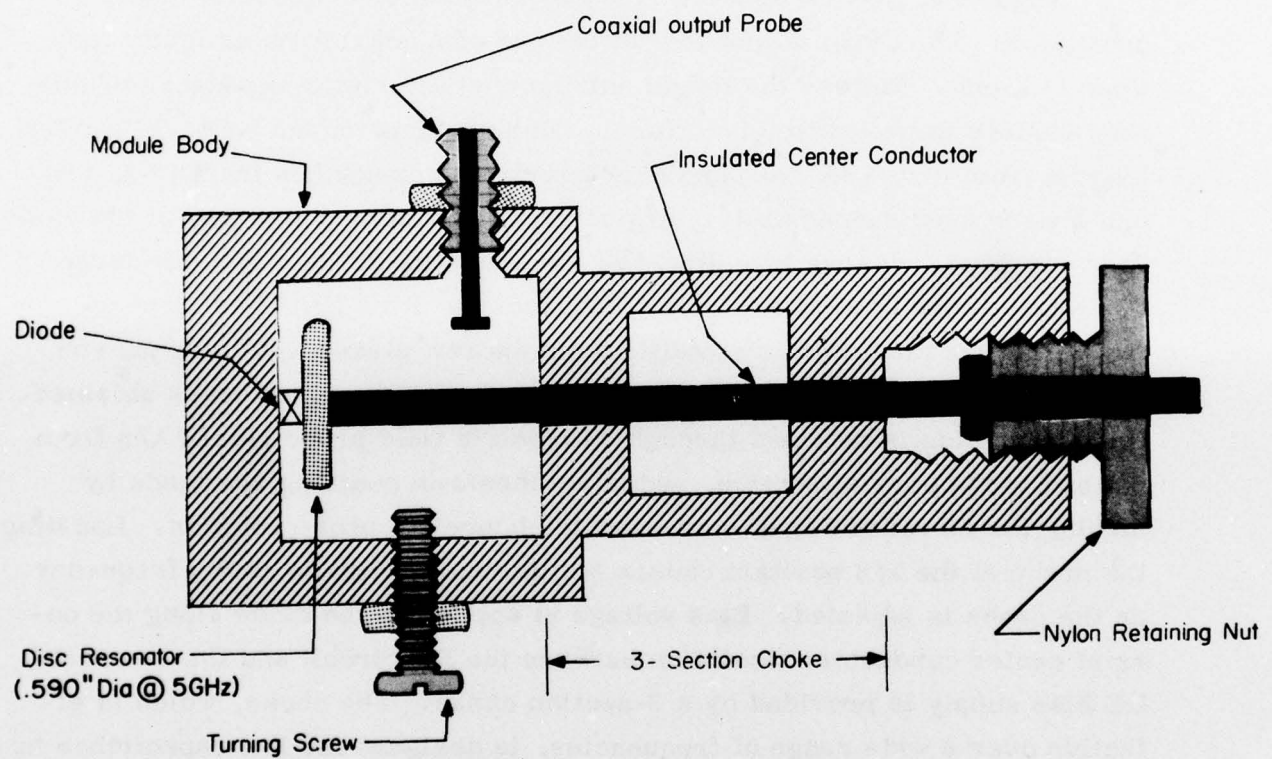
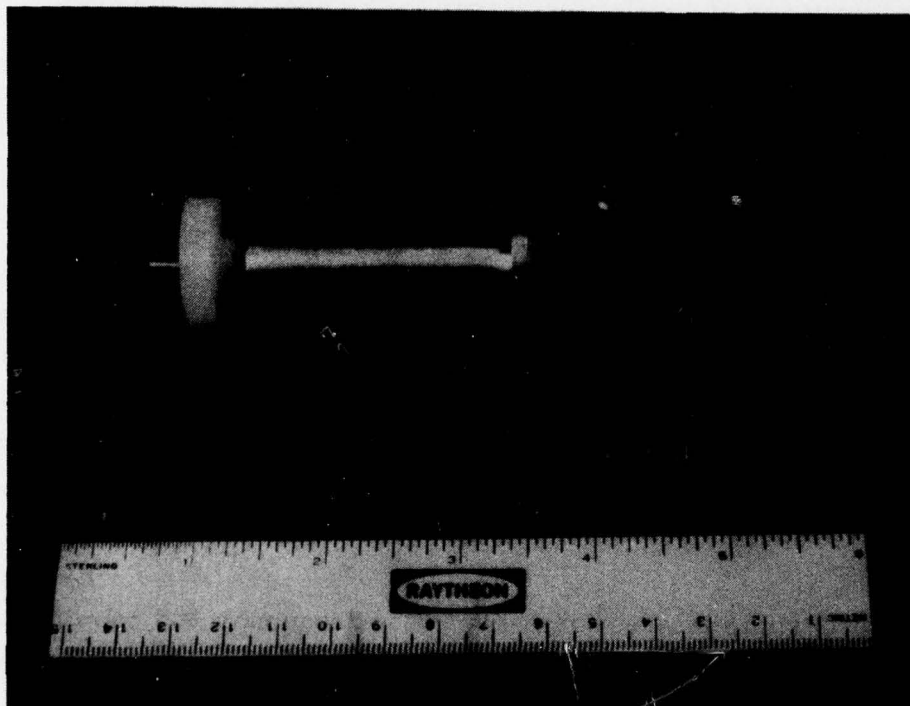Figure 56   Coaxial Cavity Oscillator Circuit.

104

Figure 57   Photograph of Coaxial Cavity Oscillator Module.

coupling. This assures starting the oscillation in the high-frequency mode. The frequency of oscillation is observed as the bias current is brought up from zero. In this undercoupled condition, the DC operating voltage of the diode is much lower than normal because the real part of the impedance presented to the diode terminals is smaller than optimum, and operation should be limited to low bias currents. However, the low current tests can be used to determine whether the size of the disc resonator should be increased or decreased to bring the frequency of oscillation closer to the desired frequency.

Ultimately, a disc resonator which, with the tuning screw withdrawn, produces a frequency of oscillation about 100 MHz above the desired operating frequency should be installed. The tuning screw can then be inserted to bring the frequency down to the desired value. The coupling probe should then be inserted farther into the cavity until the operating voltage of the diode rises to its normal value, determined in top-hat oscillator tests, at the normal operating current. Care must be taken not to push the diode to full current while undercoupled conditions still prevail, since this may provoke diode burnout. It is usually quite obvious at reduced bias current that the bias voltage is below normal, indicating undercoupled conditions, and the coupling can be increased appropriately.

There is some interaction between the frequency and coupling adjustments. However, with one or two iterations, the tuning procedure quickly converges to the correct coupling at the desired operating frequency. The only real difficulty is encountered with extremely high efficiency diodes ($\eta \sim 30$ percent). These have such a wide variation of terminal impedance between the small-signal and the large-signal condition that the tuning which gives optimum efficiency at large signal levels does not permit a normal start of oscillation as bias current is brought up from zero. Such diodes must either be tuned each time they are turned on, or operated in a slightly undercoupled condition, at some cost in power output and efficiency, in order to insure reliable starting with the application of operating bias.

106

Diodes from lots 907, 910, and 946 were tested in the coaxial cavity module. The highest power and efficiency were obtained with diodes from lot 910. The best results were 18.1 W CW output at 5.05 GHz with 29.6 percent efficiency, and 30.1 percent efficiency with 17.4 W CW output at 4.98 GHz. These diodes did require special attention in tuning as noted previously. Diodes from lots 907 and 946 could be started simply by raising the bias current from zero. A wide range of diode characteristics could be accommodated within the range of adjustments possible with the tuning screw and coupling probe. As an example, a diode from lot 910 with 3.2 pF capacitance at its 98 V breakdown, and a diode from lot 907 with 4.0 pF capacitance at its 62 V breakdown could both be tuned to 5 GHz with the same disc resonator installed. For a given diode, a frequency range of 200-300 MHz was available by adjustment of the tuning screw. The module was free from bias circuit oscillations under normal operation conditions.

Diodes from lot 946 were eventually selected for use in the deliverable transmitter. These combined smooth starting along with good power output and efficiency at 5 GHz. Reasonably good 5 GHz performance was also available from diodes in lot 907, but these required higher bias currents and lower operating voltages which made them incompatible with the existing power supply. The selected units from lot 946 were typically operated at 100 V and 525 mA, and produced 12.5 W CW Output at 5 GHz with 24 percent efficiency. This represented a very conservative operating condition. Other diodes from lot 946 had produced up to 17.5 W CW output. Operation at 12.5 W reduced the junction temperature to 175° C which is consistent with long diode life. Measurements of the external Q of the oscillator module under these operating conditions gave a value of ~ 33, sufficiently low to insure more than the required 10 MHz of locking bandwidth in the transmitter output stage. Modules were initially tuned while operating into a 50-ohm coaxial test system. Only slight readjustments of frequency were required to accommodate a small change in load impedance when the units were attached to the power combining circuit.

The design of the coaxial cavity oscillator was more conservative than proved to be necessary. The conservative approach was taken to increase the probability of success in a development effort that was conducted late in the program. It is obvious now that the cavity could be reduced substantially in size. Length could be cut by reducing the electrical length of the coaxial section to $\sim.3\ \lambda$. The one-inch-diameter bore of the cavity is much larger than necessary to accommodate the .59 in. diameter disc resonator used to reach 5 GHz. A cavity bore of 0.7 in. combined with 0.05 in. walls could reduce the outside diameter of the cavity to 0.8 in. By using a short radial-mode choke for the bias decoupling network, the overall length of the module could probably be reduced to $\sim$1.5 in. In the present situation, the bias decoupling filter actually occupies more volume than the RF portion of the circuit.

Even in its early state of development, the coaxial cavity module has shown some features which would be of value in the production of the transmitter. First, and most obvious, is the good electrical performance which contributes directly to the ease of operation and high overall efficiency of the transmitter. Second, the wide range of adjustment inherent in the design would allow it to accommodate normal manufacturing tolerances in the mechanical parts and variations in the diode characteristics. Finally, the cavity does not require any extremely precise machining, a feature which can lead to low-cost fabrication.

3.3   Multichannel Current Regulator

3.3.1   General bias circuit considerations

For bias voltages less than the breakdown voltage V_B, a reverse-biased IMPATT diode draws essentially no current. The current is a rapidly increasing function of voltage for bias voltages larger than the breakdown voltage. With this type of voltage-current characteristic, the operating point of the diode can be most smoothly controlled if bias is supplied from a current-regulated source.

The voltage-current characteristic of a high-efficiency GaAs Read IMPATT diode is quite different in the oscillating and nonoscillating states. Self-rectification of the large RF voltage across the diode tends to depress the DC operating voltage in the oscillating state. This depression may be sufficient to cause regions of incremental negative resistance to appear in the DC voltage-current characteristic of the diode. This behavior is illustrated in the curve tracer data of Fig. 58. The negative resistance may produce oscillations in the bias circuit.

Brackett[1] has given a good phenomenological explanation of the origin of the negative resistance and of the techniques required to stabilize the bias circuit. Basically, the bias circuit is stabilized by maintaining a bias source impedance that is sufficiently large to make the net bias circuit resistance (source plus load) positive under all operating conditions. Because the negative resistance may extend to frequencies above 100 MHz, stability can be assured only if the bias source impedance is kept large for frequencies well into tnis region. Passive bias networks meeting this requirement can be made, but they usually dissipate excessive amounts of power. A transistorized current regulator dissipates little power, but may not maintain high impedance into the MHz range. Efficient use of IMPATT diodes in systems usually requires a combination of active and passive bias circuit techniques.
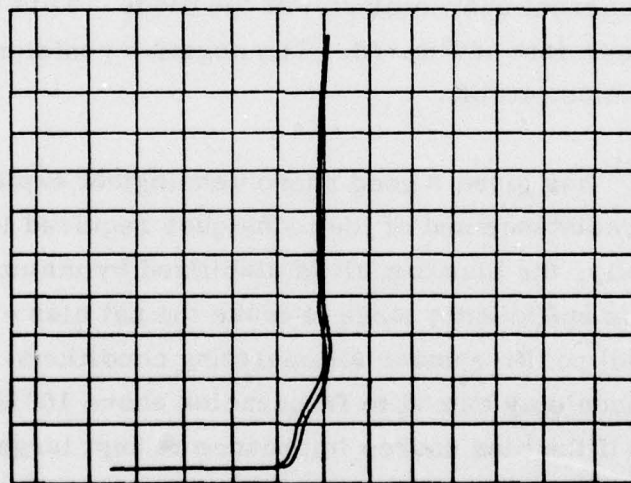
109

Diode

I

20 mA / DIV

Non oscillating

IO /DIV
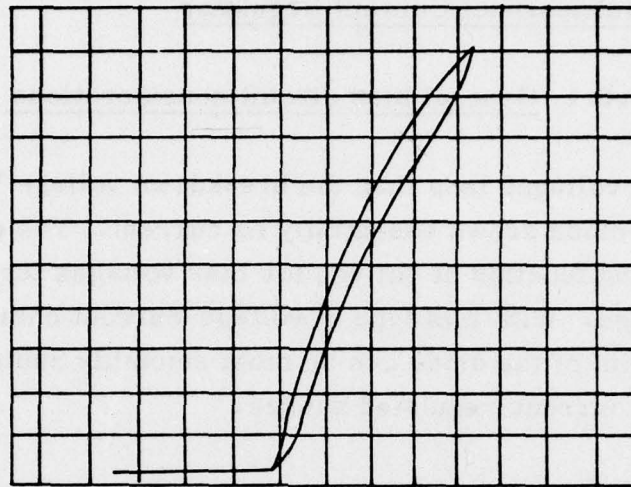
V

I

20 mA / DIV

Oscillating

IO V/DIV

V

Figure 58   V-I Characteristics of a GaAs Read Diode under
Oscillating and Nonoscillating Conditions.

110

The voltage-current characteristic of an IMPATT diode typical of the class used in the transmitter output stage is shown in Fig. 59. It was recorded under oscillating conditions. The voltage under non-oscillating conditions at the normal operating current of about 600 mA is 60 to 70 V higher than that plotted. Such a voltage produces a power dissipation which quickly causes diode failure. Consequently, operation at maximum current in the nonoscillating mode must be avoided.

The operating voltage under oscillating conditions is a strong function of the RF load impedance. Some tuning conditions may produce an operating voltage smaller than the room-temperature breakdown voltage. We can use this variation of voltage with load impedance to determine if we have achieved correct tuning of the diode, as was demonstrated in the discussion of the resonant cavity power combiner.

While the voltage-current characteristic of the oscillating Read diode may imply some stability problems, it has one feature which is of benefit in the present transmitter design. The total voltage excursion between the initial flow of current at V_B and the operating current (500-600 mA in Fig. 59) is much smaller in the oscillating state than it would be in the nonoscillating state. By choosing the injection-locked oscillator mode for the transmitter output stage, we guarantee that the diodes will always be in the oscillating state. Since the nonoscillating state never has to be accommodated, a current regulator with smaller voltage compliance, operating from a lower-voltage primary power supply, can be used. With less voltage drop across the regulator, it will dissipate less power, and the overall system efficiency will be higher.

In our work with active current regulators, we have found that an absolute minimum of 3 to 5 V across the regulator is required if control is to be maintained. Lower voltages result in saturation of the series pass transistors and loss of regulation. For the diode characteristic shown in Fig. 59, current control can be maintained through turn-on as the bias current is brought up from zero, provided a primary supply 3 to 5 volts above V_{max} is used.

111
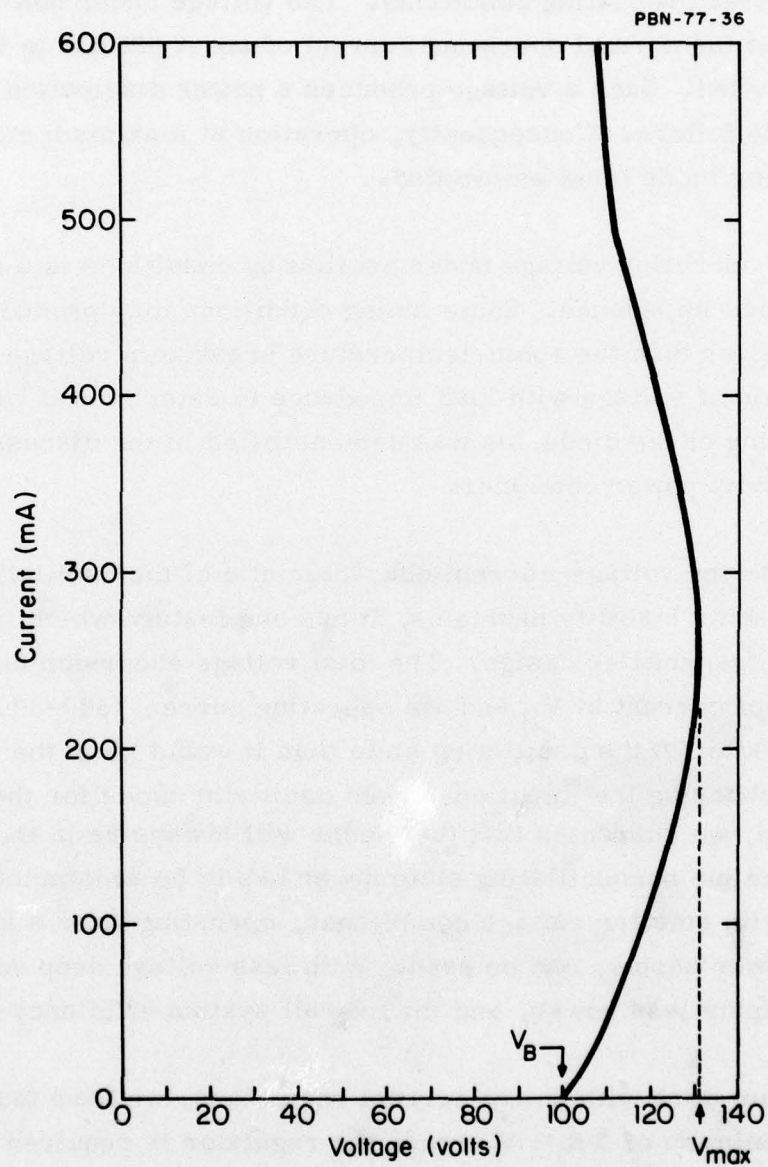
Figure 59 Voltage-Current Characteristic, Recorded under Free-Running Oscillating Conditions, of a High-Power GaAs Read IMPATT Diode Typical of Those Used in the Transmitter Delivered.

112

For the diodes from lot 946 actually used in the transmitter, V_{max} under free-running oscillating conditions was 110-112 V. The output of the inverter could be set to approximately 121 V, the minimum available, while retaining a comfortable margin in regulator voltage drop during turn-on. This resulted in a voltage drop of 22-23 V across the regulator during normal operation, representing nearly 50 W of dissipated power.

An unexpected feature of injection-locked oscillator behavior was discovered which will make it possible to reduce the DC voltage output of the inverter substantially and improve overall transmitter efficiency in future designs. If the output stage is turned on with the RF locking signal already applied, then V_{max} is reduced significantly even though the operating voltage at full current is essentially unchanged. As a specific example, for the lot 946 diodes in the transmitter, V_{max} was typically 102-103 V during turn-on with the locking signal applied. With 3V minimum drop across the current regulator, an inverter output of 105-106 V would insure proper turn-on. With diodes operating at 99-100 V, and ~ 6 V drop across the regulator, the regulator would dissipate only about 12 W. This saves ~ 40 W of inverter output capability which, given the 67 percent efficiency of the present inverter, would reduce the current drain from the 28 V prime power source by ~ 2 A.

3.3.2 Bias requirements

The transmitter design originally proposed used five diodes in the output stage. Each was to be capable of 10.7-W CW output with 23 percent efficiency at 5 GHz. When combined in a circuit having 70 percent efficiency, these diodes would produce 40-W output. Each of the five diodes would have required 465 mA of bias current at the 100 V (nominal) operating voltage, and total power consumption projected for the output stage was 232 W. The current regulator feeding the output stage would have to have five outputs capable of at least 465 mA.

By the time the Interim Report for this program had been prepared, diodes with 15 W CW output were available and a four-diode output stage

113

became feasible. Projections for a 40 W output stage, with 70 percent combining efficiency were

Devices: four diodes, 14.7-W CW each, 26.5 percent efficiency

Bias: 105 V, 528 mA each diode

Total Power Consumption: 215 W.

In the actual transmitter, a combining efficiency of 75 percent was obtained, and the nominal diode efficiency was 24 percent. The typical bias conditions for the output stage were

Devices: four diodes, 12.5 W CW each, 24 percent efficiency

Bias: 98.5 V, 527 mA each diode

Total Power Consumption: 207.6 W.

The increased combining efficiency more than offset the lower-than-projected diode efficiency. Total power consumption was well below the 232 W originally forecast, and helped to recover some of the overrun which occurred in the VCO driver subassembly.

3.3.3 Current regulator circuit

A multichannel current regulator circuit suitable for use with the older 10-W diodes was described in the Technical Proposal for this program. When initial tests of the new, large-area diodes showed that operating currents of 750 mA or more were sometimes required for maximum power output, it was thought that substantial redesign of that regulator would be required. The original circuit had a 600-mA-per-channel limit on output current. Later tests showed that 15-W output at 5 GHz was typically achieved with 500 to 570 mA of bias current, which was within the capabilities of the basic original design. Slight modifications of this design were made for the regulator actually delivered.

114

Figure 60 shows the four channel regulator circuit which was used in the deliverable transmitter. For simplicity, only two of the output channels are shown explicitly. Component values are listed in Table 6. Each of the four outputs is capable of delivering up to 600 mA.

Equivalent DC source impedance of each output is ~6000 ohms. The R_{11}-L_1 combination in each output lead served to maintain a high bias circuit impedance well into the MHz range. The output channels are driven by a single master control unit containing the integrated circuit 1C-1. Adjusting the resistor R_1 changes the currents of all outputs simultaneously, and this control is used for normal turn on of the output stage. Currents of the individual diodes are adjusted independently around the nominal value by changing the settings of the potentiometers R_9. The protective circuit operating through the zener diode D_2 shuts down the entire regulator if any one of the IMPATT diodes fails to a short-circuit condition.

This protective circuit is more conservative than is necessary. The individual output stage diodes are so well isolated from each other that the failure of one diode is not sensed by the others. The circuit would be adequately protected if only the channel supplying the failed diode were shut down. Power output degradation would occur with diode failure, as described in Section 4, but the transmitter would continue to operate.

For bench operation of the transmitter, the regulator was constructed in a standard $8 \times 8 \times 10$ in^3 instrument cabinet, shown in Fig. 61. The complete assembly weighs 8.5 lbs. Separate on-off switches were provided for each channel. Water cooling of the power transistors was provided to eliminate any chance of overheating during extended laboratory operation. This construction was extremely conservative, particularly in view of the fact that reduction of the total regulator dissipation from the present 50 W to ~10 W appears likely. The interior views of the regulator in Figs. 62a and 62b show that the volume of the regulator can be reduced substantially. A four-channel regulator occupying $6 \times 3 \times 3/4$ in^3 and weighing ~1 lb. could be fabricated now using standard components. A future size and weight reduction may be possible, particularly if reduced input voltage can be used, thereby limiting the power dissipation in the regulator.

115
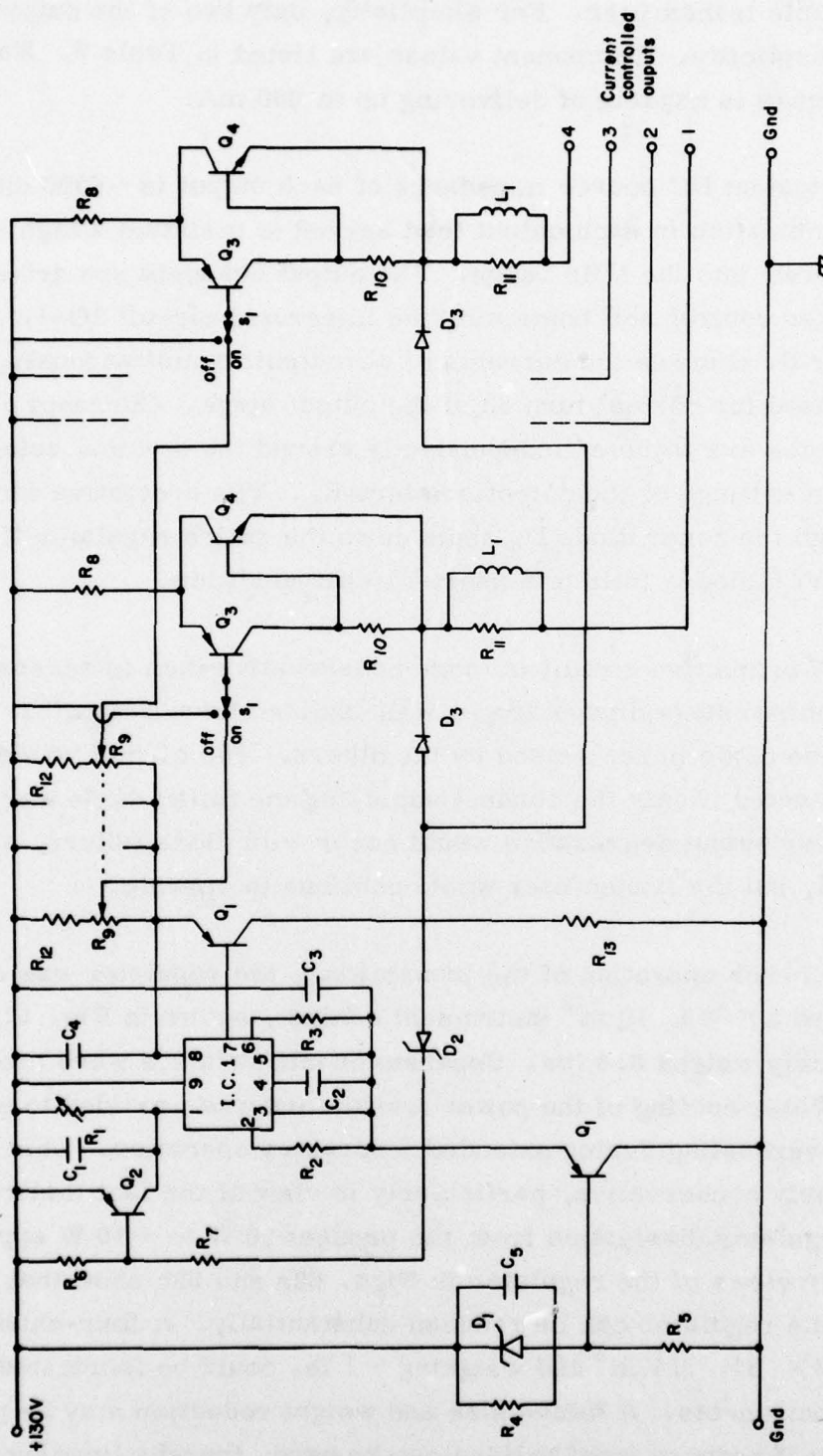
Figure 60   Circuit Diagram for the Multichannel Current Regulator.

116

TABLE 6

CIRCUIT PARTS VALUES

Item	Value	Item	Value
R_1	2.5K Ω pot	C_1, C_2, C_5	.01/200V
R_2	2.4K Ω	C_3, C_4	4.7/20V
R_3	27Ω	D_1	1N4737
R_4, R_5	27K Ω	D_2	1N4761
R_6	1K Ω	D_3	1N4005
R_7	10K Ω	Q_1, Q_3	2N5415
R_8	5Ω, 4W	Q_2	2N3906
R_9	100Ω pot	Q_4	MJ410
R_{10}	68Ω	IC1	LM304H
R_{11}	470Ω	L_1	.82μhy
R_{12}	390Ω	S_1	SPDT
R_{13}	2.15K Ω, 4 W		

117

Figure 61   Photograph of Multichannel Current Regulator (External View).
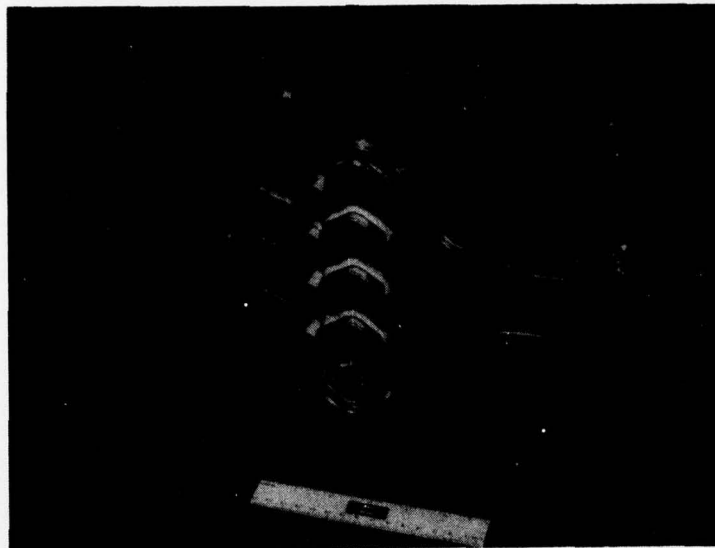
Figure 62a   Photograph of Multichannel Current Regulator (Bottom Internal View).

Figure 62b   Photograph of Multichannel Current Regulator (Top Internal View).

119

3.4 The DC-to-DC Inverter

The function of the DC-to-DC inverter is to convert the 28-VDC primary power to the 120V (nominal) level required as an input for the current regulators which feed the IMPATT diodes in the transmitter. As noted in the foregoing section, the characteristics of the high-power IMPATT diodes in the injection-locked oscillator mode are such that a substantial reduction in inverter output voltage with a corresponding increase in overall transmitter efficiency is possible. This change could be incorporated in future transmitter designs.

The multi-channel current regulator feeding the transmitter output stage and the current regulators in the VCO-driver subassembly consume essentially no current. Consequently, the total current required from the inverter is approximately equal to that consumed by the IMPATT diodes. This is 350 mA in the driver and 4 x 527 mA, or 2.11 A, in the output stage, giving a total current requirement of 2.46 A. An inverter with 2.5 A output current is thus adequate to meet the needs of the transmitter.

At the outset, we recognized that the state-of-the-art for DC-to-DC inverters was such that the size and weight goals for the entire transmitter package would be exceeded by the inverter alone. Power supply development was not considered as one of the primary objectives of this program, and it appeared unlikely that major improvements could be made in the relatively mature power supply technology. Consequently, we decided to purchase a standard commercially available inverter for use in the deliverable breadboard transmitter.

The inverter selected for use in the transmitter was the MODEL CEA2-C-130Z-252, manufactured by the CEA Division of Berkleonics, Inc., San Luis Obispo, California. The specifications of this unit are given in Table 7. The selection of 130 V nominal output was made during the middle of the program when it appeared that this higher voltage would be required to insure proper starting of the IMPATT diodes in the output stage. As it turned out, the originally-proposed 120 V was more than adequate. Fortunately, a 120 V (nominal) output could be obtained within the range of

TABLE 7

SPECIFICATIONS OF THE CEA2-C-130Z-252 INVERTER

Output Voltage:	130 VDC nominal, adjustable from 121 to 139
Output Current:	2.5 A
Input Voltage:	28 VDC nominal, 21-30 VDC acceptable
Input Current:	16 A @ 28V with output stage operating.
Efficiency:	80% maximum, 67% typical at full load.
Regulation:	Line — 1%, 21-30 V input change
	Load — 1%, .25-2.5 A load change
Ripple:	1% pp
Temperature Coefficient:	.05%/$^{\circ}$C
Size:	7 1/16 x 7 1/16 x 5 9/16 in.^{3}
Weight:	7.7 lb (5.4 lb without cover)
Cost:	$795, 1-4 units $557, 500 units

adjustment available in the chosen inverter.

A picture of the inverter with its outer cover removed is shown in Fig. 63. Only about 30 percent of the volume of the case is actually occupied by the components. Since cooling is accomplished almost entirely by conduction out through the base plate, a substantial size reduction from the volume given in Table 3-7 is possible. With existing technology, the unit could be reduced to a volume of $\sim$ 80 in^3. Weight of the modified unit would be $\sim$ 5 lb.

Some delay was encountered in obtaining the inverter from the manufacturer. Delivery required 3 months rather than the advertised 1 month. The unit was received on June 22, 1977.

Figure 63   Photograph of DC-to-DC Inverter (Internal View).

4.0   TRANSMITTER TEST RESULTS AND PERFORMANCE PROJECTIONS

4.1   Introduction

The development of the subassemblies which make up the deliverable transmitter has been described in the foregoing sections of this report.   Most of the problems encountered during the program occurred within the individual subassemblies.   A few difficulties had to be overcome during the testing of the complete transmitter.   First, after initial testing using separate power supplies for the VCO-driver and the output stage, an attempt was made to operate the transmitter from a single 28 V source, with the DC-to-DC inverter supplying the higher voltage required by the IMPATT diodes.   An interaction between the driver and the output stage through the common inverter occurred which caused a kHz-rate relaxation oscillation of the transmitter output.   This was eventually cured by inserting decoupling filters between the 28 V and the 120 V lines and the power input terminals of the VCO-driver.   (See Fig. 1).   With the filters installed, operation of the transmitter from a single power supply was the same as it had been with separate power supplies.   Second, switching transients on the inverter output caused modulation of the transmitter output in the 600-800 kHz region.   Initially, the undesired sidebands caused by these transients were only ~ 15 dB below the carrier level.   Including resonant suppression networks in the filters just mentioned reduced the level of these spurious outputs to 40-50 dB below the carrier level.   Finally, well into the testing program, one of the output stage diodes failed when a loose connection caused a transient to appear on the bias line.   The diode was replaced by one of similar but not identical characteristics.   The range of adjustment in the output stage cavity was sufficient to accommodate the new diode, and there was essentially no change in the overall transmitter performance following diode replacement.

A few other factors had to be considered during the setup and final testing of the transmitter.   These will also be noted here.

124

The original system design for the transmitter did not include a separate isolator between the VCO-driver and the output stage. However, even with a perfectly matched load connected to the transmitter output, the 17-dB (minimum) isolation of the output circulator would allow ~ 1 W to be reflected back to the VCO-driver when the transmitter operates with 40 W output. This reflected power becomes larger if there is any mismatch of the load. While there is an output isolator in the VCO-driver subassembly, it is a microstrip type having a relatively low-power termination which could be overloaded under some conditions of mismatch at the transmitter output. To avoid this possibility, and to make certain that the last stage in the VCO-driver locked to the signal injected from the Gunn diode VCO rather than to the signal reflected from the output stage, an additional isolator was inserted between the VCO-driver and the output stage (see Fig. 1). This isolator was formed by placing a 5 W termination on a Teledyne Microwave C-4S63T-10 circulator, the same model circulator used at the transmitter output. Operation of the transmitter with this isolator installed was satisfactory. No attempt was made to operate the transmitter without the interstage isolator. As an indication that the isolator was necessary, however, we noted that its termination became slightly warm, indicating the absorption of at least a few hundred milliwatts of reflected output power, during extended bench operation of the transmitter.

During initial testing of the transmitter it was discovered that the frequency of the VCO-driver subassembly was sensitive to the movement of nearby objects. The frequency could be moved more than 4 MHz by moving a finger along the top case of the unit. The problem was caused by incomplete RF shielding, and was cured by covering the gaps in the existing shield with adhesive-backed copper foil tape. However, the installation of the copper tape caused a shift in the operating band of the VCO-driver, as will be described. Also, the frequency of the VCO-driver was quite strongly dependent on temperature. A shift of 25 MHz between the frequency at turn-on and the frequency at which the unit stabilized was not unusual.

While the output circulator used in the transmitter, the Teledyne Microwave model C-4S63T-10, was rated for 50 W CW forward power, its nominal 0.3 - 0.4 dB loss represented 3 - 4 W of dissipation when the transmitter was operated at the 40 W output level. This was sufficient to make the circulator uncomfortably warm to the touch after several hours of operation. There was no evidence that this temperature rise affected the operation of the transmitter. Further, the chosen circulator had the advantage of small physical size. However, both to increase overall transmitter efficiency and to reduce the heat-removal problem in a practical transmitter, the use of a circulator with lower losses, perhaps ~0.2 dB, should be considered.

During setup of the transmitter, a fault in the 28 V primary power provided a good demonstration of the effectiveness of the DC-to-DC inverter and the multichannel current regulator in providing stable operating current for the output stage diodes. A pair of 9A power supplies connected in parallel according to the manufacturer's instructions was being used as a 28 V source. An oscillation, causing 6 V peak-to-peak voltage variations of approximately 20 Hz rate on the 28 V line, developed in the parallel-connected supplies. No effect of this oscillation could be seen in the operation of the single output-stage diode being run at the time. Thus, the transmitter is isolated from rather serious perturbations of the primary voltage supply. Subsequent tests used a single 28 V supply to feed the inverter, and no oscillations were noted.

Diodes from any one of several lots could have been chosen for use in the output stage of the transmitter. Units from lot 946 were eventually selected since they offered smooth turn-on, together with operating voltage and current requirements well within the capabilities of the DC-to-DC inverter and current regulator. Table 1 shows the free-running oscillator performance of the diodes actually used in the transmitter, both in the top-hat oscillator where they were originally qualified and in the coaxial cavity oscillator modules as tuned for use in the transmitter. Note that the diodes operate conservatively in the modules, with bias

126

TABLE 8

PERFORMANCE OF OUTPUT STAGE DIODES

DIODE	V_B (volts)	C_T @ V (pF)	V (volts)	I (mA)	P_o (W)	f (GHz)	η (%)	CIRCUIT
946C-2	87.9	3.4 @ 79	102.6	697	16.7	4.867	23.4	Top Hat
			98.4	525	12.3	5.001	23.8	Module
946D-2	88.1	3.6 @ 82	104.0	637	15.1	4.858	22.8	Top Hat
			98.3	525	12.5	5.000	24.3	Module
946E-2	89.2	3.6 @ 82	101.9	657	15.5	4.840	23.1	Top Hat
			100.6	525	12.6	4.999	23.8	Module
946E-12*	90.7	3.4 @ 83	102.0	638	15.4	4.847	23.6	Top Hat
			101.3	525	12.9	5.000	24.2	Module
946D-13+	88.6	3.6 @ 80	104.1	637	16.1	4.938	24.3	Top Hat
			97	525	-	5.000	-	Module

* Diode failed because of bias transient late in testing program.

+ Replacement for diode 946E-12; power output similar to other diodes in the module, measured through power combining circuit.

currents well below those used in the top-hat oscillator. Although no special effort was made to match the diodes to each other, the power outputs at 5 GHz with the nominal 525 mA operating current are all quite similar. This means that there is little imbalance in the combiner circuit, and the terminations in the Gysel hybrids are called upon to dissipate almost no power in normal operation. In fact, the terminations in the combiner circuit did not become at all warm to the touch when the transmitter was operated for extended periods, thus demonstrating the condition of good balance. The implication of this result is that physically smaller low-power terminations could be used in the combining circuit under normal conditions.

Figure 64 shows the output stage of the transmitter in the configuration in which it was tested. Included are the three Gysel hybrids, the four coaxial cavity oscillator modules, and the output circulator. The cooling water is run in the series through the four modules. This is acceptable because the temperature rise of the water which results from passage through one module is negligible.

The complete RF portion of the transmitter is shown in Fig. 65. Here the VCO-driver subassembly and the interstage isolator have been added to the output stage. Power and water connections to the VCO-driver were omitted to avoid cluttering the picture.

All transmitter components are shown together in Fig. 66a. The DC-to-DC inverter and the multichannel current regulator have been added to the RF components. The water and electrical interconnections have been omitted to show the individual units more clearly. In normal operation, a single series water path through all units, starting first with the output stage and then running through the VCO-driver, current regulator, and inverter, is used. After initial warm-up, the transmitter operates continuously for periods of several hours with no significant drift in its characteristics. The transmitter as delivered, with all components and electrical connections completed on a mounting board, is shown in Fig. 66b.

128
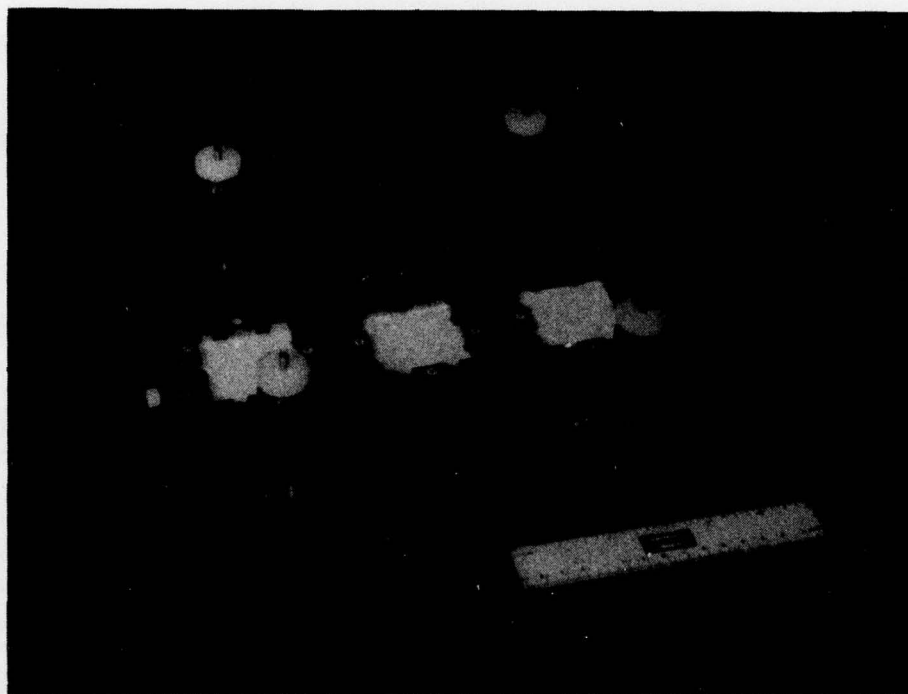
Figure 64   Photograph of the Transmitter Output Stage.

129
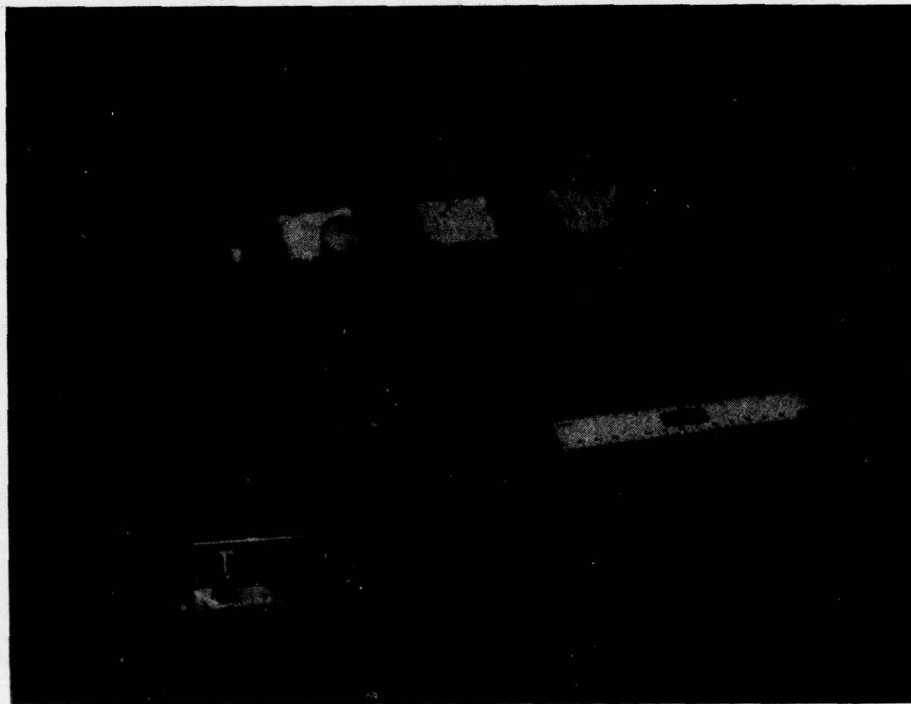
Figure 65   Photograph of the RF Portion of the Transmitter.
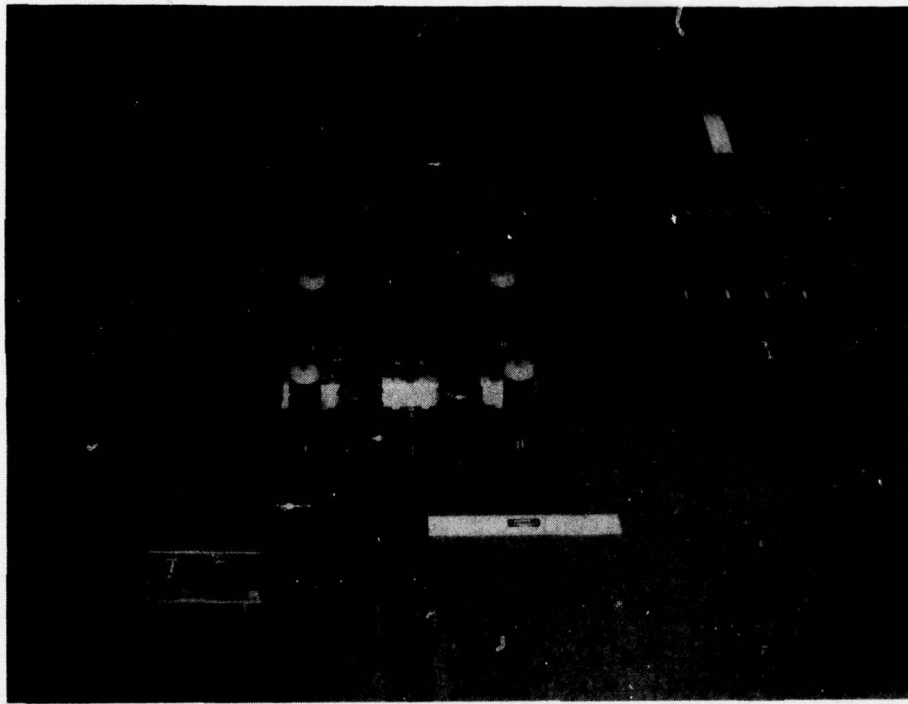
Figure 66a   Photograph of All Major Transmitter Subassemblies.
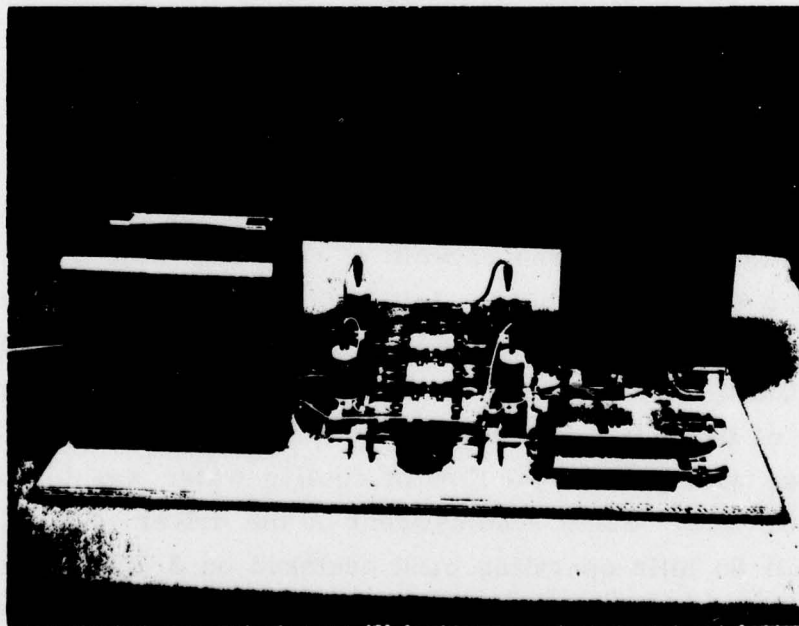
Figure 66b   Photograph of the Transmitter As Shipped.

4.2 Test Results and Performance Projections

Test results actually obtained from the complete transmitter are presented in the following subsections and compared to the original program goals. Where significant improvements relative to the goals remain to be made, projections for the performance based on reasonable extensions of the existing technology are given.

4.2.1 Center frequency

Goal: 5 GHz

Test Result: 5 GHz

Operation at 5 GHz was included within the range of frequencies to which the transmitter could be tuned. After additional shielding was placed on the VCO-driver, 5 GHz could be reached only with VCO-driver base-plate temperatures above $\sim 30°$ C.

4.2.2 Tunable bandwidth

Goal: 60 MHz

Test Result: 60 MHz demonstrated initially

The individual diode modules in the transmitter output stage could each be tuned over a range of 200-300 MHz including 5 GHz. The power combining circuit was capable of efficient, well-matched operation over the 4.8 to 5.3 GHz band. Initial tests of the VCO-driver showed that it could be electronically tuned over the 4.97 to 5.03 GHz range. After the additional shielding was added to the driver to eliminate the sensitivity of the unit to the movement of external objects, the available tuning range with the normal flow of cooling water was found to be 5.01 to 5.04 GHz. Some readjustment of the driver is required to obtain a full 60 MHz operating band centered on 5 GHz. The driver, rather than the output stage, provides the limit on tunable bandwidth.

132

4.2.3 Instantaneous bandwidth

Goal: 10 MHz (-1 dB)

Test Result: > 20 MHz demonstrated

The instantaneous bandwidth of the transmitter was checked in two ways. First, the static electronic tuning range was investigated by observing the variation in power output while adjusting the frequency of the Gunn diode master oscillator in the VCO-driver subassembly. Second, the ultimate electronic tuning bandwidth was found by operating the transmitter with frequency modulation and increasing the deviation until injection locking was lost by one of the stages in the transmitter.

In the static electronic tuning tests, to be described in more detail in the following subsection, the transmitter was tuned from 4.993 to 5.112 GHz with a power output variation of only 0.26 dB. This is well within the power variation given as a program goal.

When frequency modulation with progressively larger deviation was applied to the transmitter, it was found that locking would be lost with peak-to-peak deviations of ~ 40 MHz. Figure 67 illustrates transmitter output spectra for a less extreme case. Here, a 5 MHz modulating frequency was used. The amplitude of the modulating signal is small in the first picture, and only the first two sets of sidebands are observable. In the second case the amplitude of the modulating signal and hence the deviation have been increased until the first carrier minimum has been reached. This condition occurs when the peak-to-peak frequency deviation is 4.8 times [8] the 5 MHz modulating frequency, or 24 MHz. The depth of the carrier null, more than 32 dB, and the relatively symmetrical spectrum indicate good-quality FM with essentially no incidental AM.

Both tests indicated that the instantaneous bandwidth of the transmitter was more than twice that given as a program goal.

133
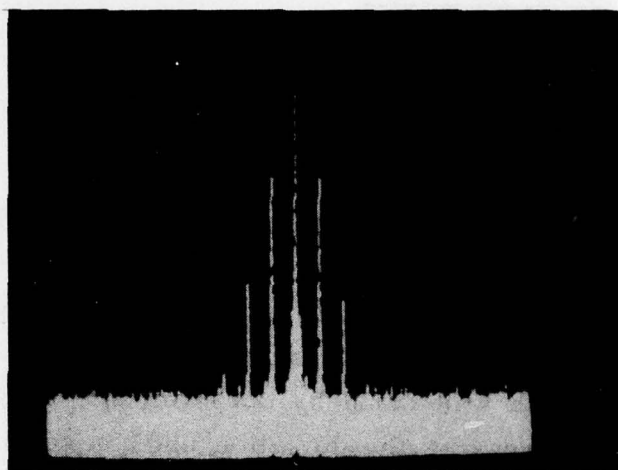
Small Deviation
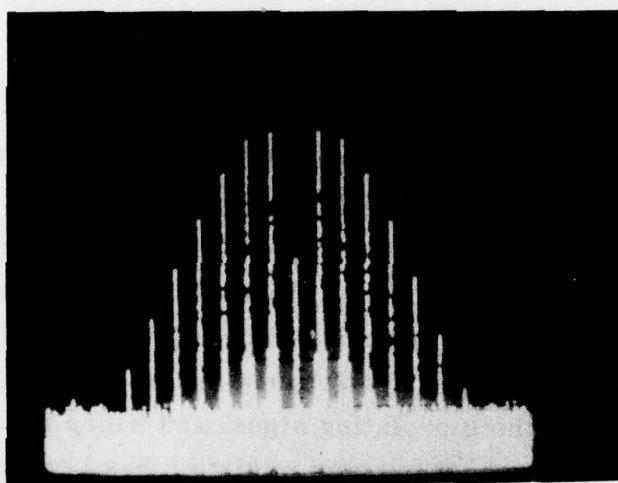
Deviation sufficient
to produce the first
carrier null.
(24 MHz peak-to-peak)

For Both Pictures:

P_o = 41.6 W
f_o = 5.0 GHz

Vertical : 10 dB/Division
Horizontal: 10 MHz/Division
           100 kHz Bandwidth

Figure 67 · Output Spectra of the Transmitter Frequency Modulated by
a 5 MHz Signal.

4.2.4 Power output

Goal: 40 W

Test Result: 42.1 W Maximum
                 (40 W Typical)

The high-power oscillator modules in the output stage of the trans-
mitter were operated at a bias current level which would permit generation
of 40 W CW output while at the same time keeping the total current demand
within the 2.5 A capability of the DC-to-DC inverter. Substantially more
output power can be obtained by raising the bias current. Table 8 shows
that each one of the diodes is capable of 15 W output. With diodes operat-
ing at the 15 W level, the transmitter power output would be $\sim$ 48 W, but
the current required from the inverter would rise to a total of 2.9 A with
the requirements of the VCO-driver (340 m A at 120 V) included.

Operation of the diodes at the 12.5 W power level keeps the total
current demand from the inverter slightly below 2.5 A. The output stage
consumes 2.1 A and the driver .34 A for a total of 2.44 A. Also, given
a typical thermal resistance of 4° C/W for the output stage diodes, 12.5 W
operation results in a junction temperature rise of 160°C. During testing
of the transmitter, heat sink temperatures were maintained at $\sim$ 15°C with
water cooling. This yields a junction temperature of 175°C which is con-
sistent with diode lifetimes in excess of 10^5 hours.

Table 9 describes the operation of the output stage at three dif-
ferent frequencies. The oscillator modules were tuned for operation at
5.000 GHz, and the data were recorded as the frequency of the VCO-
driver was reset. The power added efficiency of the output stage,
defined by $\eta = (P_o - P_{in}/P_{DC}$, was typically 18 percent. Since the
individual DC-to-RF conversion efficiencies of the diode modules were
24 percent, this implies a combining efficiency of 75 percent in the out-
put stage.

TABLE 9

OUTPUT STAGE PERFORMANCE WITH CHANGE IN VCO FREQUENCY

DIODE	V (volts)	I (mA)	P_{Dc} (W)	P_{in} (W)	P_o (W)	f (GHz)	η (%)
946C-2	96.9	527					
946D-2	96.5	530					
946E-2	98.3	530	206.1	3.46	39.7	4.993	17.6
946E-12	98.3	527					
946C-2	97.9	525					
946D-2	97.5	527					
946E-2	99.4	527	207.2	3.54	40.8	5.000*	18.0
946E-12	99.3	525					

* Nominal free-running frequency of the oscillator modules

DIODE	V (volts)	I (mA)	P_{Dc} (W)	P_{in} (W)	P_o (W)	f (GHz)	η (%)
946C-2	101.3	525					
946D-2	100.5	526					
946E-2	102.8	530	214.7	3.54	42.1	5.012	18.0
946E-12	102.8	527					

Total Current Drain = 2.1A

Combining Efficiency = 75% (Typical)

136

Somewhat unexpected was the large shift in operating voltage with frequency. This can be understood by noting that the phase offset between the injected signal and the output signal varies across the locking band of the output stage. This is true even while frequency locking is maintained. The effective impedance seen by the diode modules depends both on the passive load and on this injected signal. Consequently, because the phase difference between the injected signal and the output signal changes, the effective load impedance seen by the diode modules changes, and this influences the operating voltage.

The results of Table 9 demonstrate one technique which can be used to obtain slight increases in transmitter output power without raising the bias current applied to the output stage diodes. By setting the modules to a frequency slightly below the desired operating frequency, and pulling the output frequency up with the injected signal from the VCO-driver, one operates in the higher voltage condition. This raises the input power to the diodes and consequently their output without increasing the bias current. The overall efficiency remains virtually unchanged.

The type of combining circuit used in the output stage results in a less-than-graceful degradation in power output with diode failure. This is because a two-fold loss occurs when a diode fails: the diode power is lost to the output, and the power imbalance in the circuit is also dissipated. Isolation among the diodes in the output stage is good enough to permit them to be operated in any combination, so the transmitter can, in principle, continue to function after a diode failure. However, some combinations, such as operation of two diodes on one side of the four-port hybrid while the remaining diodes are shut down, will exceed the power dissipation ratings of the internal terminations in the hybrid. This was one reason why the current regulator feeding the output stage was designed to shut down completely on the failure of any one diode. Power output degradation with continued operation after an output stage diode failure can be computed from the known characteristics of the four-port hybrid. The results are

137

shown in Table 10. Only the cases with 0, 3, and 4 failures were verified experimentally in the present work. The power output degrades approximately twice as fast as the loss in available diode power.

4.2.5 Input Power (for 40 W RF Output)

Goal: 28 V DC, 10 A

Test Result: 28 V DC, 16.7 A

Previous Projections:

28 V DC, 13.75 A (Technical Proposal)

28 V DC, 14.96 A (Interim Report)

Estimates assuming further development

(all currents at 28 VDC):

Present IMPATT diode design, with refinements: 10.9 A

Improved IMPATT technology, with IMPATT driver: 10.5 A

Improved IMPATT technology, with FET/IMPATT driver: 8.9 A

When the program was undertaken, estimates of the power consumption for the transmitter exceeded the 28 V DC, 10 A goal given in the original statement of work. The increase in power consumption projected at the time of the Interim Report was caused primarily by the fact that the power required by the VCO-driver was larger than forecast. Power required by the complete transmitter was fairly close to the forecast made at the time of the Interim Report. The actual inverter efficiency, 67 percent, was lower than the 80 percent value used in planning the transmitter, but this efficiency loss was partially offset by the fact that power consumption in the output stage was less than forecast.

We can now make predictions of the power requirements for a refined version of the transmitter incorporating some obvious improvements of the existing design. First, assume that the same basic system design shown in Fig. 1 is retained. Output stage diodes could then be replaced

138

TABLE 10

COMPUTED POWER OUTPUT DEGRADATION WITH OUTPUT STAGE
DIODE FAILURES

Diodes Failed	Nominal Output Power*	Output Signal Loss
0	40 W	0 dB
1	22.5 W	2.5 dB
2	10 W	6 dB
3	2.5 W	12 dB
4	0 W	∞ dB

* **Neglecting feed-through from driver**

139

by units having 25 percent DC to RF conversion efficiency. Such diodes have been demonstrated, and they would raise overall efficiency without encountering the turn-on problems associated with very high efficiency ($\sim$ 30 percent) diodes. Fabrication of the power combining circuit on a single TIM substrate, the elimination of double male connectors between the diode modules and the power combiner, and use of a lower-loss circulator at the transmitter output could all be implemented to reduce losses in the output stage by $\sim$ 0.35 dB. The inverter output voltage could be reduced to 105 V to cut losses in the IMPATT diode current regulators, and substitution of an optimized inverter with 80 percent efficiency should be possible. These changes would give a total current demand of 10.9 A at 28 V DC, with 2.3 A consumed by the VCO driver and 8.6 A consumed by the output stage.

The development of multi-mesa diodes producing 25 W CW output at 5 GHz with 25 percent efficiency now appears possible. The use of such diodes in the transmitter would permit the substitution of a two-diode output stage for the four-diode stage shown in Fig. 1. A single two-port Gysel hybrid with a low-loss output circulator would reduce the loss in this output stage $\sim$ 0.55 dB below present levels. This, combined with the previously described changes in inverter output voltage and efficiency, would cut total current requirements at 28 V to 10.5 A. Of this, 8.2 A would be consumed in the output stage and 2.3 A in the VCO-driver.

The close approach to the original goal for power consumption which appears possible even with the basic IMPATT technology originally proposed results from the high output stage combining efficiency. Only 70 percent combining efficiency was initially projected, but 75 percent was actually achieved in the present work. The loss reductions which should be possible would permit a four-diode stage with 87 percent combining efficiency and a two-diode stage with 91 percent combining efficiency.

Initially we argued that the power comsumption of the VCO-driver subassembly would not have a major impact on the overall power consumption of the transmitter. As the efficiency of the output stage is

improved, however, the power consumed by the VCO-driver becomes more than 20 percent of the total. The low efficiency of the Gunn diode VCO and of the flat-profile IMPATT diode in the driver are major reasons for this relatively large power consumption.

It now appears that a significant improvement in transmitter efficiency can be achieved by redesigning the VCO-driver. The first two stages, reaching the 300 mW power level, would use FET's, and a Read IMPATT diode operating as an injection-locked oscillator would form the final stage with 3 W output. A small low-power inverter would be required to provide 10-12 V to operate the FET's. Even with this inverter, assumed to be 80 percent efficient, a VCO-driver having 15 percent overall efficiency from 28 V prime power to 5 GHz output should be possible. Such a unit would require 0.7 A at 28 V. Using the improved four-diode output stage with such a driver would produce a 40 W transmitter which would consume 9.3 A at 28 V. A further reduction to 8.9 A would be possible if the two-diode stage were used. These projections show that, with relatively simple refinements, the current consumed by the transmitter can be reduced below the original 10 A goal.

4.2.6 Cooling requirement

No Goal Stated

Present Transmitter: 0.7 gal./min. water flow
20 psi inlet pressure (427W heat load)

Projected Transmitter: .35 gal./min. water flow
(210 W heat load)

The transmitter constructed during the program was water cooled, with water circulating through channels in the individual subassemblies or through channels in cold plates on which the subassemblies were mounted. A series water path, passing through all subassemblies, was used. A water flow of 0.7 gal./min., which could be obtained with a water inlet pressure of 20 psi, was more than adequate for the 427 W heat load imposed by the power dissipated in the transmitter.

141

If the improvements described in the foregoing subsection are implemented, the transmitter efficiency will increase to ~16 percent overall, and the power dissipated within the unit will drop to 210 W. With the same heat transfer efficiency, a water flow of .35 gal./min. through the cold plate on which the transmitter is mounted should then provide adequate cooling. Suitable heat sinks for forced-air or convection cooling might also be devised.

4.2.7 Operating life and shelf life

Goals: 5000 hours operating life

7 years shelf life

Projections: > 5000 hours operating life

> 7 years shelf life

No distinct series of reliability tests was included in the program. However, some preliminary projections of the reliability of the transmitter can be made using reliability data available from independent sources. The main objective is to determine whether the IMPATT diodes would become a major limitation in attempts to reach the reliability goals. No description of ambient conditions was given with the reliability goals, so a typical laboratory environment has been assumed for initial projections.

First, consider the requirement for 5000 hours operating lifetime. Some data have been obtained by the Raytheon Special Microwave Devices Operation (SMDO) in accelerated life testing of single-mesa GaAs Read IMPATT diodes that were fabricated by essentially the same process used for the diodes in the transmitter. The test results gave lifetimes in excess of 2×10^6 hours with 200° C junction temperature and 5×10^7 hours with 175° C junction temperature. The four-mesa diode is expected to be less reliable since four separate junctions must survive the test interval. However, if one makes the assumption of independent, uncorrelated failures, a lifetime of ~10^7 hours would still be projected for four-mesa devices operating at 175° C. Assuming that all 19 semiconductor junctions in the transmitter RF section (16 in the output stage and 3 in the VCO-driver)

142

have similar but independent failure characteristics, a lifetime limit of 2.6×10^5 hours is imposed on the transmitter by the microwave semi-conductors.

Low-frequency transistor circuits of the type used in the inverter and current regulator can usually be designed for lifetimes in excess of 10^4 hours. In addition, low-power communications transmitters comparable to the VCO-driver subassembly and now manufactured by Raytheon SMDO have demonstrated lifetimes in excess of 10,000 hours in actual field service. Further, so long as the transmitter is mounted in a hermetically sealed compartment, there are no obvious fundamental mechanisms by which the passive parts of the RF circuit would degrade within a 5000 hour operating life.

The implication of all of these results is that an operating lifetime substantially in excess of 5000 hours should be possible in the transmitter. Tests of lifetime with ambient conditions prescribed should be undertaken to confirm this projection.

Projections of the shelf life of the transmitter are more difficult to make. However, the IMPATT diodes should not restrict the shelf life. Unless storage temperatures approach the normal operating temperatures for the diodes (175° C), the ordinary failure mechanism - reaction of the GaAs diode material with the contact metallization - proceeds so slowly that failures would not occur for hundreds of years. There should be no degradation of diode performance after 7 years storage so long as the diodes are placed in hermetically sealed packages to prevent contamination of the diode surfaces. In fact, we have retested GaAs Read diodes mounted in open, unsealed packages after two years of storage in a laboratory environment and found no change in characteristics.

In the prototype transmitter, no particular effort was made to insure long-term compatibility of the metals used. Brass resonators are used in the coaxial cavity oscillator modules, soft soldered joints hold some

143

mechanical parts together, and aluminum parts are mounted against copper cold plates. All of these are areas where potential corrosion problems exist. However, there is no obvious reason why the mechanical structure, given the use of appropriate materials and surface finishes, could not remain operational through a 7 year storage period. The selection of the correct materials should be the subject of future work.

The only major life-limited components in the transmitter appear to be the electrolytic filter capacitors in the DC-to-DC inverter. Such capacitors are known to degrade with time. However, units with 10-year shelf life can be obtained, so achieving a seven-year shelf-life for the transmitter as a whole should be possible.

4.2.8 Modulation

> Goal: FM, 70 kHz - 10 MHz modulating frequency;
> 10 MHz peak-to-peak deviation capability;
> Modulation sensitivity flat + 0, -1 dB, 70 kHz -
> 10 MHz.
>
> Test Result: FM, 50 kHz - 12 MHz modulating
> frequency demonstrated; > 20 MHz
> peak-to-peak deviation capability
> demonstrated; Modulation sensitivity
> 35.5 MHz/V, ± 0.2 dB from 200 kHz -
> 10 MHz, +1 dB @ 140 kHz, + 2.1 dB @ 70 kHz.

Application of a sinusoidal voltage to the modulation input of the transmitter produced classical FM output spectra. Modulation frequencies from 50 kHz to 12 MHz were used in these tests.

Figures 68, 69, and 70 show transmitter output spectra for three representative modulating frequencies: 100 kHz, 1 MHz, and 10 MHz. In each case, two different modulating voltage levels were used. A small

144
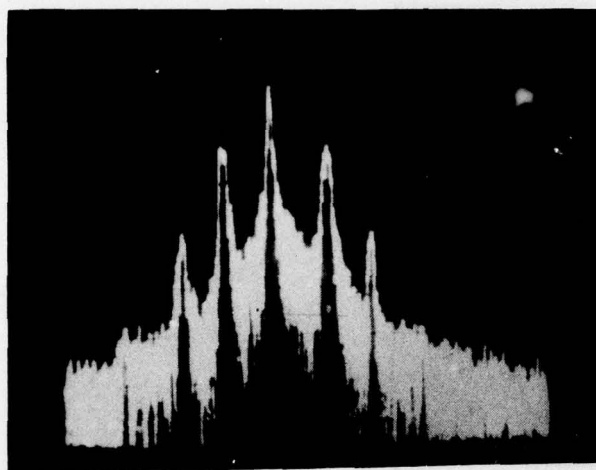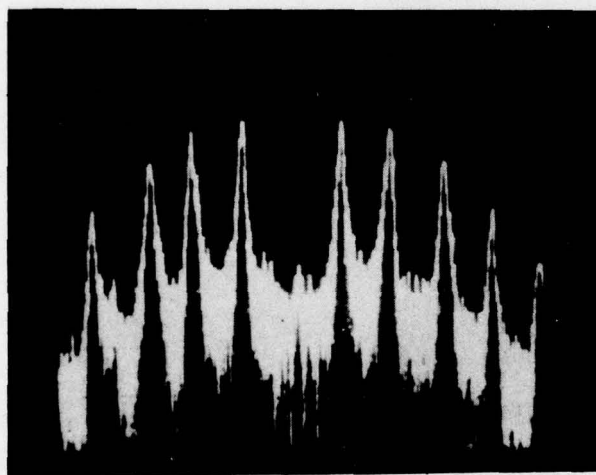
Small Deviation

Deviation sufficient to
produce carrier null.
(480 kHz peak-to-peak)

For Both Pictures:

Vertical : .10 dB/div.

Horizontal: 100 kHz/div.

10 kHz Bandwidth

f_o = 5.000 GHz

P_o = 41.6 W

Figure 68   Transmitter Output Spectra with 100 KHz Modulation.
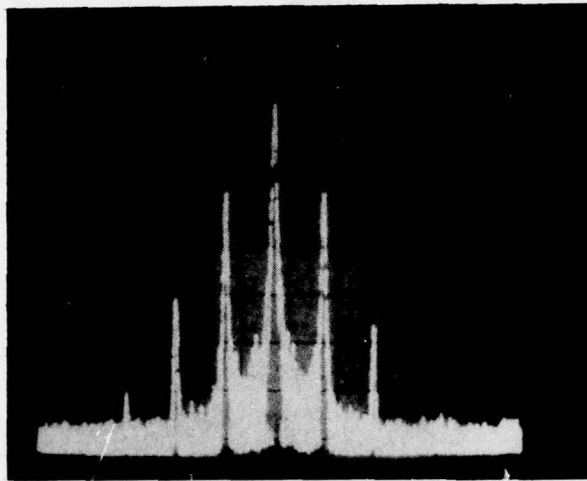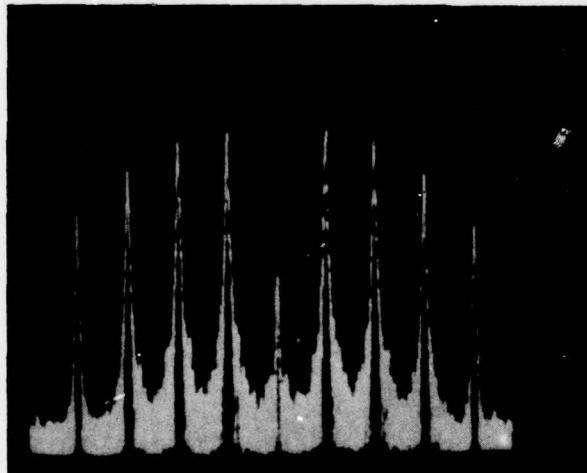
145

Small Deviation

Deviation sufficient to produce carrier null.
(4.8 MHz peak-to-peak)

For Both Pictures:

Vertical : 10 dB/div.

Horizontal: 1 MHz/div.
30 kHz Bandwidth

f_o = 5.000 GHz

P_o = 41.6 W

Figure 69   Transmitter Output Spectra with 1 MHz Modulation.
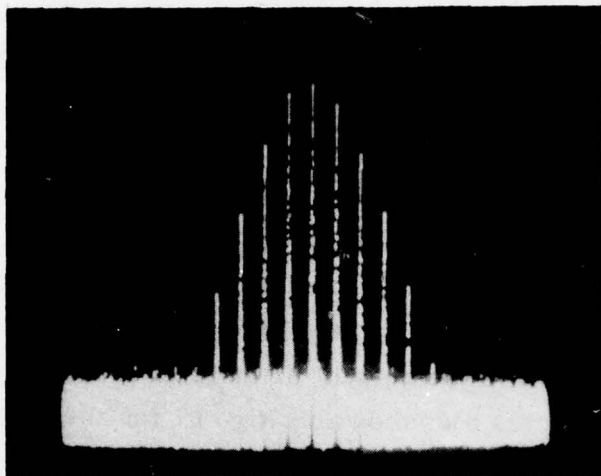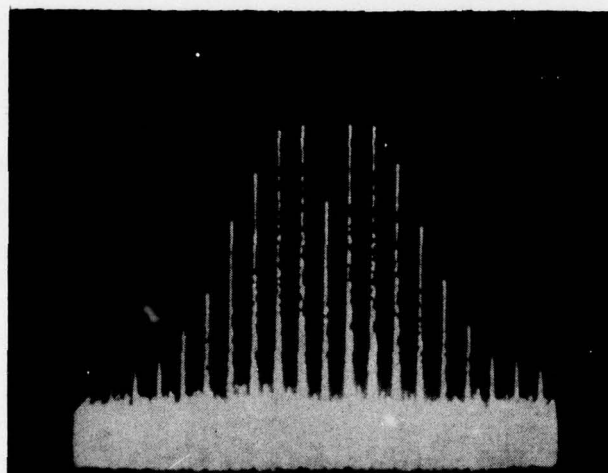
146

Small Deviation

Deviation sufficient to
produce carrier null.
(48 MHz peak-to-peak)

For Both Pictures:

Vertical :   10 dB/div.

Horizontal: 20 MHz/div.
               300 kHz Bandwidth

f_o = 5.000 GHz
P_o = 41.6 W

Figure 70   Transmitter Output Spectra with 10 MHz Modulation.

147

voltage, sufficient to display the carrier and a few sets of sidebands, was used first. A larger voltage, sufficient to produce the first carrier null was then applied. The carrier null occurs when the peak-to-peak frequency deviation is 4.8 times the modulating frequency. Note that carrier null for 10 MHz modulating frequency occurs with 48 MHz peak-to-peak deviation, more than four times the program goal. However, loss of locking was sometimes noted for deviations in excess of 40 MHz peak-to-peak. The slight asymmetry of the spectra, particularly with higher modulating frequencies and large deviations, is caused by a small amount of incidental amplitude modulation. Additional output spectra are shown in Fig. 67 for the case of 5 MHz modulating frequency. All spectra may be compared with the spectra of the unmodulated carrier shown in Figs. 72 and 73.

Modulation sensitivity was measured for modulation frequencies from 50 kHz to 10 MHz. Results are plotted in Fig. 71. The sensitivity is virtually constant from 200 kHz to 10 MHz. The rise in sensitivity at low frequencies is caused by a resonance in the circuit which superimposes the modulating signal on the bias voltage applied to the Gunn diode VCO. A modification of the circuit parameters could be made to move this resonance far below the desired band of modulating frequencies. The modulation sensitivity could then be made constant from 70 kHz to 10 MHz.

4.2.9   Size and weight

Goal: Size - 6.4 x 1.7 x 3.6 in^3

(39.2 in^3)

Weight - 3.5 lb.

Actual Transmitter: Total Volume - 1109.4 in^3

(Subassemblies only)

Weight - 25.6 lb.

Projection: Total Volume - 114.3 in.^{3}

Weight - 7.4 lb.

148

Figure 71   Modulation Sensitivity as a Function of Modulating Frequency
for the Complete Transmitter.

149
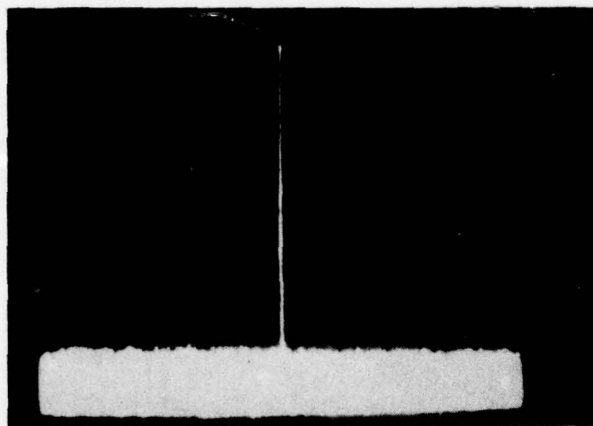
Vertical   : 10 dB/div.

Horizontal: 100 MHz/div.
             300 kHz Bandwidth

f_o = 4.999GHz

P_o = 41.5 W

Figure 72   Output Spectrum of the Unmodulated Transmitter.
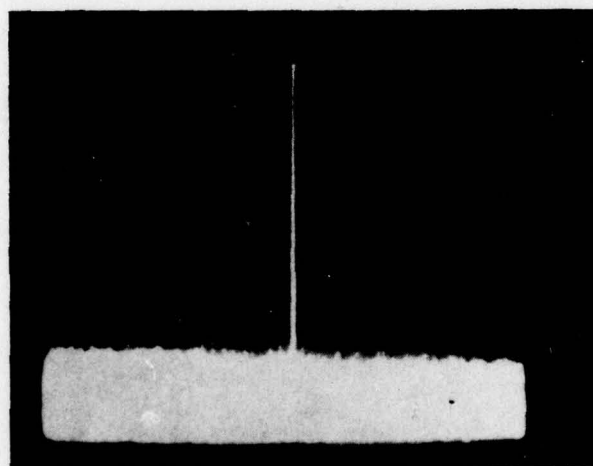
Vertical   : 10 dB/div.

Horizontal: 200 MHz/div.
             300 kHz Bandwidth

f_o = 5.000 GHz

P_o = 41.6 W

Figure 73   Output Spectrum of the Unmodulated Transmitter. Wide
Dispersion Reveals no Major Spurious Outputs in the range
4-6 GHz.

150

At the outset, it was recognized that the size and weight of the trans-
mitter package would exceed the program goals. The development work on
the deliverable transmitter occupied a greater portion of the program than
was originally planned, and little time was available for refining the mechani-
cal layout to achieve even those relatively large size and weight projections
made in the Technical Proposal. Those subassemblies included in the de-
liverable transmitter are first laboratory prototypes suitable for bench
operation, and the size and weight overruns listed above are substantial.
Actual volume and weight requirements for operation of the transmitter are
somewhat greater since the cold plates are not included in the totals listed.

Projections of the size and weight of the transmitter, assuming no
major technology improvements, do result in a more reasonable package
size with a substantial weight reduction. These projections are collected
in Table 11, describing the subassemblies, and Table 12, which sum-
marizes the projections for the complete transmitter.

The ideas leading to the projections of Table 11 will be described
first. No major changes were made in estimating the size and weight of the
VCO-driver subassembly. The existing aluminum base plate was removed
and replaced by a thin sheet which would interface with the cold plate on
which the entire transmitter would be mounted. The current regulator
would be built on a single aluminum plate rather than in a separate cabinet.
Size reduction would be accomplished by replacing the large potentiometers
with smaller trimpots and close-packing the components on the mounting
plate. Separate estimates are given for a four-channel and a two-channel
regulator. The latter would be used if 25 W diodes were available so that
a two-diode output stage could be constructed. Size and weight reductions
in the inverter were obtained by eliminating the steel outer cover (2.3 lbs.)
and by employing high-density packing of the remaining components. No
major change in components or technology was assumed, but the new high-
density packing of components will require mounting the unit against a cold
plate. Changes in the output stage include construction of the power-com-
bining circuit on a single aluminum ground plane, and use of smaller-size

151

TABLE 11

ACTUAL AND PROJECTED WEIGHTS AND VOLUMES
FOR THE TRANSMITTER SUBASSEMBLIES

Subassembly	Actual Size and Weight	Projected Size and Weight	
I. VCO-Driver	4 x 5.75 x 1.45 in.^{3} 1.67 lb.	3.4 x 4.9 x 1.25 in.^{3} 1 lb.	
II. Current Regulator	8 x 8 x 10 in.^{3} 8.5 lb.	6 x 3 x .75 in.^{3} 1 lb.	} 4 Channel
		4 x 3 x .75 in.^{3} 0.7 lb.	} 2 Channel
III. DC-to-DC Inverter	7 1/16 x 7 1/16 x 5 9/16 in.^{3} 7.7 lb.	80 in.^{3} 5.4 lb.	
IV. Output Stage	13 x 8 x 1.5 in.^{3} 7.75 lb.	2 x 5 x 1.5 in.^{3} 0.6 lb.	} 4 Diodes
		1.5 x 1.5 x 2 in.^{3} 0.25 lb.	} 2 Diodes

TABLE 12

SUMMARY OF SIZE AND WEIGHT VALUES
FOR THE COMPLETE TRANSMITTER

I. Program Goal

Volume - 39.2 in.^{3}
Weight - 3.5 lb.

II. Existing Transmitter

	RF Circuits and Regulator	DC-DC Inverter	Total
Volume -	829.4 in.^{3}	280 in.^{3}	1109.4 in.^{3}
Weight -	17.9 lb.	7.7 lb.	25.6 lb.

III. Projected Transmitter - Two-diode Output Stage

	RF Circuits and Regulator	DC-DC Inverter	Total
Volume -	34.3 in.^{3}	80 in.^{3}	114.3 in.^{3}
Weight -	2.0 lb.	5.4 lb.	7.4 lb.

IV. Projected Transmitter - Four-diode Output Stage

	RF Circuits and Regulator	DC-DC Inverter	Total
Volume -	49.3 in.^{3}	80 in.^{3}	129.3 in.^{3}
Weight -	2.6 lb.	5.4 lb.	8 lb.

153

aluminum cavities for the diodes. The cavity size reductions were described in Section 3.2.3.4. Size projections for both a four-diode stage, using existing diodes, and a two-diode stage, using 25 W diodes, are given. Cavities would be mounted against the back surface of the ground plane of the power-combining circuit to form a compact package.

Table 12 brings together the projections of Table 11, giving totals for transmitters with both the two-diode and four-diode versions of the output stage. Because it is a major contributor to the size and weight of the complete unit, the inverter is separated from the RF subassemblies and the current regulator in these projections. Note that a package excluding the inverter can be made smaller and lighter than the program goals. Without resorting to a specialized inverter, however, projections for the complete transmitter exceed the program goals by a factor of 3 in volume and a factor of 2 in weight.

4.2.10 Noise and spurious outputs

Goal: Total AM and FM noise in a 1 kHz bandwidth 100 MHz from the carrier to be 30 dB or more below carrier level.

Test Result: Noise - total AM and FM noise in a 1kHz bandwidth 100 MHz removed from the carrier was more than 90 dB below the carrier level

Spurious Output - more than 60 dB below carrier level, except as noted

1) second harmonic more than 46 dB below the fundamental output.

2) spurious sidebands ~ 600-800 kHz from the carrier, 40-50 dB below carrier level.

154

The noise output goals for the transmitter were quite modest and were easily satisfied. This is shown in Fig. 72, which shows the unmodulated output spectrum of the transmitter. The carrier is 65 dB above the noise of the detection system, which operated with 300 KHz bandwidth. This implies that the carrier level is at least 90 dB above the noise level in a 1 kHz bandwidth, giving a signal to noise ratio much better than that stated as a program goal.

There was no specified goal for the limits on spurious outputs. However, the spectrum from 10 MHz to 18 GHz was searched in an effort to find coherent spurious outputs. The second harmonic could be observed at 10 GHz, and independent measurements using a power meter coupled to the transmitter output through a high-pass filter showed it to be more than 46 dB below the 5 GHz output. No other coherent spurious outputs could be found with the spectrum analyzer. If any existed, they were more than 60 dB below the 5 GHz output level.

Figure 73 shows the spectrum from 4 to 6 GHz with the transmitter operating without modulation at 5 GHz. There are no observable spurious outputs in this range, and the limit for signal detection is at least 40 dB below the carrier level.

There are some spurious outputs close to the carrier frequency. These were caused primarily by switching transients which appeared in the output of the inverter and subsequently modulated the transmitter. The basic switching frequency of the inverter, $\sim$ 20 kHz, was fairly well suppressed on the 120 VDC line. However, each switching cycle was followed by a damped sinusoidal oscillation in the 600-800 kHz range. These transients produced sidebands 40-50 dB below the carrier level, with the actual amplitude dependent on ground loops caused by connection of the modulating signal source and the power-measuring test kit to the transmitter. Further filtering of the inverter output could reduce these spurious sidebands, shown in Fig. 74, to still lower levels. Also, there was some incidental 60 Hz FM of the transmitter caused by stray pickup from the power lines. Effects of this modulation were largely eliminated

155
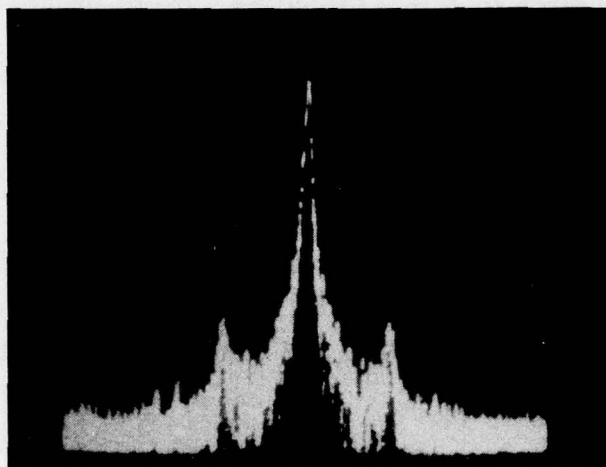
Vertical : 10 dB/div.

Horizontal: 0.5 MHz/div.
30 kHz Bandwidth

f_o = 4.999 GHz

P_o = 41.5

Figure 74   Output Spectrum of the Unmodulated Transmitter Showing
Spurious Sidebands Approximately 850 kHz from the Carrier.

during testing by triggering the sweep of the spectrum analyzer in synchronism with the AC line. With these exceptions the transmitter output was quite clean.   This demonstrated an advantage of the "straight-through" system design, with all stages operating at the output frequency, over a crystal-multiplier system or heterodyne system, in which frequencies other then the desired output frequency would always be present and would have to be suppressed by filtering.

5.0 PRODUCTION COST ESTIMATE

The validity of any estimate of the unit cost of the 40-watt C-band transmitter in quantity production is limited at present because production engineering for the component has not been undertaken. The production engineering task would form the initial phase of any large-scale production effort.

In developing the deliverable breadboard transmitter, we employed new technology for the power-combining circuitry, the individual oscillator cavities, and the diodes used in the power output stage. This was done with the foreknowledge and consent of Mr. R. H. Chilton of RADC, who was at the time the Air Force Project Engineer for the program. This approach was taken to provide new technology to the Air Force and to demonstrate the utility of such technology in the deliverable unit. The final reduction of the transmitter to a manufacturable form was judged to be of secondary importance in this program.

Our experience with military manufacturing technology contracts has shown that such efforts usually have associated with them a manufacturing engineering phase which costs 20 to 30 percent of the total contract price. In the course of such an effort, techniques for effecting substantial unit cost reductions are usually found. For the present case, we will indicate the base-line cost of parts incurred during development of the transmitter, and provide an estimate of unit costs in production lots where individual sub-assemblies would be fabricated in the same general configuration used in the prototype. The reader should be aware that the cost figures represent only rough estimates. Any substantial refinement of the figures, including mechanical redesign for reduced cost, would require an effort equal to 20 to 25 percent of the present contract.

Table 13 summarizes the cost estimates for the transmitter. Three cases are considered: costs of the single developmental unit, and costs of 100 and 500 units in serial production. In estimating costs of the developmental

158

Table 13

TRANSMITTER COST ESTIMATE

Item	Developmental Unit Cost	Unit Cost Lots of 100	Unit Cost Lots of 500
1. VCO Driver	$ 15,000	$ 2,350 - 3,000	$ 1,750 - 2,300
2. DC-to-DC Inverter	795	650	557
3. Multi-Channel Current Regulator	800	100	95
4. Combining Circuit	1,000	500	400
5. Medium Power Circulator	166	60	50
6. High Power Circulator	166	85	70
7. Four High Power Read Diodes	1,000	200	200
8. Four Oscillator Assemblies	2,000	1,000	800
9. Seven High Power OSM Loads	490	275	200
10. Labor Costs*	60,000	10,000 - 15,000	9,000 - 15,000
TOTALS	82,000	16,000 - 21,000	13,000 - 19,000

* Item 1 contains a separate labor estimate.

159

unit, work on the unsuccessful oscillator modules was omitted. An effort was made to include only that work leading directly to the deliverable unit. For all cases, costs of the VCO-driver subassembly are for a complete unit received from SMDO. Labor is included in this price. Other figures represent parts costs for the components listed.

The labor estimate is probably the least accurate of the figures included. The actual labor cost would be influenced by the success of the production engineering effort that would accompany a manufacturing program. Labor can be minimized by reducing the number of adjustable parameters in the transmitter. Fortunately, even the present design requires no adjustment of the power combining circuit, and only coupling and frequency adjustments of each high-power oscillator module. It is improbable that production quantities of 500 units would justify the capital expenditure necessary to automate such activities as diode selection, oscillator adjustment, and transmitter tuning and final adjustment. Each of these activities is labor intensive and can influence item 10.

The present transmitter design has an estimated cost which spans a range around $15,000 in quantities of 500. This is substantially in excess of the program goal of $2,000. As has been noted, an extensive production engineering effort could reduce this figure. Use of an FET-IMPATT driver and a two-diode output stage would simplify the design, and cut costs. However, the $2,000 goal does not appear to be within reach unless production lots substantially larger than 500 units are considered.

6.0   HARDWARE DELIVERIES

Two types of hardware delivery were required by the contract for this program. First, a breadboard transmitter, whose specifications, development, and performance have been described in earlier sections of this report, was to be delivered at the conclusion of the technical effort. Second, six high-power, high-efficiency GaAs Read IMPATT diodes representative of those to be used in the transmitter were to be delivered at the end of each of the first twelve months of the technical effort.

Tests of the deliverable breadboard transmitter were witnessed by Air Force personnel on 16 November 1977. The transmitter was shipped to RADC - Deputy for Electronic Technology on 23 December 1977.

The twelve diode deliveries, which included 72 high-power devices in all, were completed on March 29, 1977. The first three of these deliveries consisted of four-mesa diodes of the type originally proposed for use in the transmitter output stage. Mesa diameters were typically 7-8 mils, and nominal power outputs were near 10 W CW. The last nine shipments contained diodes with four 10-mil-diameter mesas. These larger diodes had nominal power outputs near 15 W CW, and were of the type ultimately used in the deliverable transmitter.

Condensed performance data for all diodes delivered are given in Table 14. These data were obtained in CW oscillator tests of the diodes in a disc-resonator-in-waveguide or "top-hat" circuit. More detailed data were supplied with the diode shipments.

TABLE 14

PERFORMANCE DATA AT MAXIMUM CW POWER OUTPUT
FOR DIODES DELIVERED DURING THE PROGRAM

Diode	V(Volts)	I(mA)	P_o(W)	f(GHz)	η(%)	T_J^*($^{\circ}$C)
Lot 1						
768-1	100.6	460	11.25	4.909	24.3	219
768-3	97.8	460	10.58	5.291	23.5	212
768-6	99.5	440	10.73	5.155	24.5	218
768-10	105.8	440	10.93	4.775	23.5	225
777-6	96.0	480	10.44	4.880	22.7	229
777-8	100.9	480	11.45	4.806	23.6	210
Lot 2						
756B-6	101.1	460	10.57	4.896	22.7	223
756B-8	99.8	470	10.13	4.838	21.6	220
756D-3	99.9	450	10.17	5.110	22.6	214
756D-8	100.7	460	10.03	5.078	21.7	236
768A-2	105.9	460	10.46	4.947	21.5	277
777-1	94.4	500	10.71	4.854	22.7	226
Lot 3						
756B-1	101.6	480	11.05	4.892	22.7	202
756E-3	97.0	500	10.14	5.010	20.9	255
756F-4	99.2	480	10.58	4.948	22.2	236
768B-1	98.5	450	10.16	5.141	22.9	262
777A-9	97.5	500	11.62	4.865	23.8	218
777A-10	98.3	480	11.40	4.860	24.2	230

40°C Heat Sink Assumed. Dashes indicate where thermal resistance data were not available for computation of T_J.

162

TABLE 14 (Cont'd.)

PERFORMANCE DATA AT MAXIMUM CW POWER OUTPUT
FOR DIODES DELIVERED DURING THE PROGRAM

Diode	V(Volts)	I(mA)	P_o(W)	f(GHz)	η(%)	T_J^*(°C)
Lot 4						
904D-4	64.4	820	12.50	6.630	23.7	-
904D-8	66.4	800	13.16	6.662	24.8	-
904F-1	68.8	800	12.77	6.512	23.2	222
904F-2	65.2	820	12.83	6.661	24.0	207
904G-2	63.2	840	12.50	6.629	23.6	198
904G-5	62.7	860	12.61	6.623	23.4	193
Lot 5						
907A-3	83.5	782	16.22	5.332	24.9	-
907A-4	87.4	744	15.32	5.319	23.6	-
907A-11	86.6	744	14.70	5.194	22.8	-
910-5	114.0	532	17.39	4.842	28.7	223
910-16	113.4	500	16.80	4.885	29.6	196
910A-5	114.2	560	17.02	4.855	26.6	216
Lot 6						
907B-8	88.3	782	17.17	5.210	24.9	-
907B-15	86.2	782	16.75	5.220	24.9	-
909-2	104.7	650	19.28	4.873	28.3	229
909-3	107.0	669	20.10	4.830	28.1	225
910A-6	108.5	560	15.57	4.813	25.6	215
910C-9	114.1	560	17.06	4.831	26.7	-

---

* 40°C Heat Sink Assumed. Dashes indicate where thermal resistance data
were not available for computation of T_J.

TABLE 14 (Cont'd.)

PERFORMANCE DATA AT MAXIMUM CW POWER OUTPUT
FOR DIODES DELIVERED DURING THE PROGRAM

Diode	V(Volts)	I(mA)	P_o(W)	f(GHz)	η(%)	T_J^*(°C)
Lot 7						
907C-1	89.7	782	17.60	5.160	25.1	---
907C-5	89.2	762	16.96	5.397	25.0	---
909C-4	106.0	630	19.37	4.841	29.0	---
909C-15	105.6	650	19.26	4.860	28.1	236
910A-2	110.6	540	16.00	4.820	26.8	206
910C-4	111.1	580	17.35	4.835	26.9	---
Lot 8						
946-2	103.1	633	15.61	4.863	23.9	238
947-1	99.5	594	14.42	4.992	24.4	206
947-3	107.8	555	15.28	4.986	25.6	210
947-9	106.5	576	15.47	4.994	25.2	211
949-1	103.4	537	15.50	5.215	27.9	190
949-4	102.4	555	14.84	5.202	26.1	208
Lot 9						
910D-6	114.5	516	17.62	4.929	29.8	200
910D-9	111.6	516	16.31	4.927	28.3	---
946A-9	98.0	693	15.31	4.874	22.5	---
947A-1	103.0	633	16.20	4.977	24.9	234
946A-6	97.4	733	14.94	4.852	20.9	---
947A-8	102.5	613	15.76	4.950	25.1	---

---

* 40°C Heat Sink Assumed. Dashes indicate where thermal resistance data were not available for computation of T_J.

TABLE 14 (Cont'd.)

PERFORMANCE DATA AT MAXIMUM CW POWER OUTPUT
FOR DIODES DELIVERED DURING THE PROGRAM

Diode	V (Volts)	I (mA)	P_O (W)	f (GHz)	η (%)	T_J^* (°C)
Lot 10						
946A-12	102.2	674	16.03	4.872	23.3	276
946A-3	101.4	714	17.03	4.872	23.5	219
946A-7	103	653	16.35	4.913	24.3	—
946A-8	100.3	733	16.52	4.855	22.5	—
949-5	100.5	537	14.13	5.185	26.2	204
952-5	108.4	450	13.31	5.197	27.3	195
Lot 11						
946B-2	103.1	657	16.77	5.048	24.8	236
946B-4	103.0	677	17,47	5.024	25.1	236
946B-6	101.6	677	16.26	5.006	23.7	237
949B-7	109.8	559	16.35	4.808	26.7	—
949B-8	112.2	539	15.47	4.826	25.6	—
949B-10	106.1	559	16.05	4.843	27.1	—
Lot 12						
946B-9	103.5	677	17.37	5.021	24.8	242
946C-4	104.1	677	17.11	4.888	24.3	—
946C-10	103.8	677	17.21	4.919	24.5	—
949C-13	105.6	617	16.36	4.823	25.1	—
949C-5	109.7	598	17.35	4.822	26.5	—
949C-9	108.8	597	16.28	4.805	25.9	—

---

* 40° C Heat Sink Assumed. Dashes indicate where thermal resistance data were not available for computation of T_J.

165

7.0 CONCLUSIONS AND SUGGESTIONS FOR FUTURE WORK

The present program has demonstrated that a 40-W FM CW transmitter operating at 5 GHz and meeting the electrical performance goals set initially can be constructed using GaAs Read IMPATT diodes as active elements. The prototype transmitter actually fabricated either met these goals or came sufficiently close to demonstrate that simple refinements of existing technology would be adequate to achieve them. In particular, minor changes in the DC-to-DC inverter and in the multi-channel current regulator could improve the overall transmitter efficiency to the original 14 percent goal from the 9 percent actually obtained. A change in modulation input circuitry would extend the frequency range over which the modulation sensitivity remains constant. Further, the electrical performance was achieved with the IMPATT diodes operating at a conservative 175° C junction temperature. Finally, the simple "straight-through" design having all stages of the transmitter operating at 5 GHz without frequency multiplication or frequency conversion produced a unit which was free from spurious outputs, even without elaborate filtering.

The size, weight, and cost objectives for the transmitter appear to be beyond the capabilities of present technology. It is possible to fit the entire transmitter (exclusive of the DC-to-DC inverter) within the weight and volume originally given as program goals. This might be an acceptable solution in some applications. Also, a further development effort might substantially reduce the size and weight of the inverter, making it possible to include this unit with the transmitter. Cost of the present transmitter at $ 15,000 per unit in lots of 500 is well above the $ 2,000 program goal. An intensive production engineering effort, combined with development of a simpler two-diode output stage and an FET-IMPATT driver might reduce the cost to the $ 4,000-$ 6,000 range, but additional work would be required to judge the validity of this cost projection.

The technology is available for constructing IMPATT transmitters with powers substantially greater than 40 W CW output at 5 GHz. The TIM-line power combining circuitry used in the present work could be extended

166

to the combination of 16 diodes, with total power outputs between 100 and 200 W. A cavity circuit producing 120 W at 5 GHz was in fact demonstrated in the present work, although the junction temperatures of the diodes used, $\sim 240°$ C, were not consistent with reliable long-term operation.

The present program effort revealed a number of areas in which additional work is required. These tasks include both basic development engineering and production engineering, and would be directed toward improving the performance and reducing the cost of the transmitter.

Additional study of the TIM-line oscillator circuit is required to determine whether an efficient and smoothly-operating circuit can be constructed in this medium. The possibility of a fully integrated transmitter output stage, with TIM-line oscillator modules and TIM-line power combining circuitry is attractive. Also, TIM oscillators will probably offer wider locking bandwidths than cavity-type oscillators. However, the performance of TIM-line oscillators in the present work was not sufficiently good to include them in the deliverable transmitter.

The usable bandwidth of the Gysel-type hybrids constructed in TIM-line during the present program was between 10 and 20 percent. The circuit is not truly nonresonant, since it depends on certain of its internal line segments being $\lambda/4$ long for correct operation. If still larger bandwidths are required, it may be worthwhile to investigate the radial-line combining circuit further. This circuit is truly nonresonant, but has in the past offered insufficient isolation between the diode ports to insure stability against undesired modes of oscillation.

One way to simplify the transmitter, and so reduce costs, would be to combine a smaller number of diodes, each with higher power capability, in the output stage. Diodes with 30-40 W CW power capability at 5 GHz appear to be possible. These would make a two-diode output stage, requiring a simpler current regulator and simpler power-combining circuitry, possible. Development of such diodes should be undertaken in the future.

It now appears that simpler adjustment and higher overall efficiency can be obtained in the transmitter by using FET's in the low-level stages in preference to the Gunn and flat-profile IMPATT diodes used in the prototype. The power level to which FET's are used should be the subject of a cost-efficiency tradeoff study, but it now appears that FET's could be employed effectively up to about 300 mW. At least one IMPATT stage would still be required in the VCO-driver subassembly to reach the 3W level.

The foregoing suggestions for development work may lead to a transmitter system design substantially different from that used in the deliverable prototype constructed during the present program. Whatever form the transmitter ultimately takes, there are several additional tasks which must be completed before it can be regarded as a manufacturable product. First, the reliability of the high-power, four-mesa GaAs Read IMPATT diodes must be confirmed in actual tests to determine whether reliability objectives for the transmitter can in fact be achieved. Next, the transmitter package must be designed to withstand shock, vibration, and extremes of temperature, humidity and altitude that will be encountered in actual field use. Finally, a substantial production engineering effort must be undertaken to reduce fabrication costs.

8.0 REFERENCES

1. C. A. Brackett, "The Elimination of Tuning-Induced Burnout and Bias Circuit Oscillations in IMPATT Oscillators," Bell System Technical J. <u>52</u>, 271 (March 1973).

2. "High-Efficiency Solid-State C-Band Generator," Contract F30602-74-C-0306, work carried out at Raytheon Research Division from 24 June 1974 to 24 June 1975.

3. "High-Efficiency Solid-State C-Band Generator," Final Technical Report RADC-TR-75-286, Rome Air Development Center, Air Force Systems Command, Griffiss Air Force Base, New York 13441, November 1975.

4. E. J. Wilkinson, "An N-Way Hybrid Power Divider," IRE Transactions <u>MTT-8</u>, 116 (January 1960).

5. U. H. Gysel, "A New N-Way Power Divider/Combiner Suitable for High-Power Applications," 1975 IEEE MTT Symposium Digest, p. 116.

6. C. Buntschuh, "A Study of the Transmission Line Properties of Trapped Inverted Microstrip Line," Final Technical Report RADC-TR-74-311, Rome Air Development Center, Air Force Systems Command, Griffiss Air Force Base, New York 13441, December 1974.

7. D. J. Coleman, Jr., W. R. Wisseman, and D. W. Shaw, "Reaction Rates for Pt on GaAs," Appl. Phys. Lett. <u>24</u>, 355 (April 1974).

8. <u>Reference Data for Radio Engineers</u>, 5th Ed., p. 21-8, New York: Howard W. Sams & Co., Inc., 1968.

MISSION
of
Rome Air Development Center

RADC plans and conducts research, exploratory and advanced development programs in command, control, and communications (C^3) activities, and in the C^3 areas of information sciences and intelligence. The principal technical mission areas are communications, electromagnetic guidance and control, surveillance of ground and aerospace objects, intelligence data collection and handling, information system technology, ionospheric propagation, solid state sciences, microwave physics and electronic reliability, maintainability and compatibility.